METAL-CHALCOGEN-NITROGEN RING COMPLEXES & CRYSTALLOGRAPHICS STUDIES

Paul Gordon Waddell

A Thesis Submitted for the Degree of PhD
at the
University of St Andrews

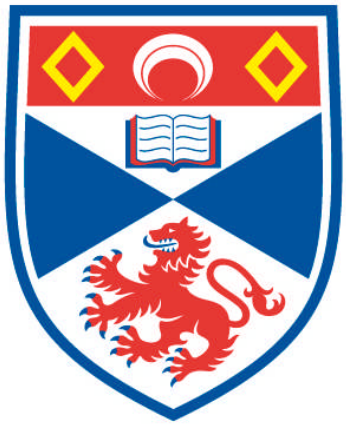

2010

Metal-Chalcogen-Nitrogen Ring Complexes & Crystallographic Studies

A thesis submitted by

Paul Gordon Waddell

In partial fulfillment for the award of

Doctor of Philosophy, University of St Andrews

School of Chemistry, University of St Andrews

North Haugh, St Andrews, Fife, KY16 9ST

19 February 2010

Declarations

I, Paul Gordon Waddell, hereby certify that this thesis, which is approximately 40,000 words in length, has been written by me, that it is the record of work carried out by me and that it has not been submitted in any previous application for a higher degree.

I was admitted as a research student in September, 2006 and as a candidate for the degree of Doctor of Philosophy in February 2010; the higher study for which this is a record was carried out in the University of St Andrews between 2006 and 2010.

Date: Signature of candidate:

I hereby certify that the candidate has fulfilled the conditions of the Resolution and Regulations appropriate for the degree of Doctor of Philosophy in the University of St Andrews and that the candidate is qualified to submit this thesis in application for that degree.

Date: Signature of supervisor:

In submitting this thesis to the University of St Andrews we understand that we are giving permission for it to be made available for use in accordance with the regulations of the University Library for the time being in force, subject to any copyright vested in the work not being affected thereby. We also understand that the title and the abstract will be published, and that a copy of the work may be made and

supplied to any *bona fide* library or research worker, that my thesis will be electronically accessible for personal or research use unless exempt by award of an embargo as requested below, and that the library has the right to migrate my thesis into new electronic forms as required to ensure continued access to the thesis. We have obtained any third-party copyright permissions that may be required in order to allow such access and migration, or have requested the appropriate embargo below.

The following is an agreed request by candidate and supervisor regarding the electronic publication of this thesis: embargo on both all or part of printed copy and electronic copy for the same fixed period of 1 year on the following ground: publication would preclude future publication.

Date: Signature of candidate:

Signature of supervisor:

Acknowledgments

My thanks first and foremost go to my supervisors, Prof. Alex Slawin and to Prof. Derek Woollins for their patience, help whenever it was needed, no matter how trivial the question (I should really say patience twice) and for giving me this shot in the first place. I will be eternally grateful for their support over the last four years.

My thanks also go to all those in the Woollins/Slawin/Kilian conglomerate I've had the pleasure of sharing a lab with over the course of my postgraduate studies for their banter and friendship, especially Dr Sahrah Parveen and Dr Vit Matuska for all their help getting me started, Dr Amy Fuller for her ability to solve a few of my crystallographic issues and 'my' project students Ben Read, Emma Whitelaw, Ally Robertson and Catherine Bromley.

This thesis would be a lot harder to read without the help of Dr Piotr Wawrzyniak, whose understanding of the workings of Microsoft Word and Endnote (the authors of which I would also like to thank) has been invaluable. Thanks also to Jacks Garland for taking the time to proof-read the whole thing.

Special thanks to Prof. Takayoshi Fujii and his group for supplying me with the ndsdsd ligand. A debt of gratitude goes also to Sylvia Williamson, one of the departments unsung heroines, for performing the microanalyses presented in this thesis. My thanks go also to EPSRC for funding my research.

I would also like to give my thanks and love to Gwen for tolerating my research-related mood swings. Whether pretending to understand when I enthusiastically pontificated about chemistry or genuinely understanding when things weren't going well she was always supportive and for that I am grateful.

Finally, I'd like to thank my friends and family, especially my Dad, to whom I would like to dedicate this thesis.

Abstract

A series of $Pt(S_2N_2)(P(OR)_nR'_{3-n})_2$ complexes were prepared and analysed using ^{31}P NMR and IR spectroscopy, elemental analysis and X-ray crystallography. Similarly, a series of $Pt(SeSN_2)(P(OR)_nR'_{3-n})_2$ complexes were also prepared and analysed. The $^1J_{Pt-P}$ coupling constants and Pt-P bond lengths for these complexes are influenced by the oxygen content of their phosphorus ligands. The ^{31}P NMR spectra for a series of $[Pt(S_3N)(P(OR)_nR'_{3-n})_2][BF_4]$ complexes are also reported. Planar $[S_2N_2H]^-$ complexes were prepared and the X-ray crystal structure of $[Pd(S_2N_2H)(bipy)][Cl]$ is reported.

The X-ray structures of $MX_2(P(OR)_nR'_{3-n})_2$ are reported and compared with the previously reported analogues. The magnitude of the $^1J_{Pt-P}$ varies linearly with the Pt-P bond length ($l_{Pt-P} = 2.421 - J/24255$) for the 12 platinum-containing complexes. This correlation is compared to that of a larger series of complexes.

A series of $M(ndsdsd)L_2$ (ndsdsd = bis[(nitrilo(diphenyl)-λ^6-sulfanyl)](diphenyl)-λ^6-sulfanediimide ($Ph_2S(=N\text{-}(Ph_2)S\equiv N)_2$)) complexes were prepared and characterised using elemental analysis and multinuclear NMR and IR spectroscopy where appropriate. The X-ray crystal structures of five examples are reported.

Contents

Declarations **2**

Acknowledgments **4**

Abstract **6**

Contents **7**

List of Figures **14**

List of Tables **17**

Abbreviations **20**

General Abbreviations 20

NMR Spectroscopy Abbreviations 21

IR Spectroscopy Abbreviations 22

CHAPTER 1: Introduction **23**

1. Metal-Chalcogen-Nitrogen Complexes **23**

1.1. Metal-Sulfur-Nitrogen complexes 23

1.1.1. Introduction 23

1.1.2. Preparations involving tetrasulfur tetranitride 23

1.1.3. Preparations involving sodium trisulfur trinitride 28

1.1.4. Reactivity of $Pt(S_2N_2)(PR_3)_2$ complexes 29

1.1.5. Reactions involving transmetallation using $[R_2SnS_2N_2]_2$ 30

1.1.6. Reactions in liquid ammonia 31

1.1.7. Reactions involving heptasulfur imide 35

1.2. Selenium-containing Metal-Chalcogen-Nitrogen Complexes 36

1.2.1. Introduction 36

1.2.2. Selenium-sulfur-nitrogen analogues 37

1.2.3. Selenium-nitrogen analogues 38

1.3. Tellurium-containing Metal-Chalcogen-Nitrogen Complexes 40

1.4. λ^6-sulfanenitrile-Metal Complexes 43

1.4.1. Introduction 43

1.4.2. λ^6-sulfanenitriles in organic chemistry 44

1.4.3. λ^6-sulfanenitrile-metal complexes 48

1.5. Characterisation, Structural Elucidation and Spectroscopy 49

2. Bis(phosphino)Platinum(II) Dihalides 50

2.1. Introduction 50

2.2. Synthesis of $PtX_2(PR_3)_2$ Complexes 51

2.3. ^{31}P NMR of $PtX_2(PR_3)_2$ Complexes 52

2.4. X-ray Crystallography of $PtX_2(PR_3)_2$ Complexes 55

3. Inorganic 1-D Complexes 58

3.1. Introduction 58

3.2. 1-D Metal Complexes 58

3.3. 1-D Electrical Conducting Systems 60

3.3.1. Introduction 60

3.3.2. Magnus' Green Salt 60

3.3.3. Krogmann Salts 61

3.4. Potential of Metal-Chalcogen-Nitrogen Complexes 62

CHAPTER 2: 5-membered Metal-Sulfur-Nitrogen Complexes 66

4. $Pt(S_2N_2)(P(OR)_nR'_{3-n})_2$ Complexes 66

4.1. Introduction 66

4.2. Synthesis of $Pt(S_2N_2)(P(OR)_nR'_{3-n})_2$ Complexes 67

4.3. NMR Spectroscopy 70

4.4. IR Spectroscopy 75

4.5. X-ray Crystal Structures 76

4.5.1. Low-temperature X-ray crystal structure of $Pt(S_2N_2)(PMe_2Ph)_2$ 76

4.5.2. X-ray crystal structures of $Pt(S_2N_2)(P(OR)_3)_2$ Complexes 78

4.5.3. X-ray crystal structures of $Pt(S_2N_2)(P(OMe)_nPh_{3-n})_2$ 81

5. 1-D Disulfur-Dinitrido Complexes 85

5.1. Introduction 85

5.2. Synthesis of Planar $[S_2N_2]^{2-}$ or $[S_2N_2H]^-$-containing Complexes 86

5.3. NMR Spectroscopy 88

5.4. X-ray Crystal Structures 90

6. Trisulfur-Mononitrido Complexes 94

6.1. Introduction 94

6.2. Synthesis of $[Pt(S_3N)(P(OR)_nR'_{3-n})_2][BF_4]$ Complexes 94

6.3. NMR Spectroscopy 95

CHAPTER 3: 5-membered Selenium-containing Metal-Chalcogen-Nitrogen Complexes 98

7. Monoselenium-Monosulfur-Dinitrido Complexes 98

7.1. Introduction 98

7.2. Synthesis of $Pt(SeSN_2)(P(OR)_nR'_{3-n})_2$ Complexes 99

7.3. NMR Spectroscopy 101

7.4. IR Spectroscopy 104

7.5. X-ray Crystal Structures 104

Chapter 4: Correlating Pt-P Bond lengths and Pt-P Coupling Constants 109

8. $MX_2(P(OR)_nR'_{3-n})_2$ Complexes 109

8.1. Introduction 109

8.2. Synthesis of $MX_2(P(OR)_nR'_{3-n})_2$ Complexes 110

8.2.1. Synthesis of *cis*-$PtCl_2(P(OR)_nR'_{3-n})_2$ complexes 110

8.2.2. Synthesis of $PtBr_2(P(OR)_nR'_{3-n})_2$ and $PtI_2(P(OR)_nR'_{3-n})_2$ complexes 111

8.2.3. Synthesis of *cis*-$PdCl_2(P(OR)_nR'_{3-n})_2$ complexes 113

8.3. NMR Spectroscopy 113

8.4. X-ray Crystal Structures 117

8.5. Correlating Pt-P Bond Lengths and Pt-P Coupling Constants 125

Chapter 5: Metal λ^6-Sulfanenitrile Complexes 129

9. Metal-ndsdsd Complexes 129

9.1. Introduction 129

9.2. Synthesis of Metal-ndsdsd Complexes 129

9.3. Spectroscopic Analysis 133

9.4. X-ray Crystal Structures 135

Chapter 6: Experimental 141

10. Experimental 141

10.1. General Experimental 141

10.2. Preparation of Starting Materials and Reagents 142

10.2.1. Preparation of $[S_4N_3]Cl$ 142

10.2.2. Preparation of S_7NH 142

10.2.3. Preparation of $PtCl_2(COD)$ 143

10.2.4. Preparation of $PtCl_2(PhCN)_2$ 143

10.2.5. Preparation of $PtCl_2(bipy)$ 144

10.2.6. Preparation of *trans*-$PtBr_2(PhCN)_2$ 144

10.2.7. Preparation of *trans*-$PtI_2(PhCN)_2$ 144

10.2.8. Preparation of $Pd(COD)Cl_2$ 145

10.2.9. Preparation of $PdCl_2$(bipy) 145

10.3. Preparation of $MX_2(PR_3)_2$ Complexes 145

10.3.1. Preparation of *cis*-$PtCl_2(PMe_2Ph)_2$ 145

10.3.2. Preparation of *cis*-$PtCl_2(P(OPh)_3)_2$ 146

10.3.3. Preparation of *cis*-$PtCl_2(P(O^nBu)_3)_2$ 146

10.3.4. Preparation of *cis*-$PtCl_2(P(O^iPr)_3)_2$ 146

10.3.5. Preparation of *cis*-$PtCl_2(P(OEt)_3)_2$ 147

10.3.6. Preparation of *cis*-$PtCl_2(P(OMe)_3)_2$ 147

10.3.7. Preparation of *cis*-$PtCl_2(P(OMe)_2Ph)_2$ 147

10.3.8. Preparation of $PtCl_2(P(OMe)Ph_2)_2$ 148

10.3.9. Preparation of *cis*-$PtCl_2(PPh_3)_2$ 148

10.3.10. Preparation of *cis*-$PtBr_2(P(OMe)_3)_2$ 149

10.3.11. Preparation of *cis*-$PtBr_2(P(OMe)_2Ph)_2$ 149

10.3.12. Preparation of *cis*-$PtBr_2(P(OMe)Ph_2)_2$ 149

10.3.13. Preparation of $PtBr_2(PPh_3)_2$ 150

10.3.14. Preparation of *cis*-$PtI_2(P(OMe)_3)_2$ 150

10.3.15. Preparation of *cis*-$PtI_2(P(OMe)_2Ph)_2$ 151

10.3.16. Preparation of *cis*-$PtI_2(P(OMe)Ph_2)_2$ 151

10.3.17. Preparation of *cis*-$PtI_2(PPh_3)_2$ 152

10.3.18. Preparation of *trans*-$PtI_2(PPh_3)_2$ 152

10.3.19. Preparation of *cis*-$PdCl_2(P(OMe)_3)_2$ 153

10.3.20. Preparation of *cis*-$PdCl_2(P(OMe)_2Ph)_2$ 153

10.3.21. Preparation of *cis*-$Pd_2Cl_4(P(OMe)_2Ph)_2$ 154

10.4. Preparation of Disulfur-Dinitrido Complexes 154

10.4.1. Preparation of $Sb(S_2N_2)Ph_3$ 154

10.4.2. Preparation of $Pt(S_2N_2)(PMe_2Ph)_2$ 155

10.4.3. Preparation of $Pt(S_2N_2)(P(OPh)_3)_2$ 155

10.4.4. Preparation of $Pt(S_2N_2)(P(O^nBu)_3)_2$ 156

10.4.5. Preparation of $Pt(S_2N_2)(P(OEt)_3)_2$ 157

10.4.6. Preparation of $Pt(S_2N_2)(P(OMe)_3)_2$ 157

10.4.7. Preparation of $Pt(S_2N_2)(P(OMe)_2Ph)_2$ 158

10.4.8. Preparation of $Pt(S_2N_2)(P(OMe)Ph_2)_2$ 159

10.4.9. Preparation of $[Pd(S_2N_2H)(bipy)][^nBu_2SnCl_3]$ 160

10.4.10. Preparation of $[Pd(S_2N_2H)(bipy)][Cl]$ 160

10.4.11. Preparation of $Pd(S_2N_2)(bipy)$ 161

10.4.12. Preparation of $Pt(S_2N_2)(bipy)$ 161

10.4.13. Preparation of $[Pt(S_2N_2H)(bipy)][BF_4]$ 162

10.4.14. Attempted preparation of $Pt(S_2N_2)(PPh_3)_2$ 163

10.5. Preparation of Trisulfur-Mononitrido Complexes 163

10.5.1. Preparation of $[Pt(S_3N)(P(OMe)_3)_2][BF_4]$ 163

10.5.2. Preparation of $[Pt(S_3N)(P(OMe)_2Ph)_2][BF_4]$ 164

10.5.3. Preparation of $[Pt(S_3N)(P(OMe)Ph_2)_2][BF_4]$ 164

10.6. Preparation of Monoselenium-Monosulfur-Dinitrido Complexes 165

10.6.1. Preparation of $Pt(SeSN_2)(P(OMe)_3)_2$ 165

10.6.2. Preparation of $Pt(SeSN_2)(P(OMe)_2Ph)_2$ 166

10.6.3. Preparation of $Pt(SeSN_2)(P(OMe)Ph_2)_2$ 167

10.6.4. Preparation of $Pt(SeSN_2)(PPh_3)_2$ 168

10.7. Preparation of ndsdsd-containing Complexes 168

10.7.1. Preparation of [Pt(ndsdsd)(COD)][2Cl] 168

10.7.2. Preparation of $[Pt(ndsdsd)(P(OMe)_3)(P(O)(OMe)_2)][Cl]$ 169

10.7.3. Preparation of $[Pd(ndsdsd)_2][Pd_2Cl_6]$ 169

10.7.4. Preparation of [Pd(ndsdsd)(bipy)][2Cl] 170

10.7.5. Preparation of $[AuCl_2(ndsdsd)][AuCl_4]$ 170

10.7.6. Preparation of $[AuCl_2(ndsdsd)][PF_6]$ 171

Further Work 172

References 174

Appendices 180

A: Crystallographic Data 181

B: Publications 214

List of Figures

1: S_4N_4 24

2: *mer*-$Pt(S_4N_4)Cl_2(PMe_2Ph)$ (a), *fac*-$Pt(S_4N_4)Cl_2(PMe_2Ph)$ (**b**) 27

3: Proposed structure for $Pt(S_4N_4)[P(OPh_3)]_2$ 27

4: $[Me_2SnS_2N_2]_2$ 30

5: $Co(S_2N_2H)_2$ 31

6: Apparatus used for reactions in liquid ammonia 33

7: $[Pt\{SO_2(NH)_2\}(PR_3)_2]$ (**a**), $Pt(NSO)_2(PR_3)_2$ (**b**) 35

8: $[Cu(S_3N)_2]^-$ 35

9: $[(\eta^5\text{-}C_5H_5)_2Ti(S_7NH)]$ 36

10: $PtCl(Se_3N)(PMe_2Ph)_2$ (**a**), $[Pt(Se_2N_2H)_2(PMe_2Ph)_2]^+$ (**b**) 39

11: $Te_2N_2SCl_2$ 41

12: $Te_3N_2SCl_2$ 42

13: Structures of λ^6-sulfanenitriles. Trifluoronitrilosulfur (**a**) and difluoro(heptafluoroisopropyl)nitrilosulfur (**b**) 43

14: Structure of 2,2-biphenylylene(phenyl)-λ^6-sulfanenitrile 44

15: Structures of $[CoCl_2(ndsdsd)]$ (**a**) and $[Ni(ndsdsd)_2]^{2+}$ (**b**) 49

16: π-back bonding in M-P bonds in *cis*-$PtCl_2(PR_3)_2$ (**a**) and *trans*-$PtCl_2(PR_3)_2$ (**b**) .. 54

17: *cis*-$PtBr_2(P(OPh)_3)_2$ (**a**)[94] and *trans*-$PtCl_2(PEt_3)_2$ (**b**)[95] 56

18: Correlation between $^1J_{Pt\text{-}P}$ (Hz) and bond length (Å) for known $PtX_2(PR_3)_2$ complexes 57

19: Schematic diagram of the four structural classes of 1D transition metal polymers 59

20: Schematic of Magnus' Green Salt 61

21: Diagram showing the overlap of d_z^2 orbitals of platinum within a Krogmann Salt (**a**) and the decreased interplanar separation observed upon oxidation with bromine (**b**) 62

22: Stacking arrangement in $[Pt(S_2N_2H)(PMe_2Ph)_2]^+$ dimer unit 64

23: $Pt(S_2N_2)(P(OR)_nR'_{3-n})_2$ showing correct labelling of the phosphorus atoms. 71

24: $^{31}P-\{^1H\}$ NMR spectrum (109 MHz, CH_2Cl_2 solution) of **5** 71

25: Variation of ^1J_A and ^1J_X in $Pt(S_2N_2)(P(OMe)_nPh_{3-n})_2$ complexes 72

26: X-ray crystal structure of **1** 76

27: X-ray crystal structure of **2**. 78

28: X-ray crystal structure of **4** showing two-fold disorder about the $[S_2N_2]^{2-}$ fragment 80

29: X-ray crystal structure of **7**. 82

30: Variation of Pt-P(A) and Pt-P(X) distances in $Pt(S_2N_2)(P(OMe)_nPh_{3-n})_2$ complexes 83

31: ^1H environments in $[Pd(S_2N_2H)(bipy)]^+$ 88

32: X-ray crystal structure of $\mathbf{9}^1$ showing hydrogen bonding to Cl^- 91

33: X-ray crystal structure of **9** showing stacking between $[Pd(S_2N_2H)(bipy)]^+$ units 93

34: Fragment of $[Pt(S_3N)(P(OR)_nR'_{3-n})_2][X]$ with important atoms labelled 96

35: Variation of ^1J_A and ^1J_X in $[Pt(S_3N)(P(OMe)_nPh_{3-n})_2][X]$ complexes 97

36: Variation of ^1J_A and ^1J_X in $Pt(SeSN_2)(P(OMe)_nPh_{3-n})_2$ complexes 103

37: X-ray crystal structure of **18**. 105

38: Variation of Pt-P(A) and Pt-P(X) distances in $Pt(SeSN_2)(P(OMe)_nPh_{3-n})_2$ complexes 107

39: Variation of $^1J_{Pt-P}$ in $[PtCl_2(P(OMe)_nPh_{3-n})_2]$ complexes 114

40: X-ray crystal structure of **24**. 117

41: X-ray crystal structure of **28**. 119

42: X-ray crystal structure of **32**. 121

43: X-ray crystal structure of **34** 123

44: Variation of Pt-P distances in $PtX_2(P(OMe)_nPh_{3-n})_2$ complexes 124

45: Correlation of $^1J_{Pt-P}$ with Pt-P bond length in **22-33** 126

46: Correlation of $^1J_{Pt-P}$ with Pt-P bond length in large range of Platinum-Phosphorus complexes 127

47: ndsdsd 130

48: X-ray crystal structure of **38** 136

49: X-ray crystal structure of the backbone in **40** showing the twist-boat conformation 137

50: X-ray crystal structure of **39** 137

51: X-ray crystal structure of **37** 138

List of Tables

1: Microanalyses, yields and melting points for **2** and **4**-**7** 70

2: ^{31}P NMR chemical shifts and coupling constants for **1**-**7** and $Pt(S_2N_2)(PPh_3)_2$ 74

3: Selected IR absorptions (cm^{-1}) for **2** and **4**-**7** 75

4: Selected bond distances (Å) and angles (°) of **1** 77

5: Selected bond lengths (Å) and angles (^{o}) for **2**, **4** and **5** 79

6: Selected bond lengths (Å) and angles (^{o}) for **5**-**7** and $Pt(S_2N_2)(PPh_3)_2$ 84

7: Microanalyses and yields for **8**-**12** 88

8: ^{1}H NMR data for 9 $[Pd(S_2N_2H)(bipy)][Cl]$ 89

9: Selected bond lengths (Å) and angles (^{o}) for **9** and **9**[1] 92

10: ^{31}P NMR chemical shifts and coupling constants for **13**-**15** and $[Pt(S_3N)(PPh)_3)_2][PF_6]$ 96

11: Microanalyses, yields and melting points for **16**-**18** 100

12: ^{31}P NMR chemical shifts and coupling constants for **16**-**19** 102

13: Selected IR absorptions (cm^{-1}) for **16**-**19** 104

14: Selected bond lengths (Å) and angles (^{o}) for **16**-**19** 108

15: Microanalyses, yields and melting points for **31** and **32** 112

16: ^{31}P NMR chemical shifts, coupling constants and isolated yields for **20**-**35** 115

17: ^{1}H NMR data for **31** and **32** 116

18: Selected bond lengths (Å) and angles (^{o}) for **20**-**25** 118

19: Selected bond lengths (Å) and angles (^{o}) for **26**-**29** and **29a** 120

20: Selected bond lengths (Å) and angles (^{o}) for **30**-**33**. 122

21: Selected bond lengths (Å) and angles (^{o}) for **34**-**35**. 123

22: Coupling constants and bond lengths calculated and observed for selected compounds 128

23: Microanalyses and yields for **36**-**41** 132

24: ^{1}H NMR data for 41 [$AuCl_2$(ndsdsd)][PF_6] 133

25: Selected bond lengths (Å) for **36**-**40** 139

26: Selected bond angles (^{o}) for **34**-**38** 140

A. 1: Crystal data and structure refinement for **1** 181

A. 2: Crystal data and structure refinement for **2** 182

A. 3: Crystal data and structure refinement for **4** 183

A. 4: Crystal data and structure refinement for **5** 184

A. 5: Crystal data and structure refinement for **6** 185

A. 6: Crystal data and structure refinement for **7** 186

A. 7: Crystal data and structure refinement for **8** 187

A. 8: Crystal data and structure refinement for **9** 188

A. 9: Crystal data and structure refinement for **16** 189

A. 10: Crystal data and structure refinement for **17** 190

A. 11: Crystal data and structure refinement for **18** 191

A. 12: Crystal data and structure refinement for **19** 192

A. 13: Crystal data and structure refinement for **20** 193

A. 14: Crystal data and structure refinement for **21** 194

A. 15: Crystal data and structure refinement for **23** 195

A. 16: Crystal data and structure refinement for **24** 196

A. 17: Crystal data and structure refinement for **26** 197

A. 18: Crystal data and structure refinement for **27** 198

A. 19: Crystal data and structure refinement for **28** 199

A. 20: Crystal data and structure refinement for **29**.....200

A. 21: Crystal data and structure refinement for **29a**.....201

A. 22: Crystal data and structure refinement for **30**.....202

A. 23: Crystal data and structure refinement for **31**.....203

A. 24: Crystal data and structure refinement for **32**.....204

A. 25: Crystal data and structure refinement for **33**.....205

A. 26: Crystal data and structure refinement for **33a**.....206

A. 27: Crystal data and structure refinement for **34**.....207

A. 28: Crystal data and structure refinement for **35**.....208

A. 29: Crystal data and structure refinement for **36**.....209

A. 30: Crystal data and structure refinement for **37**.....210

A. 31: Crystal data and structure refinement for **38**.....211

A. 32: Crystal data and structure refinement for **39**.....212

A. 33: Crystal data and structure refinement for **40**.....213

Abbreviations

General Abbreviations

°C	degrees Celsius
Å	Ångström, 1×10^{-10} m
bipy	2,2′-bipyridyl
^{n}Bu	*normal*-butyl
ca.	*circa*
calc.	calculated
COD	1,5-cyclooctadiene
DBU	1,8-diazabicyclo[5.4.0]undec-7-ene
dppe	1,2-bis(diphenylphosphino)ethane
dppoe	1,2-bis(diphenylphosphoryl)ethane
EPR	electron paramagnetic resonance
Et	ethyl
fac	facial
HMPA	hexamethylphosphoramide
IR	infra red
LT	low temperature
Me	methyl
mer	meridional
MGS	Magnus' Green Salt
MP	melting point

M-S-N	metal-sulfur-nitrogen
ndsdsd	bis[(nitrilo(diphenyl)-λ^6-sulfanyl)](diphenyl)-λ^6-sulfanediimide
NMR	nuclear magnetic resonance
OTf	triflate
Ph	phenyl
^{i}Pr	*iso*-propyl
P(OR′)$_3$	phosphite
P(OR′)$_2$R	phosphonite
P(OR′)R$_2$	phosphinite
PR$_3$	phosphine
SN	sulfur-nitrogen
TCNQ	tetracyanoquinodimethane
TTF	tetrathiafulvalene
RT	room temperature
UV-VIS	ultra violet-visible

NMR Spectroscopy Abbreviations

d	doublet
dd	doublet of doublets
Hz	Hertz
m	multiplet
ppm	parts per million
s	singlet
sep	septet

IR Spectroscopy Abbreviations

m	medium
s	strong
w	weak
δ	deformation

CHAPTER 1: Introduction

1. Metal-Chalcogen-Nitrogen Complexes

1.1. Metal-Sulfur-Nitrogen complexes

1.1.1. Introduction

Metal sulfur-nitrogen complexes have been an area of interest for inorganic chemists for some years now and many examples have been synthesised.[1] One of the most common examples of a sulfur-nitrogen ligand is the disulfur dinitrido ligand $[S_2N_2]^{2-}$ and the closely-related protonated version $[S_2N_2H]^-$. As the examples that follow will testify, the most common metal centre to which this ligand is attached is platinum (typically platinum phosphines) although there are many examples which involve other metal centres. Over the years a great many different synthetic strategies have been utilised to create this ligand, though it is not available as a free ion.

1.1.2. Preparations involving tetrasulfur tetranitride

Tetrasulfur tetranitride is a very important species with regards to sulfur-nitrogen chemistry as a whole. Its preparation involves passing gaseous ammonia through a solution of either sulfur dichloride or sulfur monochloride.[2] The crystal structure reveals a caged structure where all four nitrogen atoms can be viewed in the same

plane.[3] As one would expect of a cage structure with such a high nitrogen content S_4N_4 is explosive, detonating under heat and shock.

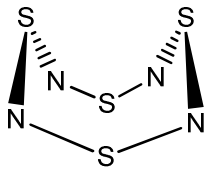

Figure 1: S_4N_4

Tetrasulfur tetranitride (Figure 1) can be used as the source for a number of sulfur-nitrogen ligands including $[S_2N_2]^{2-}$, $[S_3N]^-$, $[S_2N_3]^{3-}$ and $[S_3N_2]^{2-}$. One example requires roughly two equivalents of $PtCl_2(PMe_2Ph)_2$ suspended with S_4N_4 in xylene to be heated to 150 °C until the platinum compound has dissolved. The solution is heated further to 170 °C at which point an oily precipitate forms and the solution is cooled and evaporated to dryness. The residue is dissolved in dichloromethane and eluted through a bio-beads gel-permeation column from which a red band is collected and concentrated before being placed on a silica preparative thin-layer chromatography plate and eluted once more with dichloromethane giving two bands, yellow and purple, which were found to be $Pt(S_2N_2H)Cl(PMe_2Ph)$ and $Pt(S_3N)Cl(PMe_2Ph)$ respectively (Equation 1).[4]

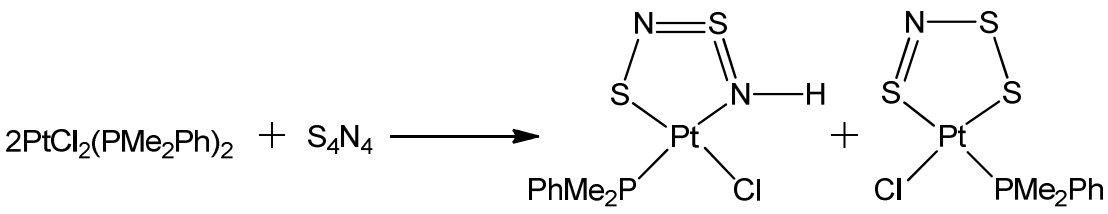

Equation 1

The same reaction can also be performed *via* photochemical activation of S_4N_4.[5] Equimolar amounts of the two starting reagents are stirred in dichloromethane for an hour whilst being photolysed with a 125 W mercury-discharge lamp (265-579 nm) which activates the S_4N_4 to react with the platinum compound. One advantage of this method is that the S_4N_4 need not be heated to high temperatures and is less likely to explode.

Tetrasulfur tetranitride is also used in the preparation of $[PPh_4]_2[Pd_2(\mu\text{-}S_2N_2)Cl_6]$ and $[PPh_4]_2[Pd_2(\mu\text{-}S_3N_2)Cl_4]$.[6] These two compounds are formed in the reaction of $[PPh_4]_2[Pd_2Cl_6]$ and two equivalents of S_4N_4 in dichloromethane (Equation 2). The first of these compounds, $[PPh_4]_2[Pd_2(\mu\text{-}S_2N_2)Cl_6]$ contains a bridging neutral $[S_2N_2]$ ligand with each nitrogen atom bonded to one of the palladium atoms with a yield from this reaction of 38 %. This neutral S_2N_2 ligand can also be achieved with antimony and copper centres as in $[S_2N_2]\cdot 2SbCl_5$[7] and $[S_2N_2]\cdot 2CuCl_2$.[8] The second molecule, $[PPh_4]_2[Pd_2(\mu\text{-}S_3N_2)Cl_4]$, contains a more unusual bridging $[S_3N_2]^{2-}$ ligand, with both palladium atoms coordinated to the same two sulfur atoms, as produced in low yield in a similar reaction involving S_4N_4 and $PdCl_2$, which gives $[Pd_2(\mu\text{-}S_3N_2)(S_2N_2)_2]$[9] along with a small amount of an $[S_2N_2H]^-$ containing compound, $[PPh_4][Pd(S_2N_2H)Cl_2]$, in a yield of 4 %.[10] As with other observed protonated compounds this latter complex exhibits hydrogen-bonding in the crystal structure showing dimers with the NH of the $[S_2N_2H]^-$ ligand hydrogen-bonding to one of the chlorine atoms of the adjacent molecule.

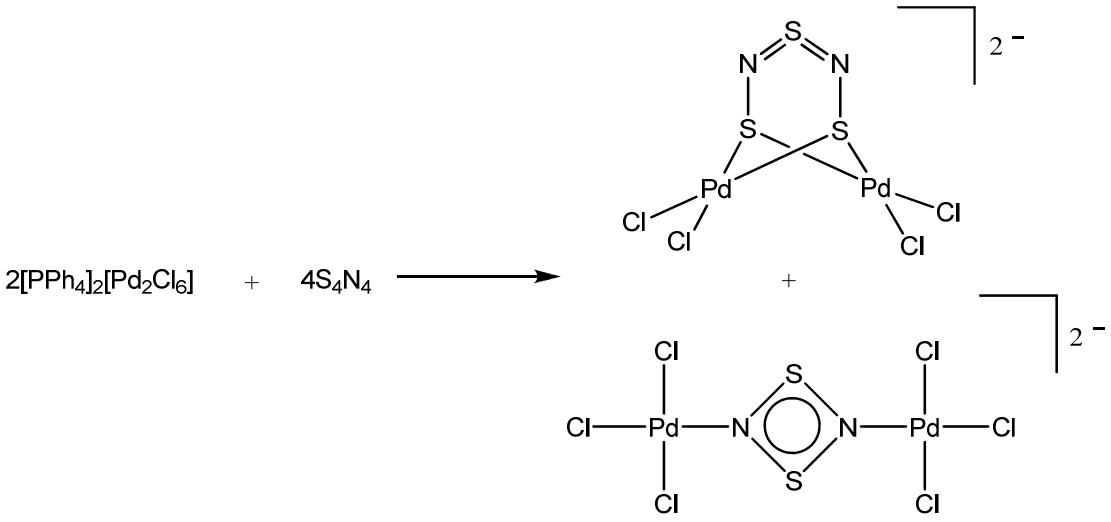

Equation 2

Tetrasulfur tetranitride can also co-ordinate as the $[S_4N_4]^{2-}$ anion. This can be observed when adding two equivalents of S_4N_4 to platinum chlorophosphines.[11] $[PtCl_2(PMe_2Ph)]_2$ in dichloromethane was added slowly to a solution of S_4N_4 in dichloromethane and stirred for 15 minutes. The product was isolated as a red band when the solution was passed through a bio-beads gel-permeation column. The crystal structure shows the ligand taking a meridional tridentate form coordinating *via* two sulfur and one nitrogen atom around an octahedral platinum centre in $Pt(S_4N_4)Cl_2(PMe_2Ph)$ (Figure 2 (**a**)). The bonding within the six-membered and five-membered rings is still not fully understood. The facial isomer (Figure 2 (**b**)) of $Pt(S_4N_4)Cl_2(PMe_2Ph)$ can also be produced by heating the meridional isomer in chloroform to between 75-80°C with the isomerisation being effectively complete after three hours.[12] The structure of this isomer was first thought to have the platinum atom co-ordinated to one nitrogen and two sulfur atoms but was later found to be to two nitrogen atoms and one sulfur atom.[13] The $[S_4N_4]^{2-}$ anion is also known to co-ordinate to iridium through the reaction of $IrCl(CO)(PPh_3)_2$ with S_4N_4.[14]

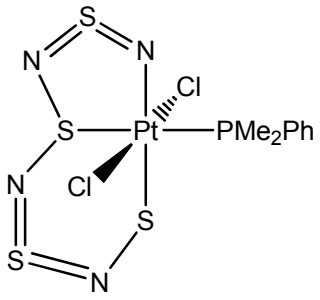

a

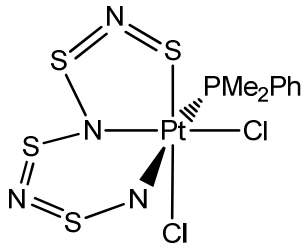

b

Figure 2: *mer*-$Pt(S_4N_4)Cl_2(PMe_2Ph)$ (**a**), *fac*-$Pt(S_4N_4)Cl_2(PMe_2Ph)$ (**b**)

The above compounds are not the only examples of S_4N_4 reacting to form a complex where the reagent is not broken into smaller units. The compound $Pt(S_4N_4)[P(OPh_3)]_2$ (Figure 3) has also been reported as being made *via* the addition of a benzene solution of $Pt(P(OPh_3))_4$ to a benzene solution of S_4N_4, though the existence of this species is based solely on elemental analysis and IR spectroscopy[15] and in the light of the more well characterised examples above the proposed structure seems unlikely.

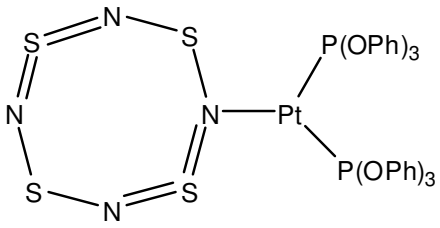

Figure 3: Proposed structure for $Pt(S_4N_4)[P(OPh_3)]_2$

There are also examples of S_4N_4 reacting to form complexes at metal centres other than the precious metals highlighted previously. One such example is the reaction of $Co(CO)_2(C_5H_5)$ with S_4N_4 in benzene which gives $Co(S_2N_2)(C_5H_5)$.[16]

As well as S_4N_4, its reduced analogue, tetrasulfur tetraimide ($S_4N_4H_4$) can also be used in the synthesis of metal sulfur-nitrogen complexes. An early example of the preparation of a metal sulfur-nitrogen complex uses this reagent to produce $Pt(S_2N_2)(PPh_3)_2 \cdot 4CHCl_3$.[17] For this, $S_4N_4H_4$ was treated with tris(triphenylphosphine) platinum in toluene (Equation 3).

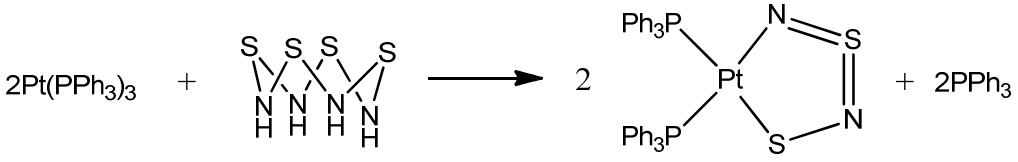

Equation 3

The product was obtained as a chloroform solvate in a 45 % yield and the procedure is also hampered by the necessity of preparing the tetrasulfur tetraimide by reducing S_4N_4.

Common factors in most reported procedures involving S_4N_4 are the low yields and the tendency for multiple products to be produced. In light of this and the explosive nature of the compound, accentuated by the fact that high temperatures are often required, this reagent is best avoided in favour of safer and more reliable methods.

1.1.3. Preparations involving sodium trisulfur trinitride

Sodium trisulfur trinitride is a salt of $[S_3N_3]^-$ and another source of SN ligands. It can be formed *via* the reaction of $NaNH_2$ and S_4N_4 in liquid ammonia.[18] Like S_4N_4, $Na[S_3N_3]$ is also explosive and decomposes below 120 °C.

Early examples of disulfur dinitrido platinum phosphine complexes were prepared *via* procedures involving sodium trisulfur trinitride (Equation 4).[19] The tetrasulfur tetranitride produced as a by-product was removed by washing with cyclohexane.[20]

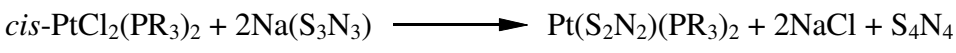

Equation 4

The same method can also be applied to $PdCl_2(dppe)$ to afford $Pd(S_2N_2)(dppe)$.[19] However, one downside of this strategy is the explosive nature of sodium trisulfur trinitride although yields were improved compared to the routes involving S_4N_4, reaching 60-70 %.

1.1.4. Reactivity of $Pt(S_2N_2)(PR_3)_2$ complexes

Complexes of the formula $Pt(S_2N_2)(PR_3)_2$ can also act as precursors for other compounds. The $[S_2N_2H]^-$ ligand, the protonated version of the $[S_2N_2]^{2-}$ ligand,[21-23] can easily be prepared from a disulfur dinitrido complex by addition of HBF_4, which protonates the ring leaving $[BF_4]^-$ to act as the counter-ion.[20] The yield of this reaction is reported as 60%. This protonation can also be performed using HCl.[24]

The reaction of $Pt(S_2N_2)(PR_3)_2$ with $SOCl_2$ produces the sulfur-nitrogen heterocycle Roesky's sulfoxide (S_3N_2O)[25], in 35 % yield and $PtCl_2(PR_3)_2$ which can be recycled and used to make more starting material (Equation 5).[24]

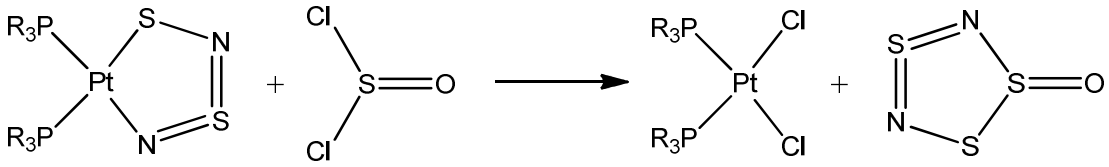

Equation 5

1.1.5. Reactions involving transmetallation using $[R_2SnS_2N_2]_2$

The first reported species of the type $[R_2SnS_2N_2]_2$ was $[Me_2SnS_2N_2]_2$ which can be formed *via* the reaction of $N(SnMe_3)_3$ and S_4N_4 (Figure 4).[26] Rather more conveniently, $[^nBu_2SnS_2N_2]_2$ can be obtained *via* reaction of $^nBu_2SnCl_2$ with $[S_4N_3]Cl$ in liquid ammonia. These compounds can both be used in transmetallation reactions as a source of $[S_2N_2]^{2-}$, though in most cases the protonated form, $[S_2N_2H]^-$ is obtained (Equation 6).

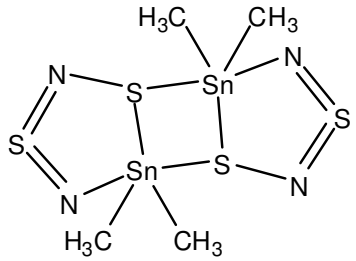

Figure 4: $[Me_2SnS_2N_2]_2$

$$[PtCl_2(PR_3)_2] + [Me_2SnS_2N_2]_2 \longrightarrow [Pt(S_2N_2H)(PR_3)_2][Me_2SnCl_3]$$

Equation 6

The $Me_2SnCl_3^-$ counter-ion probably forms due to the presence of HCl in the dichloromethane.[26] The same method was also used in attaching the $[S_2N_2H]^-$ to a cobalt centre.[26] For this reaction two equivalents of $CoCl_2$(dppoe) was stirred with

$[Me_2SnS_2N_2]_2$ in dichloromethane for 20 hours to give [{$Co(S_2N_2H)_2$}(dppoe)]. The X-ray structure of this compound reveals two homoleptic $Co(S_2N_2H)_2$ molecules (Figure 5) hydrogen-bonded to the oxygen atoms of the dppoe group. The use of this hydrogen-bonding property could be investigated further as large arrays may be possible much in the same way that platinum $[S_2N_2H]^-$ complexes of this type can be used to produce stacking compounds.[27]

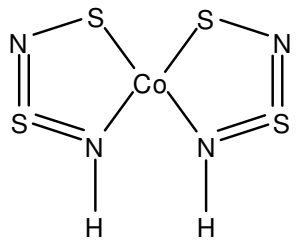

Figure 5: $Co(S_2N_2H)_2$

1.1.6. Reactions in liquid ammonia

Another very useful method of preparing $[S_2N_2]^{2-}$ complexes and other sulfur-nitrogen containing compounds is using liquid ammonia as a solvent though less work has been completed this way.[28] This route can be seen as preferable as it eliminates the need for explosive reagents such a S_4N_4 and $Na[S_3N_3]$. Instead reagents such as $[S_4N_3]Cl$ and $[S_3N_2Cl]Cl$ can be used to much the same effect as S_4N_4. Insights into which species are formed upon dissolving sulfur or sulfur-nitrogen heterocycles in liquid ammonia are to be found in a number of studies, though the solutions themselves and the equilibria involved are notoriously complex. Cyclo-octasulfur, when dissolved in liquid ammonia, gives rise to a variety of sulfur-nitrogen species such as $[S_4N]^-$, $[S_3N]^-$ and $[S_7N]^-$ according to the UV-VIS absorption spectrum of the

solution.[29] Dissolution of Li_2S_6 in liquid ammonia has also been shown to produce the $[S_4N]^-$ anion as it exists in equilibrium with $[S_6]^{2-}$ as well as a variety of other polysulfide anions.[30] It is thought from ^{14}N NMR studies that the major reactive species formed by $[S_4N_3]Cl$ and $[S_3N_2Cl]Cl$ in liquid ammonia is $[S_3N_3]^-$,[31] suggesting that ammonia not only acts as a solvent but also as a nitrogen source as it would also have to produce $[S_4N]^-$ upon the dissolution of sulfur. Though other sulfur nitrogen species are most likely present in lower concentrations and in equilibrium with $[S_3N_3]^-$, the equilibria demonstrated in (Equation 7-8) are thought to be involved.

$$7[S_4N_3]^+ + 6NH_3 \rightleftharpoons 9[S_3N_3]^- + H_2S + 16H^+$$

Equation 7

$$[S_3N_2Cl]^+ + NH_3 \rightleftharpoons [S_3N_3]^- + 3H^+ + Cl^-$$

Equation 8

The $[S_2N_2H]^-$ ion can also be formed in liquid ammonia by treating $S_4N_4H_4$ with potassium azide or by deprotonating S_7NH, again with potassium azide, the latter proceeding *via* the sequential formation of the anions $[S_7N]^-$, $[S_4N]^-$ and $[S_3N]^-$.[32] $[S_2N_2H]^-$, which has been characterised by ^{14}N and ^{15}N NMR spectroscopy, is however a fairly short-lived species decomposing to give $[S_3N_3]^-$ as the final product.

In a general reaction either one of the two compounds $[S_4N_3]Cl$ or $[S_3N_2Cl]Cl$ is added to liquid ammonia at -78 °C after which the metal complex to which the disulfur dinitrido ligand is to be attached is added and after stirring at low temperature for some time, the solution is allowed to warm to room temperature with the ammonia being blown off under a stream of nitrogen (Figure 6).

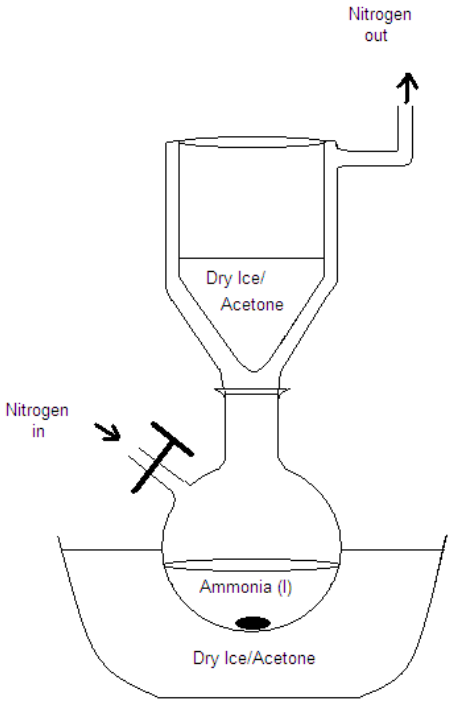

Figure 6: Apparatus used for reactions in liquid ammonia

Each manipulation is performed under nitrogen due to the tendency of $[S_4N_3]Cl$ and $[S_3N_2Cl]Cl$ to hydrolyse in air. After the ammonia has evaporated the product can be dissolved in dichloromethane and recrystallised. This method has proved to be a most promising avenue due to its relative simplicity and its use of relatively stable reagents.

Using liquid ammonia as a solvent can also provide a route to numerous other sulfur-nitrogen ligands *via* a range of other reagents. The ligand $[S_2N_3(SO_2NH_2)]^{2-}$ is prepared *via* reaction in liquid ammonia using $S_4N_4O_2$ as the reagent (Equation 9).[33]

$$[PtCl_2(PR_3)_2] + S_4N_4O_2 + 3NH_3 \longrightarrow [Pt\{S_2N_3(SO_2NH_2)\}(PR_3)_2] + NH_4Cl + \text{'SN'}$$

Equation 9

This reaction can be performed with platinum and palladium dichlorophosphines in an analogous way to that of $[S_4N_3]Cl$ in liquid ammonia. In a similar fashion SO_2Cl_2 in liquid ammonia produces the $[SO_2(NH)_2]^{2-}$ ligand (Equation 10).[31] Reaction of this with $[PtCl_2(PR_3)_2]$ in liquid ammonia (Equation 11) gives $[Pt\{SO_2(NH)_2\}(PR_3)_2]$ (Figure 7 (**a**)) in 54-75 % yield.

$$SO_2Cl_2 + 4NH_3 \longrightarrow SO_2(NH_2)_2 + 2NH_4Cl$$

Equation 10

$$[PtCl_2(PR_3)_2] + SO_2(NH_2)_2 + 2NH_3 \longrightarrow [Pt\{SO_2(NH)_2\}(PR_3)_2] + 2NH_4Cl$$

Equation 11

Yet another liquid ammonia reaction involves $SOCl_2$ to give $[NSO]^-$ ligands. $Pt(NSO)_2(PR_3)_2$[34, 35] (Figure 7 (**b**)) and $Ti(NSO)_2(C_5H_5)_2$[31] can both be isolated *via* addition of the corresponding dichlorides to $SOCl_2$ in liquid ammonia at -78 °C (equation 12) in yields of 70 % and 45 % respectively.

$$MCl_2L_2 + 2SOCl_2 + 8NH_3(l) \longrightarrow M(NSO)_2L_2 + 2NH_4Cl$$

Equation 12

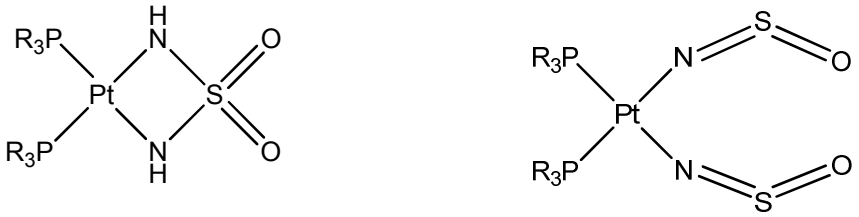

a **b**

Figure 7: $[Pt\{SO_2(NH)_2\}(PR_3)_2]$ (**a**), $Pt(NSO)_2(PR_3)_2$ (**b**)

1.1.7. Reactions involving heptasulfur imide

The preparation of a number of other sulfur-nitrogen ligands is also possible *via* various methods. The S_3N^- ligand can be produced using the well-known reagent heptasulfur imide (S_7NH) as its source.[1] This ligand, unlike $[S_2N_2]^{2-}$, binds to the metal centre *via* two sulfur atoms. An example of this is the preparation of the copper complex $[AsPh_4][Cu(S_3N)Cl]$,[36] produced by adding S_7NH in a 1:1 ratio to a solution of $CuCl_2$ and $[AsPh_4]OH$ in methanol. With four equivalents of S_7NH the products $[AsPh_4][Cu(S_3N)_2]$ (Figure 8) and $[AsPh_4][Cu(S_3N)]_2S_2O_3$ are also isolated.[37] Nickel[36] and palladium[38] complexes containing the $[S_3N]^-$ ligand can also be obtained using S_7NH.

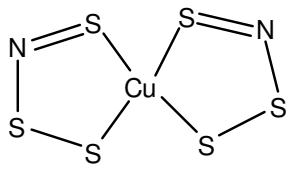

Figure 8: $[Cu(S_3N)_2]^-$

A similar reaction involving a copper centre can produce an $[S_7N]^-$ containing compound. In this reaction $[(PPh_3)_2N]OH$ and S_7NH and $CuCl_2{\cdot}2H_2O$ in a 5:1 ratio

react to give $[(PPh_3)_2N][Cu(S_3N)(S_7N)]$.[38] The protonated analogue of this anion is observed in the complex $[(\eta^5\text{-}C_5H_5)_2Ti(S_7NH)]$ (Figure 9) which is produced *via* the reaction of S_7NH and $[(\eta^5\text{-}C_5H_5)_2Ti(CO)_2]$ in hexane at room temperature.[39]

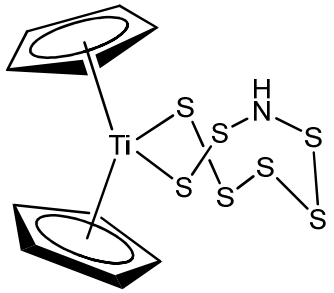

Figure 9: $[(\eta^5\text{-}C_5H_5)_2Ti(S_7NH)]$

1.2. Selenium-containing Metal-Chalcogen-Nitrogen Complexes

1.2.1. Introduction

As well as the metal sulfur-nitrogen complexes, a number of analogues containing selenium are also known. Much of the chemistry involved is analogous although given the larger covalent radius of selenium compared to sulfur and the lower bond strength of selenium-nitrogen and selenium-metal bonds in comparison to their sulfur analogues the stability of selenium containing compounds is generally (although not always) lower. As a consequence of this their synthesis often proves more difficult than that of their sulfur analogues. In fact there are very few reported selenium-nitrogen heterocycles. Tetraselenium tetranitride (Se_4N_4), which is extremely shock sensitive, is the most prominent example and cyclic Se_2N_2 has also

been observed as evidenced by the synthesis of the Se_2N_2 adducts $[Pd_2(\mu\text{-}Se_2N_2)X_6]^{2-}$.[40, 41] However selenium-nitrogen analogues of some of the sulfur-nitrogen ligands mentioned have already been synthesised and the complexes containing selenium-nitrogen fragments are just as stable as their sulfur-nitrogen analogues. Mixed chalcogen ligands, *i.e.* those containing both selenium and sulfur atoms have also been synthesised.

1.2.2. Selenium-sulfur-nitrogen analogues

Mixed chalcogen ligands of the type $[SeSN_2]^{2-}$ and the protonated $[SeSN_2H]^-$ can be synthesised using liquid ammonia as a solvent and nitrogen-donor[42] in the same way that $[S_4N_3]Cl$ and $[S_3N_2]Cl_2$ were used to produce $[S_2N_2]^{2-}$ ligands, here $[Se_2SN_2]_2Cl_2$ is used to produce the $[SeSN_2]^{2-}$ ligand (Equation 13).

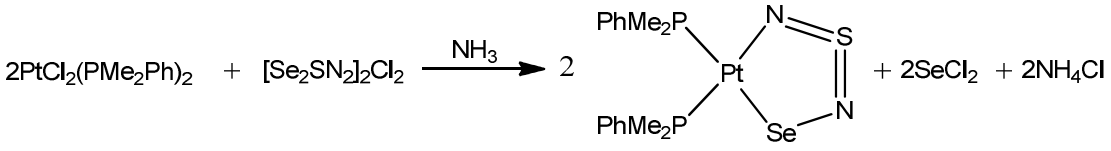

Equation 13

A reported yield of 70 % was found for this reaction. The compound was found to be isostructural with the disulfur equivalent.

A second method for making this compound was also reported.[43] Again using liquid ammonia as a solvent, $SeCl_4$ and $[S_4N_3]Cl$ are added together and stirred 30 minutes before the platinum dichlorophosphine is added. If the two reagents are added in a 5:1 excess of $SeCl_4$, the monoselenated compound is formed with trace amounts

of the disulfur dinitrido complex and no diselenated rings are found. In both methods the crystal structure revealed a metal-bound selenium atom. Protonation of the ring to give the $[SeSN_2H]^-$ ligand is achieved using HBF_4 in tetrahydrofuran-benzene with a yield of 70 %.[42] Both compounds were found to be isostructural with the previously reported sulfur analogues.[43]

1.2.3. Selenium-nitrogen analogues

The diselenated compound can also be obtained using liquid ammonia as a solvent. $SeCl_4$ is used in a 3:1 ratio with the platinum dichlorophosphine to produce a platinum complex with an $[Se_2N_2]^{2-}$ ligand (Equation 14):

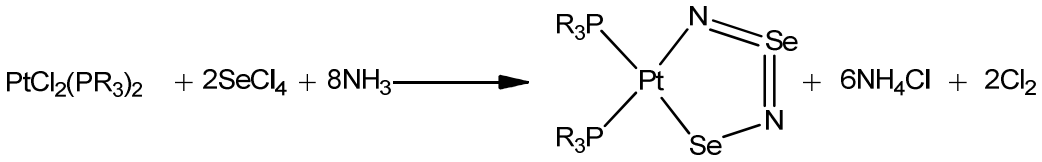

Equation 14

This reaction was reported to give a 74 % yield.[43] The diselenated compounds were also found to be isostructural to their sulfur equivalents.

Another similarity between sulfur and selenium chemistry as regards these ligands is that Se_4N_4 can also be used to produce $[Se_2N_2]^{2-}$ and $[Se_2N_2H]^-$ ligands. Se_4N_4 can be synthesised from a reaction of NH_3 and $(EtO)_2SeO$.[44] Although Se_4N_4 is highly explosive, reactions can be carried out using the correct precautions. $Pt(Se_2N_2H)(PMe_2Ph)Cl$ can be synthesised by refluxing Se_4N_4 and $PtCl_2(PMe_2Ph)_2$ in chloroform[45], although this is accompanied by the formation of $PtCl(Se_3N)(PMe_2Ph)$

(Figure 10 (**a**)). Reaction of this crude mixture with phosphine gives $[Pt(Se_2N_2H)(PMe_2Ph)_2]Cl$ (Figure 10 (**b**)), which, like its sulfur analogue can form stacking arrays. However the call for a high temperature and the low yield recorded makes this an unsatisfactory process.

a **b**

Figure 10: $PtCl(Se_3N)(PMe_2Ph)_2$ (**a**), $[Pt(Se_2N_2H)_2(PMe_2Ph)_2]^+$ (**b**)

Se_4N_4 also reacts with zerovalent $Pt(PPh_3)_3$ to give $[Pt(Se_2N_2)(PPh_3)_2]_2$ and a short lived intermediate species, which decomposes with the loss of PPh_3.[46] A suspension of Se_4N_4 in dichloromethane is stirred to give a fine dispersion and added to a solution of $Pt(PPh_3)_3$ in dichloromethane to give an equimolar mixture of the two compounds before the decomposition of the dimer (Equation 15).

$$Pt(PPh_3)_3 + Se_4N_4 \longrightarrow [Pt(Se_2N_2)(PPh_3)_2]_2 + Pt_2(Se_2N_2)_2(PPh_3)_3$$

$$\longrightarrow 2[Pt(Se_2N_2)(PPh_3)_2]_2$$

Equation 15

Tetraselenium tetranitride has also been found to react in liquid ammonia.[47] However, the process by which it can be made to dissolve involves high temperature and pressure. To achieve this, a suspension of Se_4N_4 in liquid ammonia is heated until

the internal pressure of the pressure tube is 50 atmospheres. If $PtCl_2(PMe_2Ph)_2$ is present in a near equimolar amount during this procedure then $Pt(Se_2N_2)(PMe_2Ph)_2$ is produced.

Alternatively, $PtCl_2(PMe_2Ph)_2$ is added to liquid ammonia in a thick-walled Young's tube and stirred until thoroughly dissolved. At this point the mixture is frozen at -196 °C and $SeOCl_2$ is added drop-wise. The tube is then sealed and allowed to warm to room temperature with stirring before the red solid produced is extracted with dichloromethane.[48]

Other selenium analogues of the afore-mentioned sulfur compounds include $[Se_3N_2]^{2+}$ and $[Se_2SN_2]^{2+}$.[49] Due to their positive charges they are not suitable for addition to most metal centres, though they could be useful precursors in liquid ammonia reactions.

1.3. Tellurium-containing Metal-Chalcogen-Nitrogen Complexes

Introducing tellurium into chalcogen-nitrogen inorganic ring systems is a very interesting challenge in that very few species have been isolated. A few examples do exist; these are generally mixed chalcogen systems. With the increase in metallic character as chalcogens increase in atomic radius it can be assumed that the chemistry involved in making these compounds will be very different to that of sulfur and selenium. The lack of obvious reagents for any potential compounds makes this a very

challenging area in which to experiment. Very few heterocycles consisting purely of tellurium and nitrogen, such as Te_6N_8,[50] have been reported to date although mixed-chalcogen compounds such as $Te_2N_2SCl_2$[51] (Figure 11) exist and may be useful in producing new ligands.

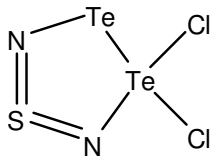

Figure 11: $Te_2N_2SCl_2$

A mixed chalcogen-nitrogen example of a tellurium containing ring system is $Pt(TeSN_2)(PMe_2Ph)_2$.[52] This is produced by stirring an equimolar amount of $TeCl_4$ and S_4N_4 in dichloromethane until a red solid is deposited. After this settles the solution is decanted before being suspended in more dichloromethane. At this point $PtCl_2(PMe_2Ph)_2$ is added and this mixture is stirred before the addition of DBU which gives a dark solution. The solvent is then removed to leave a mixture of $Pt(TeSN_2)(PMe_2Ph)_2$ and $Pt(S_2N_2)(Me_2Ph)_2$.[48] Typical of reactions involving S_4N_4 multiple products are observed. A more effective way of producing this compound is the addition of $Te_3N_2SCl_2$ (Figure 12) to $PtCl_2(PMe_2Ph)_2$.[52] This product was observed *via* ^{31}P NMR, but protonation of the ring using HBF_4 gave crystals of $Pt(TeSN_2H)(PMe_2Ph)_2$ due to the increased order provided by the hydrogen-bonding these compounds exhibit.

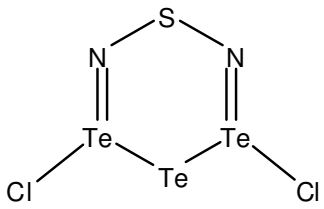

Figure 12: $Te_3N_2SCl_2$

Not yet reported is whether there has been any success in attempting to make these tellurium-nitrogen complexes using liquid ammonia. It may be possible, as was possible with selenium reagents, to use a mixture of $TeCl_4$ and $[S_4N_3]Cl$ in liquid ammonia to produce the same result. There is also a possibility of forming the $[Te_2N_2]^{2-}$ ligand in an analogous reaction to that used to create the $[Se_2N_2]^{2-}$ ligand in liquid ammonia with the use of $TeCl_4$. The synthesis of $[Te_2N_2]^{2-}$ and $[TeSeN_2]^{2-}$ may also be possible using similar reagents as were used to make $Te_3N_2SCl_2$. The precursor to this species is $S[N(SiMe_3)_2]_2$[53], for which selenium and tellurium analogues can also be made from $LiN(SiMe_3)_2$ by adding Se_2Cl_2 and $TeCl_4$ respectively.[54] It can be hypothesised that by reacting these compounds with $TeCl_4$ in dioxane as in the preparation of $Te_3N_2SCl_2$ that the compounds $Te_3N_2SeCl_2$ and $Te_4N_2Cl_2$ may be made from which the ligands $[Te_2N_2]^{2-}$ and $[TeSeN_2]^{2-}$ may also be formed.

1.4. λ^6-sulfanenitrile-Metal Complexes

1.4.1. Introduction

λ^6-sulfanenitriles are a class of compounds with the general formula $X_3S{\equiv}N$ with a terminal, triply-bonded nitrogen atom and six bonds coordinated to the sulfur atom. The compound $F_3S{\equiv}N$ (Figure 13(**a**)) has been known for some time, although it was first believed to exist as the $F_2S{=}NF$ isomer[55] before the correct structure was confirmed spectroscopically.[56-58] $F_3S{\equiv}N$ is produced along with the compound SNF *via* the reaction of S_4N_4 and AgF_2. The first λ^6-sulfanenitrile to contain a carbon-sulfur bond was produced soon afterwards in the form of $N{\equiv}SF_2CF(F_3C)_2$ (Figure 13 (**b**)), which was prepared *via* the reaction of $F_3S{\equiv}N$ with perfluoropropene and caesium fluoride.[59] Since then a whole host of derivatives of $F_3S{\equiv}N$ have been reported.[60]

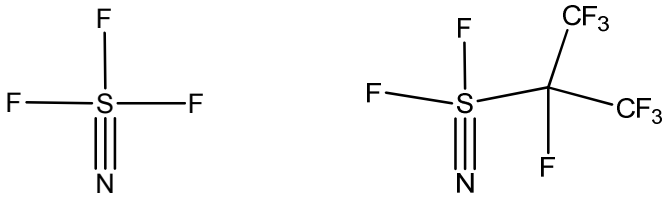

a **b**

Figure 13: Structures of λ^6-sulfanenitriles. Trifluoronitrilosulfur (**a**) and difluoro(heptafluoroisopropyl)nitrilosulfur (**b**)

λ6-sulfanenitriles of the type $Ph_2FS{\equiv}N$ can also be prepared from the corresponding sulfimide. Using the electrophilic fluorinating agent SelectFluor™ (1-chloromethyl-4-fluoro-1,4-diazoniabicyclo-[2,2,2]octane bis(tetrafluoroborate)) the

intermediate $Ph_2S{=}NF$ is formed which undergoes a 1,2-migration of the fluorine atom to produce the diaryl(fluoro)-λ6-sulfanenitrile (Equation 16).

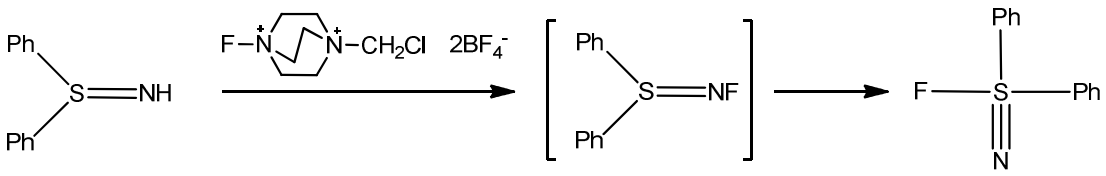

Equation 16

1.4.2. λ^6-sulfanenitriles in organic chemistry

Despite the long history of these compounds in the field of fluorine chemistry until recently little interest was shown by organic chemists. The first truly organic λ^6-sulfanenitrile to be fully characterised was the compound $Ph_3S{\equiv}N$, which was reported in 1997 and produced *via* reaction of $Ph_2FS{\equiv}N$ with phenyl lithium in THF at -78 °C.[61] A heterocyclic λ^6-sulfanenitrile has also been reported (Figure 14). 2,2-biphenylylene(phenyl)-λ^6-sulfanenitrile is produced *via* reaction of $Ph_2FS{\equiv}N$ and 2,2-dilithiobiphenyl in THF at -78 °C.[62]

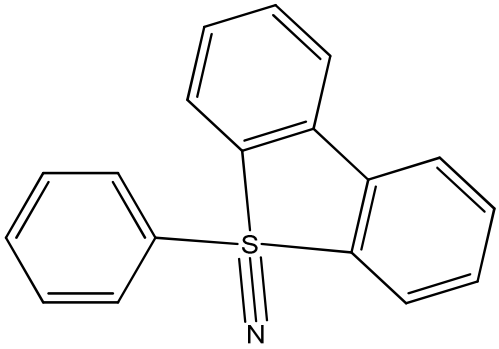

Figure 14: Structure of 2,2-biphenylylene(phenyl)-λ^6-sulfanenitrile

The compounds were found to be quite basic as would be expected of compounds containing such electron-rich atoms as the triply bonded nitrogen observed in λ^6-sulfanenitriles. As a result of this the nitrogen atom was found to be nucleophilic and hence *N*-alkylated derivatives of $Ph_3S{\equiv}N$ could also be produced following treatment with alkyl halides to form compounds with the formula $[Ph_3S{=}NR][X]$.

N-sulfenylation of $Ph_3S{\equiv}N$ can be used as a source of sulfenylnitrenes *via* reaction with arenesulfenyl chloride in dichloromethane at -30 °C which affords $[Ph_3S{=}NSAr][Cl]$.[63] The sulfenylnitrene fragment can then be trapped using an alkene to give the corresponding aziridine (Equation 17).

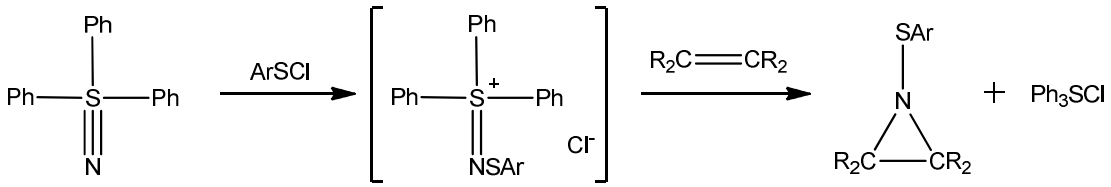

Equation 17

Similarly, the reaction of $Ph_3S{\equiv}N$ with sulfur dichloride affords thiazyl chloride which is in equilibrium with its cyclic trimer $(ClSN)_3$, which can be used to synthesise sulfur-nitrogen heterocycles (Equation 18).

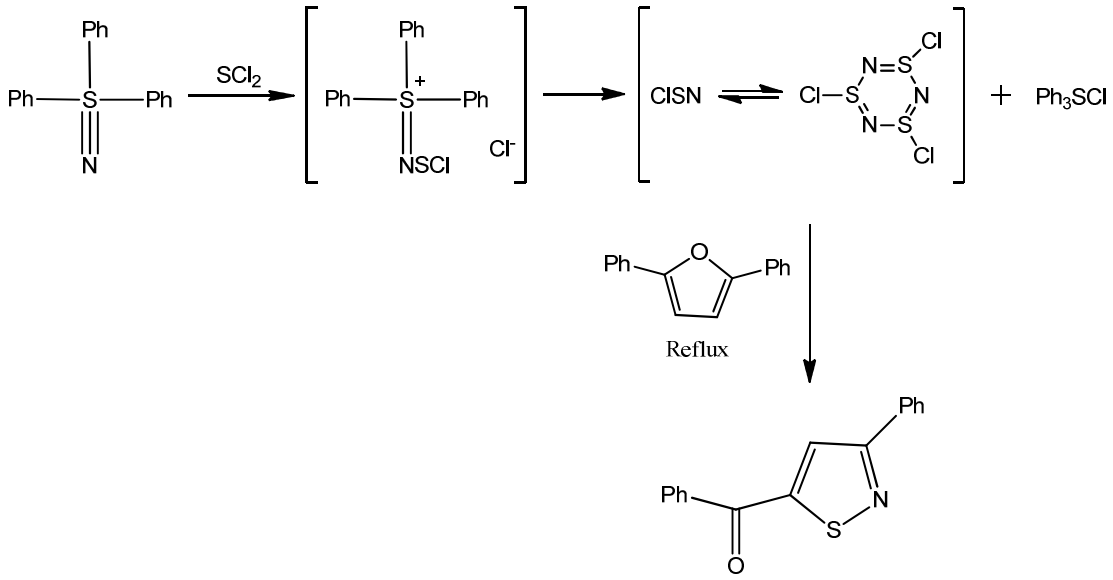

Equation 18

The λ^6-sulfanenitrile $Ph_2FS{\equiv}N$ in particular has proven itself to be a useful building block in sulfur-nitrogen chemistry as is demonstrated by its ability to react to form systems containing sulfur-nitrogen chains. Reaction of $Ph_2FS{\equiv}N$ with diphenyl-sulfoximide under reflux in benzene and treatment of the resulting solution with perchloric acid produces the $[Ph_2OS\text{-}N\text{-}SPh_2NH]^+$ cation, which contains a 4-membered sulfur nitrogen chain. A similar cation $[Ph_2NHS\text{-}N\text{-}SPh_2NH]^+$ which contains a 5-membered sulfur-nitrogen chain can be produced *via* reaction of diphenyl-sulfodiimide and $Ph_2FS{\equiv}N$ under similar conditions (Equation 19).[64]

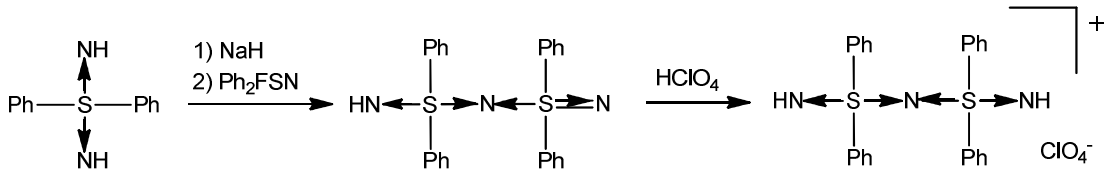

Equation 19

Neutral λ^6-sulfanenitrile equivalents of these cations can be produced if the treatment with perchloric acid is omitted giving rise to longer sulfur-nitrogen chains with a terminal nitrogen atom.[65]

Furthermore, treatment of the sulfimide $Ph_2S{=}NH$ with three equivalents of $Ph_2FS{\equiv}N$ affords the $[(Ph_2S(=N\text{-}(Ph_2)S{=}NH)_2]^{2+}$ cation, which when treated with base, forms the compound bis[(nitrilo(diphenyl)-λ^6-sulfanyl)](diphenyl)-λ^6-sulfanediimide ($Ph_2S(=N\text{-}(Ph_2)S{\equiv}N)_2$, ndsdsd) (Equation 20). This compound is neutral and contains a 7-membered sulfur nitrogen chain with two terminal, triply-bonded nitrogen atoms.[66]

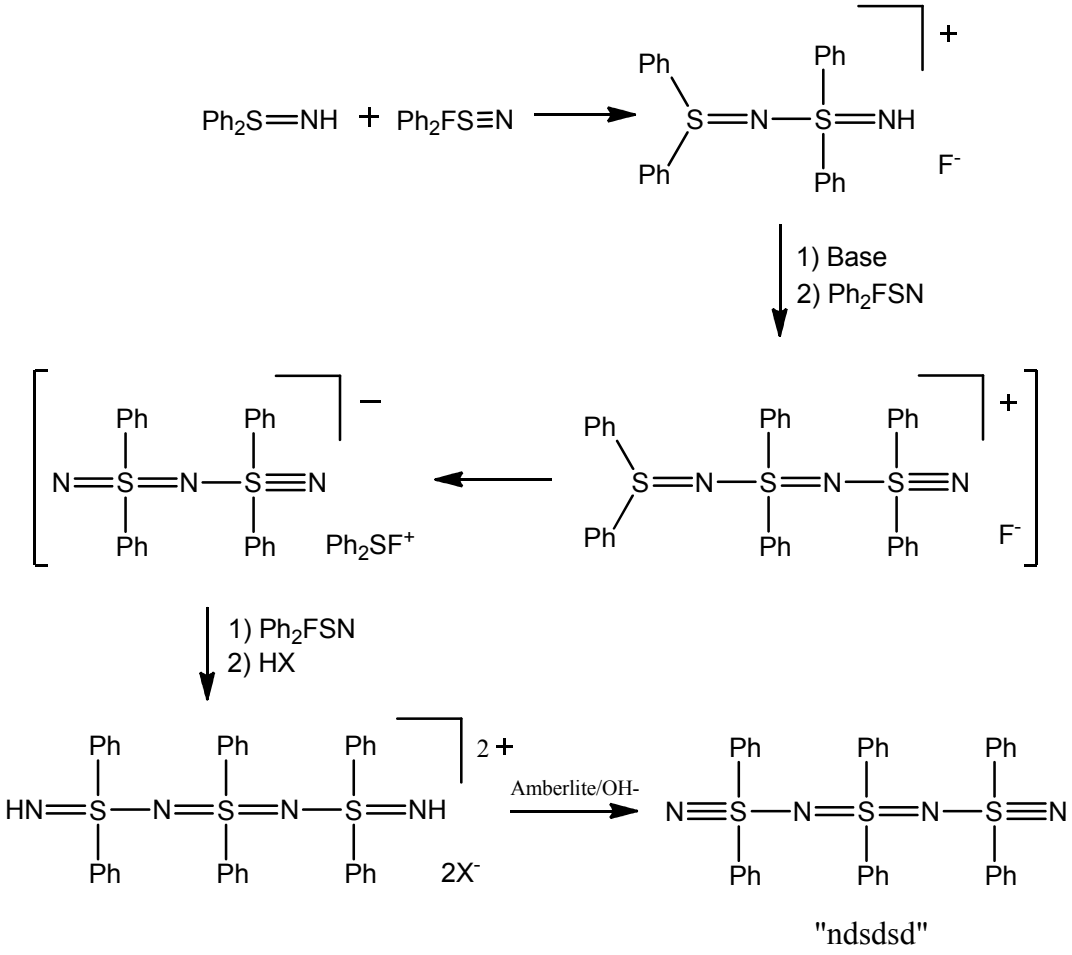

Equation 20

As with $Ph_3S{\equiv}N$, ndsdsd can also be alkylated; one equivalent of TfOMe gives $[(Ph_2(N{\equiv})S\text{-}N{=}(Ph_2)S{=}N\text{-}(Ph_2)S{=}N\text{-}Me)][TfO]$ and two equivalents gives $[(Ph_2S(=N\text{-}(Ph_2)S{=}NMe)_2][2TfO]$. Much like the alkylation of $Ph_3S{\equiv}N$ this is testament to the nucleophilicity of the triply-bonded nitrogen. The same can be said for the *N*-sulfenylation of ndsdsd which has also been reported.

1.4.3. λ^6-sulfanenitrile-metal complexes

λ^6-sulfanenitriles have been shown to behave as coordinating ligands though few examples have been characterised. $Ph_3S{\equiv}N$ has been shown to coordinate to copper in the bridged complex $[CuCl_2(\mu\text{-}NSPh_3)]_2$ from a reaction of one equivalent of $Ph_3S{\equiv}N$ with $CuCl_2$ in acetonitrile at room temperature.[67] The same reaction employing two equivalents of $Ph_3S{\equiv}N$ affords the complex $[CuCl_2(NSPh_3)_2]$ (Equation 21).

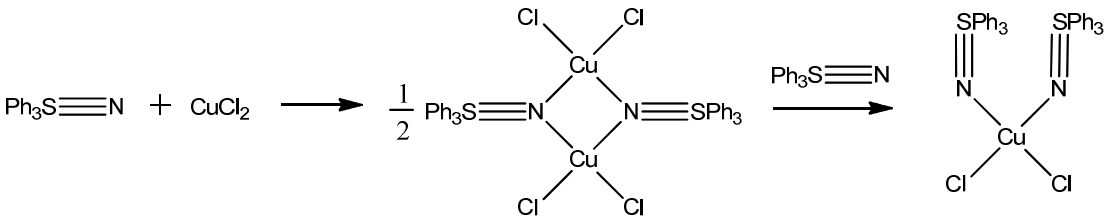

Equation 21

Interestingly the ndsdsd λ^6-sulfanenitrile has been observed to coordinate to some metal centres to form 8-membered sulfur-nitrogen chelate rings.[68] The complexes $[MCl_2(ndsdsd)]$ and the homoleptic $[M(ndsdsd)_2][2Cl]$ (M = Co(II), Ni(II) and Cu(II)) have all been fully characterised.

Successful coordination of the ligand is indicated by a lower frequency being observed for the S≡N stretching of the complexed ligand (*ca.* 1270 cm^{-1}) compared to that of the free ligand (1313 cm^{-1}) as was observed for the $Ph_3S{\equiv}N$ complexes. X-ray crystal structures of these complexes confirm the presence of the S≡N bond within the complex (1.47 Å) and exhibit both tetrahedral geometry about the metal in the cases of all $[MCl_2(ndsdsd)]$ complexes and $[Co(ndsdsd)_2]^{2+}$ and square planar geometry about the metal for $[Ni(ndsdsd)_2]^{2+}$ and $[Cu(ndsdsd)_2]^{2+}$. In all cases the rings adopt a twist-boat conformation.

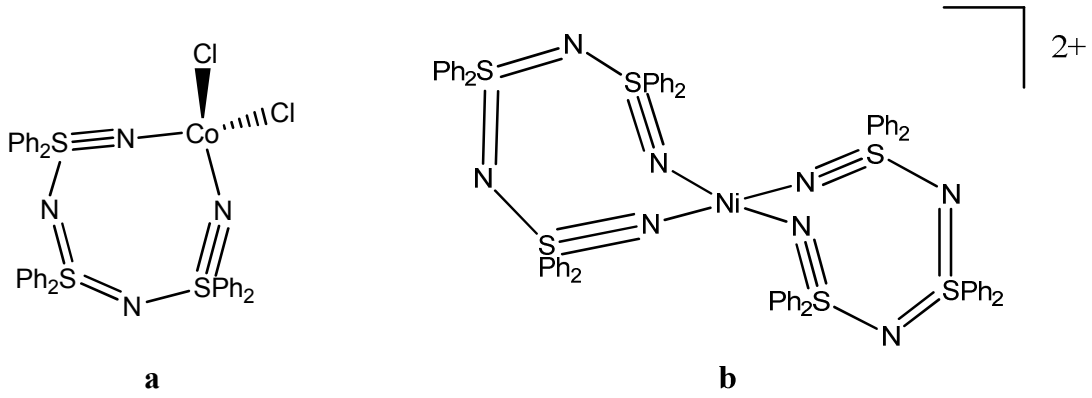

a **b**

Figure 15: Structures of $[CoCl_2(ndsdsd)]$ (**a**) and $[Ni(ndsdsd)_2]^{2+}$ (**b**)

1.5. Characterisation, Structural Elucidation and Spectroscopy

In most of the examples given above the starting materials used are of the formula $MX_2(PR_3)_2$. This aids the characterisation of the final product as in a standard reaction *e.g.* Equation 3, where there is one phosphorus environment in the starting material and two in the final product. This, in tandem with the close proximity of the

phosphorus atoms to each other, produces the characteristic AX splitting in the ^{31}P NMR spectrum.[19] In cases where platinum is present, satellites due to ^{195}Pt are seen either side of each of the doublets representing ^{31}P nuclei. The larger of the two platinum-phosphorus coupling constants is assigned to the phosphorus *trans*- to the nitrogen as this is generally the shorter platinum-phosphorus bond length. As one would expect, the same pattern is observed for complexes containing selenium[43, 45] and tellurium.[52] Other nuclei which could be observed, such as ^{15}N, would require atomic labelling.

IR spectroscopy is a little less useful, although for $[S_2N_2]^{2-}$ complexes there are some characteristic stretches observed for ν_{SN} (*ca*. 1050, 680 cm^{-1}), δ_{SN} (*ca*. 610, 360 cm^{-1}), ν_{PtN} (*ca*. 450 cm^{-1}) and ν_{PtS} (*ca*. 345 cm^{-1}).[19] In $[Se_2N_2]^{2-}$ complexes the absorptions associated with ν_{SeN} are also known (*ca*. 810, 600, 370 cm^{-1}).[43]

Single crystal X-ray crystallography is by far the most useful method for determining the structure of these complexes. Almost all of the structures in this introduction were confirmed *via* this method.

2. Bis(phosphino)Platinum(II) Dihalides

2.1. Introduction

Compounds of the formula $PtX_2(PR_3)_2$, where X can be Cl, Br, I and on rare occasions, F and PR_3 can be a phosphine, phosphinite, phosphonite or phosphite

ligand, have been known and studied for a great many years. They have been proven to be useful in the field of catalysis as well as starting materials in synthetic reactions. Platinum complexes containing phosphorus ligands are of particular interest as the ^{31}P NMR spectra contain ^{195}Pt satellite peaks, which allow the ^{31}P-^{195}Pt coupling constant to be measured giving insight into the nature of bonding around the platinum centre. Compounds of this type are also seen to exhibit the square planar geometry typical of platinum(II) compounds and therefore many can be synthesised as both *cis*- and *trans*-isomers. Palladium(II) analogues of many of these systems are also known and are chemically and structurally similar.

2.2. Synthesis of $PtX_2(PR_3)_2$ Complexes

There are a large variety of synthetic routes to bis(phosphino)platinum(II) dihalides employing some typically trivial chemistry. One example is the displacement of the 1,5-cyclooctadiene ligand in the complex $PtCl_2(COD)$ with two equivalents of PR_3 in dichloromethane to produce *cis*-$PtCl_2(PR_3)_2$ (Equation 22).[69]

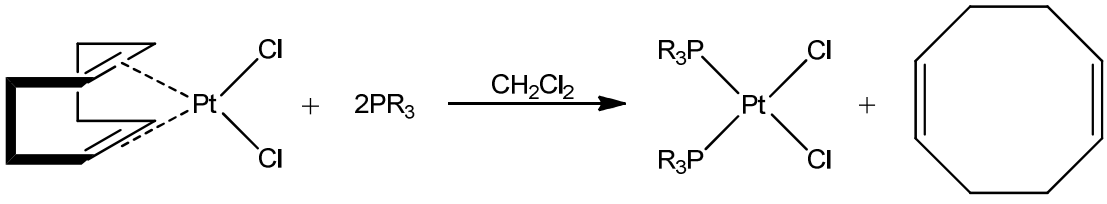

Equation 22

Most other syntheses for *cis*-$PtX_2(PR_3)_2$ complexes are equally simplistic. Another example would be the preparation of *cis*-$PtX_2(P(OMe)_3)_2$, which is achieved

via the addition of two equivalents of $P(OMe)_3$ to a suspension of *trans*-$PtX_2(PhCN)_2$ in acetone with the halides about the platinum rearranging to give the *cis*- product.[70] In some cases the phosphine can be seen to displace halides, such as the synthesis of *cis*-$PtCl_2(PPh_3)_2$, where a solution of PPh_3 in ethanol is added to a solution of potassium tetrachloroplatinate in water.[71] Isomerisation of these *cis*- products to *trans*- is typically achieved *via* light irradiation.[71-74]

Exchanging the halides in *cis*-$PtX_2(PR_3)_2$ can be achieved *via* metathesis. Smaller halides can only be exchanged with larger ones *i.e.* the reaction of *cis*-$PtCl_2(PPh_3)_2$ with excess LiBr under reflux in 95 % ethanol-chloroform forms *cis*-$PtBr_2(PPh_3)_2$[74] with the elimination of LiCl providing the driving force with its greater stability relative to the bromide. Similarly *cis*-$PtI_2(PPh_3)_2$ can be prepared from either *cis*-$PtCl_2(PPh_3)_2$ or *cis*-$PtBr_2(PPh_3)_2$ using excess NaI in an equivolume mixture of water, ethanol, acetone and chloroform.[74] Interestingly, though relatively unstable, difluoride analogues of certain *cis*-$PtX_2(PR_3)_2$ complexes have been synthesised *via* the reaction of $(PR_3)_2Pt(Ph)_2$ with XeF_2 in dichloromethane.[75]

2.3. ^{31}P NMR of $PtX_2(PR_3)_2$ Complexes

One of the most useful methods of characterising $PtX_2(PR_3)_2$ complexes is using ^{31}P NMR spectroscopy. The ^{31}P nucleus has a spin of ½ and an abundance of 100 % making it near perfect for NMR spectroscopy. In the case of $PtX_2(PR_3)_2$ there is only one phosphorus environment present so the splitting pattern is observed as a singlet. Satellite peaks are also observed due to the *ca.* 34 % abundance of the ^{195}Pt nucleus,

which also has a spin of ½. The presence of these satellite peaks allows the ^{31}P-^{195}Pt coupling constant ($^{1}J_{Pt\text{-}P}$) to be measured.

It is generally accepted that the magnitude of coupling constants is an indication of the s-character of the orbitals involved in the bond in question, and can be equated to bond strength. Hence, the stronger the bond, the larger the $^{1}J_{Pt\text{-}P}$ value.[76] This effect can be explained in electronic terms by considering the role of π-back-bonding in the Pt-P bond. Phosphorus ligands are known to be good σ-donors and, in the case of $PtX_2(PR_3)_2$ complexes, the Pt-P is a coordinate covalent bond using the lone pair on the phosphorus atom, however the stronger the bond, the more π-back-bonding is thought to be the dominating factor. In cases where a high coupling constant is observed there is a greater degree of π-back-bonding as the phosphorus ligand involved is a better π-acceptor.[77] The opposite is true in cases where a low coupling constant is observed. It is thought that the anti-bonding σ*-orbitals of phosphorus to carbon or oxygen are the π-acceptor orbitals on phosphorus.[78, 79]

The amount of π-back-bonding in a metal-phosphorus bond can be described in terms of the σ-basicity and π-acidity of the specific phosphorus ligand. Previous studies measuring the CO stretching frequencies of the complexes $Ni(PR_3)(CO)_3$ and $Cr(PR_3)(CO)_5$[80, 81] have shown that phosphorus ligands are strong σ-donors to the metal creating a high electron density at the metal centre. For phosphorus ligands of lower π-acidity the IR stretch was seen to be at lower frequency due to strong back-donation into π* orbitals of the CO. For more π-acidic phosphorus ligands the ν_{CO} frequencies are increased as they compete with CO for π-back-donation. These observations also apply to bonding within the Pt-P bond in $PtX_2(PR_3)_2$ complexes.

The *trans*-influence, defined as the ability of a ligand to weaken the bond *trans*- to it, is also a factor in the magnitude of $^{1}J_{Pt\text{-}P}$.[76, 82] Ligands with lower *trans*-influence, such as halides, are usually poor π-acceptors and therefore offer little competition with the phosphorus ligands for electron back-donation (Figure 16 (**a**)). Ligands with higher *trans*-influence, such as phosphorus ligands themselves, offer more in the way of competition for electron back-donation and hence give lower coupling constants (Figure 16 (**b**).[83]

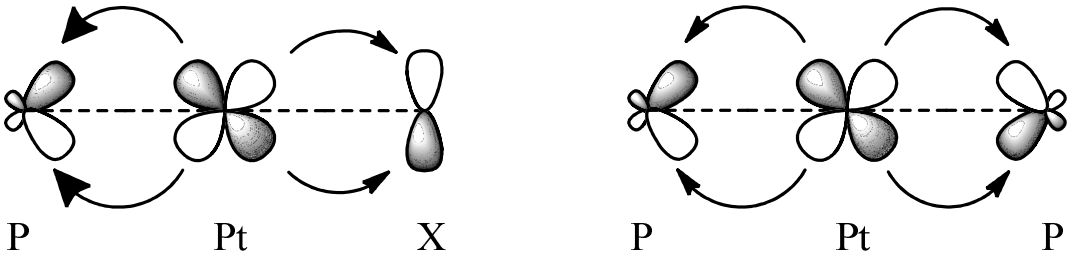

(**a**) Strong π-back bonding, low *trans*-influence of X

(**b**) Competition for π-back bonding, higher *trans*-influence of P

Figure 16: π-back bonding in M-P bonds in *cis*-$PtCl_2(PR_3)_2$ (**a**) and *trans*-$PtCl_2(PR_3)_2$ (**b**)

For complexes of the type $PtCl_2(PR_3)_2$, where PR_3 denotes a phosphine ligand, there is a great amount of ^{31}P NMR data available.[84-91] For these types of compounds $^{1}J_{Pt\text{-}P}$ ranges from *ca.* 3400-3700 Hz in *cis*- and *ca.* 2400-2650 Hz in the *trans*-complexes. Higher values are seen for the more electron-withdrawing R-groups. For example $^{1}J_{Pt\text{-}P}$ increases in the order $PMe_3 < PMe_2Ph < PMePh_2 < PPh_3$ as the methyl groups are replaced by the more electron withdrawing phenyl groups. Where the phosphorus ligand is a phosphite the $^{1}J_{Pt\text{-}P}$ value is *ca.* 2000 Hz larger than for phosphines due to their much greater π-acidity.[83, 92] Intermediate values are found for phosphonites and phosphinites as their mixture of both phosphine and phosphite

character would suggest.[93] *trans*- complexes exhibit a $^{1}J_{Pt\text{-}P}$ value *ca.* 1000 Hz lower than their *cis*- isomers due to the higher *trans*-influence of phosphorus ligands compared to halides.[85, 86, 88, 89] For the halides $^{1}J_{Pt\text{-}P}$ decreases in the order Cl > Br > I implying that the larger the halide the better a π-acceptor it is and the more it is able to compete for electron back-donation.

Although very similar to their platinum-centred counterparts, the ^{31}P NMR spectra of the palladium analogues cannot give us the same information. ^{105}Pd has a lower natural abundance and sensitivity than ^{195}Pt and a higher spin therefore for $PdX_2(PR_3)_2$ systems only a singlet is seen and satellite peaks are generally not observed.[94-96]

2.4. X-ray Crystallography of $PtX_2(PR_3)_2$ Complexes

As would be expected of such well-known and much used compounds a substantial number a $PtX_2(PR_3)_2$ structures have been reported all of which exhibit square planar geometry about platinum (Figure 17). These can prove useful when looking for a correlation between $^{1}J_{Pt\text{-}P}$ and the Pt-P bond length. Unfortunately surprisingly few compounds for which both ^{31}P NMR and crystallographic data is available have been reported.

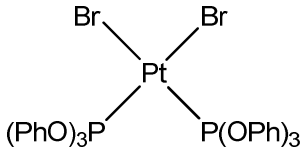

a

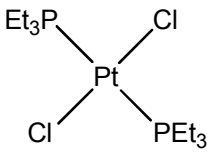

b

Figure 17: *cis*-$PtBr_2(P(OPh)_3)_2$ (**a**)[97] and *trans*-$PtCl_2(PEt_3)_2$ (**b**)[98]

Most of the structures reported with readily available ^{31}P NMR spectra are *cis*-$PtCl_2(PR_3)_2$ compounds with phosphine ligands,[87, 99-105] though some examples with phosphite ligands have also been reported.[83, 106] Even fewer structures of this type where X is Br or I have been reported[97, 107, 108] and no structures of phosphonite and phosphinite complexes are known. A number of *trans*-$PtX_2(PR_3)_2$ complexes where X is Cl or I and PR_3 is a phosphine are also known.[98, 109-112]

A number of $PdX_2(PR_3)_2$ have also been analysed by this method including an array of both isomers of $PdCl_2(PR_3)_2$ where PR_3 is a phosphine,[110, 113-118] phosphinite[119, 120] or phosphite.[121] X-ray crystal structures of $PdX_2(PR_3)_2$ systems where X is Br or I have also been reported.[122-124] These structures have generally been found to be isostructural, if not isomorphous, to platinum analogues.

The correlation between the $^1J_{Pt\text{-}P}$ coupling constant and the Pt-P bond length has been the subject of various studies, which have tended to acknowledge that there is indeed a crude correlation between the two measurements.[83, 125, 126] It is not unreasonable to assume a correlation between the two as the magnitude $^1J_{Pt\text{-}P}$ is an indication of bond strength and classically the stronger the bond the shorter it is. However, other factors will influence the bond length, such as angle and steric effects.

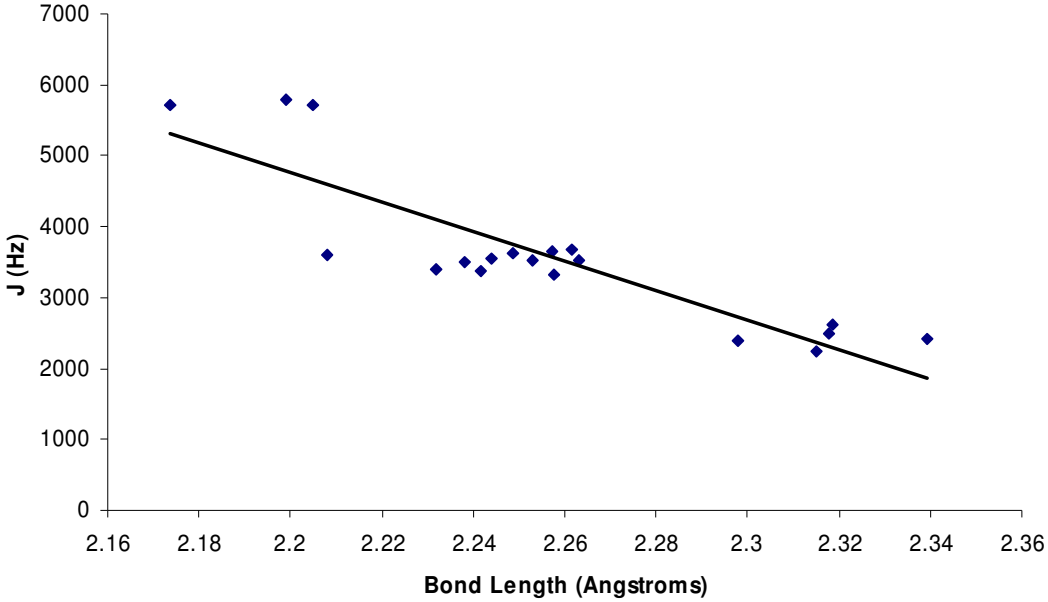

Figure 18: Correlation between $^{1}J_{Pt\text{-}P}$ (Hz) and bond length (Å) for known $PtX_2(PR_3)_2$ complexes

Comparing the ^{31}P NMR and crystallographic data for those examples where both are available, a crude correlation can indeed be seen (Figure 18). *trans*-Phosphine-containing complexes are seen to have the lowest $^{1}J_{Pt\text{-}P}$ coupling constants and the longest Pt-P bond lengths, whereas the *cis*- phosphite complexes have the highest $^{1}J_{Pt\text{-}P}$ values and the shortest bond lengths. The *cis*- phosphine complexes exhibit intermediate values and lie between the two aforementioned classes of compounds. A better picture could surely be achieved through the study of both *cis*- and *trans*- phosphinite and phosphonite and *trans*- phosphite complexes.

3. Inorganic 1-D Complexes

3.1. Introduction

A great many different types of 1-D solid-state systems are known and have been studied, such as covalent polymers. Inorganic examples are less common although one well known example is the SN polymer, polysulfur nitride, which has shown interesting electrical properties primarily, the ability to act as a semi-conductor. A number of square planar metal complexes also exhibit 1-D stacking arrangements conducive to electrical conduction.

3.2. 1-D Metal Complexes

Typically, metal complexes which exhibit 1-D qualities can be separated into four structural groups by considering their inter-molecular interactions and arrangement relative to the 1-D stacking axis (Figure 19).[127] Class I shows the repeating units stacked with a 90° angle between the molecular plane of the unit cell and the 1-D axis producing an optimum metal-metal distance. As a result, as conduction in 1-D complexes is dependant on metal-metal interactions, Class I is the most common configuration observed in known organometallic semi-conductors. Class II solids are similar to Class I compounds though the angle between the molecular plane of the unit cell and the 1-D axis is no longer 90°. This increases the

metal-metal distance and places more emphasis on ligand-metal interactions as a factor in defining their physical properties.

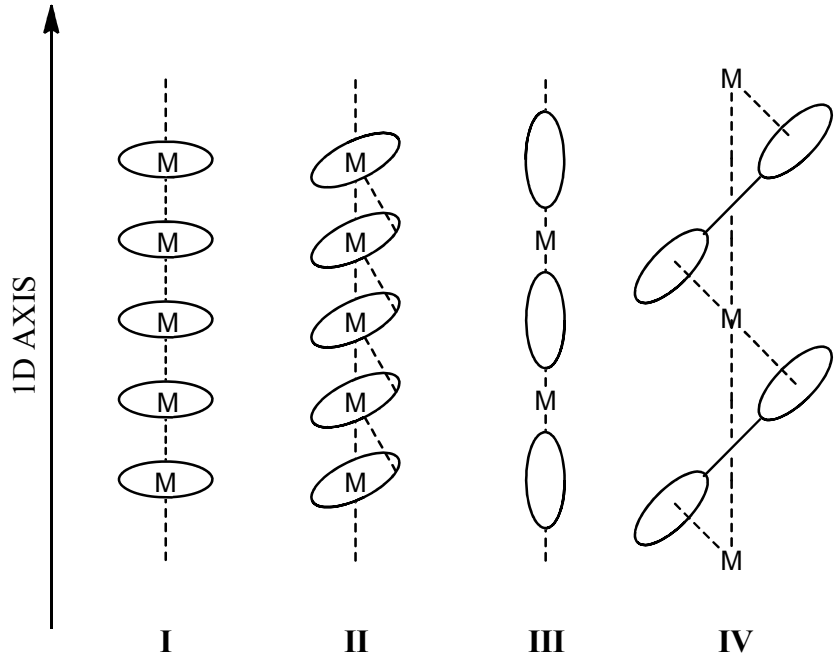

Figure 19: Schematic diagram of the four structural classes of 1D transition metal polymers

Class III compounds are stacked so as to eliminate metal-metal interaction altogether creating a system where metal-ligand interactions are dominant. Metallocene polymers of Class IV are more complex, yet metal-ligand interaction is still thought to be dominant.[128] In all cases the formation of 1-D complexes requires strong intermolecular interactions. The effect is more likely to be seen in planar complexes such as those exhibiting square-planar geometry and with planar or less sterically hindering ligands where the close proximity required for these compounds can be achieved. The occupation of molecular orbitals perpendicular to the plane of the molecule is also required for the formation of a 1-D system.

3.3. 1-D Electrical Conducting Systems

3.3.1. Introduction

Interest in 1-D electrical conducting systems seems to have been sparked by the discovery of superconductivity in the 1-D "organic metal" salt tetrathiafulvalene·tetracyanoquinodimethane ([TTF]·[TCNQ]).[129] The two planar molecules are seen to form stacking arrays of TTF cations and anionic TCNQ radicals with an intermolecular distance of 3.47 Å.[130] By comparison the intermolecular distance in neutral TTF is only 3.62 Å, which suggests that the contraction is a key factor in the delocalisation of electrons down each stack. [TTF]·[TCNQ], which becomes a superconductor at *ca.* 56 K, exhibits anisotropic contraction along the 1-D axis at low temperatures,[131] which could be a factor in its conducting ability. Another mechanism for this property could be that the lattice vibrations experienced at room temperature are reduced at lower temperatures, allowing for a more stable inter-molecular overlap.

3.3.2. Magnus' Green Salt

An example of an inorganic 1-D solid is Magnus' Green Salt (MGS). First synthesised in the early 1800s MGS is produced upon dissolving $PtCl_2$ in hydrochloric acid and adding ammonia to produce the green-coloured salt $[Pt(NH_3)_4][PtCl_4]$.[132] The structure consists of planar $[Pt(NH_3)_4]^{2+}$ and $[PtCl_4]^{2-}$ units forming stacking arrays of alternate ions with a 3.25 Å distance between platinum atoms (Figure 20).[127] This distance suggests that the structure relies more heavily on

ionic bonding than any Pt-Pt interactions, though these interactions still exist.[133] The semiconducting properties of MGS are well documented.[127] Just as [TTF]·[TCNQ] was seen to be a better conductor at low temperature, MGS's ability to conduct improves with increased pressure, which decreases the distance between platinum atoms to 2.95 Å.[134]

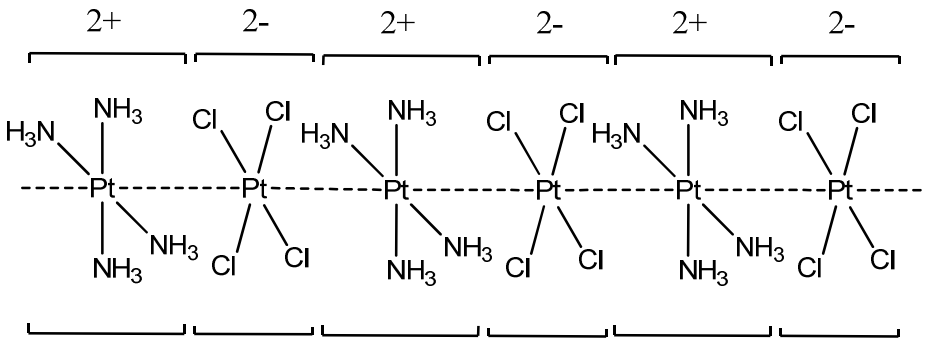

Figure 20: Schematic of Magnus' Green Salt

The applications of MGS as a semiconductor have long been hampered by its poor solubility which makes manipulation of the salt difficult. Derivatives of MGS of the type $[Pt(NH_2R)_4][PtCl_4]$ can be produced, where the R group increases solubility though this is often at the risk of increasing the distance between platinum atoms and thus decreasing conductivity.[135] One such $[Pt(NH_2R)_4][PtCl_4]$ salt where R = (S)-3,7-dimethyloctane[132] has however shown to be soluble in organic solvents with no loss of conduction.

3.3.3. Krogmann Salts

Another example of inorganic 1-D conductors are Krogmann Salts (KS). In this case the salts are formed by stacking units of d^8 transition metals such as Ir^+ and Pt^{2+} with planar ligands where a weak overlap between the d_z^2 orbitals on the metal can be

improved *via* oxidation with chlorine or bromine.[127, 136-138] One example is the tetracyanoplatinate salt $K_2[Pt(CN)_4]Br_{0.3}\cdot(H_2O)_n$,[139] where the platinum has an average oxidation state of 2.3. Due to the partial oxidation, the distance between the $[Pt(CN)_4]^{2-}$ units decreases from 3.35 Å to 2.89 Å (Figure 21) which increases the conductivity down the stacks. The compound $Rb_2[Pt(CN)_4][FHF]_{0.4}$ has been shown to exhibit almost metal-like conductivity due to the 2.798 Å distance between platinum atoms, supporting the fact that in these compounds the shorter the Pt-Pt distance the higher the conductivity.[140]

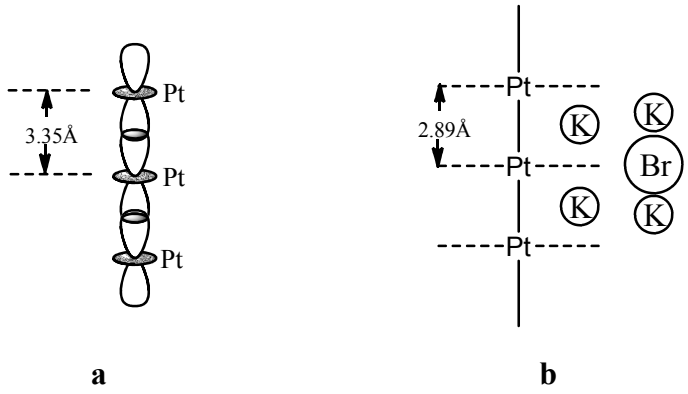

Figure 21: Diagram showing the overlap of d_z^2 orbitals of platinum within a Krogmann Salt (**a**) and the decreased interplanar separation observed upon oxidation with bromine (**b**)

3.4. Potential of Metal-Chalcogen-Nitrogen Complexes

The discovery of the unexpected electrical conductivity of polysulfur nitride $((SN)_x)$[141] prompted a resurgence in interest in sulfur-nitrogen compounds.[142] Sulfur-nitrogen complexes containing planar ligands such as $[S_2N_2]^{2-}$, $[S_2N_2H]^-$ and $[S_3N]^-$ are of particular interest with regards to 1-D systems due to their planar

nature.[1, 4, 17, 23, 143] In addition to the planarity of the S-N fragments in these complexes several have also been shown to form π-stacking arrays.[20, 26, 27, 144]

Stacking arrays in sulfur-nitrogen systems have been observed in ionic $[S_2N_2H]^-$ systems such as the complexes $[Pt(S_2N_2H)(PMe_3)_2]BF_4$ and $[Pt(S_2N_2H)(PMe_2Ph)_2]PF_6$.[20] The structures of these complexes were seen to produce stacking columns of both cations and anions. In these cases the $Pt(S_2N_2)$ rings were seen to stack nearly directly on top of each other with the reversal of each alternate $[Pt(S_2N_2H)(PR_3)_2]^+$ cation accommodating the non-planar phosphine groups. In both cases the platinum atom was seen to be positioned directly above and below the non-platinum-bound sulfur atom of its nearest neighbour. The interplanar distance for $[Pt(S_2N_2H)(PMe_3)_2]^+$ was observed to be 3.8 Å. $[Pt(S_2N_2H)(PMe_2Ph)_2]^+$ was seen to form dimer-like units with interplanar distances of 3.5 Å within the dimer and 4.6 Å between dimer units. This discrepancy between the complexes can be attributed to the greater steric bulk of the PMe_2Ph ligand compared to PMe_3.

Further studies into the phenomenon of stacking in $[S_2N_2H]^-$ compounds have shown that the interplanar distance can be manipulated by changing the anion. For compounds of the type $[Pt(S_2N_2H)(PMe_2Ph)_2]X$ the interplanar distance within the dimers decreases from 3.58 Å to 3.48 Å in the order $X = PF_6 > BF_4 > Cl$.[27] This can be explained as an electrostatic effect as the anions are always observed to be hydrogen-bonding through the N-H on the ring, hence the electrostatic repulsion between anions, which in turn depends on the size of the anion, will be a factor in the close approach of the cations. In addition to this a palladium analogue of one of these compounds was found to stack in the same manner.

The mechanism of orbital overlap which allows for the close approach of the cations in these systems has also been considered (Figure 22). It was also observed that the S(1)-N(2) bond distance increases as the anion size and intercation distance decreases. As this bond is known to possess substantial π-character and it is also known that there is an empty low-lying π^* orbital associated with the $[S_2N_2H]^-$ ligand it was suggested that electron density is transferred from the d_z^2 orbital on the platinum to an orbital which is antibonding with respect to S(1)-N(2). This would allow for the close approach of the platinum atom and S(1) on adjacent cations as well as accounting for the lengthening of the S(1)-N(2) bond.

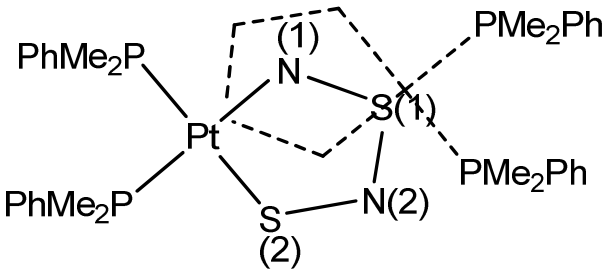

Figure 22: Stacking arrangement in $[Pt(S_2N_2H)(PMe_2Ph)_2]^+$ dimer unit

Stacking has also been observed in iridium-centred $[S_2N_2AuPPh_3]^+$ complexes such as $[(\eta^5\text{-}C_5Me_5)Ir(S_2N_2)Au(PPh_3)][ClO_4]$ in which the interplanar distance is reported to be 3.4 Å.[144]

The interplanar distances observed in these systems are still too large for any potential use as electrically conducting systems. This is further compounded in the systems which form dimer-like units where the distances between these units are even greater. The proposed mechanism for orbital overlap also suggests a Class III 1-D

solid of which few are known conductors. However these could be factors associated with the non-planar nature of phosphine ligands. Potentially, a smaller interplanar distance and better orbital overlap could be achieved with a completely planar molecule where close approach of the platinum atoms on each adjacent cation would be possible without being hindered by steric bulk.

CHAPTER 2: 5-membered Metal-Sulfur-Nitrogen Complexes

4. $Pt(S_2N_2)(P(OR)_nR'_{3-n})_2$ Complexes

4.1. Introduction

The discovery of the unexpected electrical properties of the $(SN)_x$ polymer in 1973 led to sustained interest in this area though M-S-N chemistry has been of interest since the 1950s.[141] The disulfur dinitride dianion ($[S_2N_2]^{2-}$) is not known in simple salts but can be isolated in metal complexes and as fragments in heterocycles.[17, 19, 20, 31, 143, 145] These complexes may be protonated at the metal-coordinated nitrogen and structural consequences of this protonation have been investigated.[26, 27] M-S-N complexes may be prepared by a variety of routes *e.g.* oxidative addition of S_4N_4 or $S_4N_4H_4$ with $Pt(PPh)_4$, reaction of $Na[S_3N_3]$ with $PtCl_2(PR_3)_2$ or transmetallation using $[Me_2SnS_2N_2]_2$ or $[^nBu_2SnS_2N_2]_2$. The use of $[S_4N_3]Cl$ in liquid ammonia as a solvent in these reaction has also been shown to be valuable yet it has not been established for the synthesis of $M(S_2N_2)$ systems.[144, 146]

Surprisingly there is some ambiguity about the bond length pattern within the $M(S_2N_2)$ ring in some $Pt(S_2N_2)(PR_3)_2$ complexes.[147] Increasing the number of characterised $M(S_2N_2)$ systems should help to give better insight into this ambiguity.

Analysis of known $Pt(S_2N_2)(PR_3)_2$ complexes *via* X-ray crystallography at low temperature, where before analysis at room temperature was reported, would presumably achieve the same end by yielding a more accurate result.

We were interested to see if further insight into the bond length pattern could also be achieved by altering the electronic properties of the phosphorus ligands *trans*- to the metallacycle. As most complexes of the formula $Pt(S_2N_2)(PR_3)_2$ contain phosphine ligands, we anticipated that investigating complexes containing phosphite, phosphonite and phosphinite ligands could yield interesting results. The electron withdrawing ability of these ligands increases in the order $PR_3 < P(OR')R_2 < P(OR')_2R < P(OR')_3$ and it is reasonable to hypothesise that this may have some effect on the bonding within the metallacycle. Thus far there is only one reported example of a $Pt(S_2N_2)(P(OR)_3)_2$ complex whose formulation was proposed using only IR spectroscopy and microanalysis data.[15] The formulation of this complex remains doubtful. In this section the results of investigations into the spectral and structural properties of complexes of the type $Pt(S_2N_2)(P(OR)_nR'_{3-n})_2$ are reported.

4.2. Synthesis of $Pt(S_2N_2)(P(OR)_nR'_{3-n})_2$ Complexes

The compound $[S_4N_3]Cl$ was prepared by standard methods.[2] The starting materials *cis*-$[PtCl_2(P(OR)_nR'_{3-n})_2]$ ($(P(OR)_nR'_{3-n})$ = PMe_2Ph, $P(OMe)_3$, $P(OMe)_2Ph$, $P(OMe)Ph_2$, $P(OPh)_3$, $P(O^nBu)_3$ or $P(OEt)_3$) were prepared from $PtCl_2(COD)$[69] and two equivalents of the phosphite, phosphonite, phosphinite or phosphine in dichloromethane. The choice of these starting materials was based on the need to

establish the liquid ammonia route to $Pt(S_2N_2)(PR_3)_2$ complexes and the relatively simple preparation of $PtCl_2(COD)$.[148] The compound $Pt(S_2N_2)(COD)$, formed *via* reaction of $PtBr_2(COD)$ and the metathetical reagent $[Me_2SnS_2N_2]_2$ is known, yet no examples of its use as a starting material for $Pt(S_2N_2)(PR_3)_2$ complexes have been reported.[149] Though potentially useful this route would negate the need to use liquid ammonia as a solvent and was hence not employed.

In a typical reaction liquid ammonia (30 mL) was condensed using a condenser filled with dry ice and acetone into a Schlenk tube in a dry ice/acetone bath. To this $[S_4N_3]Cl$ (0.78 mmol) was added rapidly to produce a dark red solution. After stirring for 30 mins $PtCl_2(P(OR)_nR'_{3-n})_2$ (0.5 mmol) was added. Over the course of one hour the solution lightened to a pale orange colour. After stirring the reaction mixture at -78 °C for 3 h the solution was allowed to warm to RT and the ammonia was evaporated under a stream of nitrogen. The resulting orange or brown residue was dried *in vacuo* then dissolved in dichloromethane (10 mL) and filtered through celite. The products $[Pt(S_2N_2)(P(OR)_nR'_{3-n})_2]$ (**1**, $(P(OR)_nR'_{3-n}) = PMe_2Ph$; **2**, $((P(OR)_nR'_{3-n}) = P(OPh)_3$; **3**, $(P(OR)_nR'_{3-n}) = P(O^nBu)_3$; **4**, $(P(OR)_nR'_{3-n}) = P(OEt)_3$; **5**, $(P(OR)_nR'_{3-n}) = P(OMe)_3$; **6**, $(P(OR)_nR'_{3-n}) = P(OMe)_2Ph$; **7,** $(P(OR)_nR'_{3-n}) = P(OMe)_2Ph$) were precipitated via slow addition of hexane. Isolated yields were 30-65 % (Table 1). Crystals suitable for X-ray crystallography were grown by slow diffusion of hexane into a solution of the complex in dichloromethane. In the case of **3** attempts to isolate the compound for further characterisation yielded only oils. Though **1** is a known complex and has been characterised, crystals were grown for low-temperature X-ray crystallography as its structure has only previously been determined at room temperature.[27]

Based on thin-layer chromatography and X-ray crystallography the reaction was shown to produce S_4N_4 as a by-product. S_4N_4 explodes upon mechanical or heat shock. Its explosiveness increases with the purity of the substance and therefore, as it was mostly observed as part of the residue after the reaction, it was unlikely to detonate. Residues of S_4N_4 were disposed of by decomposition with aqueous NaOH.

A correct ratio of reagent to starting material was calculated using the proposed equilibria for $[S_4N_3]^+$ in liquid ammonia in which 7 equivalents of $[S_4N_3]^+$ give rise to 9 equivalents of $[S_3N_3]^-$(Equation 7). Given that $[S_3N_3]^-$ is thought to be the reactive species in sulfur-nitrogen liquid ammonia solutions[31] and that both $[S_2N_2]^{2-}$ complexes and S_4N_4 are formed during the course of the reaction it can be theorised that 2 equivalents of $[S_3N_3]^-$ are needed to fulfil the reaction stoichiometry (Equation 23).

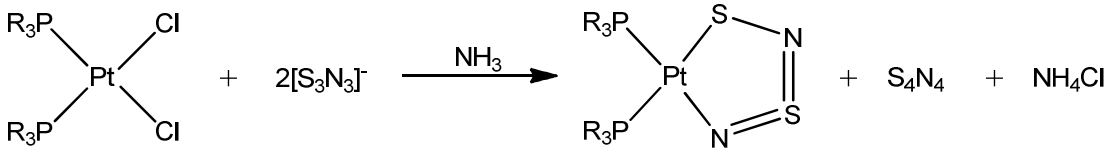

Equation 23

The overall stoichiometry for the reaction is therefore that 14 equivalents of $[S_4N_3]Cl$ are required to produce 9 equivalents of the product.

For complexes with lower oxygen content, a greater amount of starting material was observed in the $^{31}P\{^1H\}$ NMR spectrum of the crude reaction residue. This can be attributed to the increasing solubility of the starting materials in liquid ammonia in the

order $PR_3 < P(OR')R_2 < P(OR')_2R < P(OR')_3$ or the increasing lability of the chlorides in the same order. The same trend was observed in both products and starting material in the case of their solubility in dichloromethane suggesting that solubility is the dominating factor limiting the reaction rate.

Table 1: Microanalyses, yields and melting points for **2** and **4**-**7**

Compound	%C (calc.)	%H (calc.)	%N (calc.)	Yield (%)	MP (°C)
2 $Pt(S_2N_2)(P(OPh)_3)_2$*	45.90 (46.13)	3.12 (3.28)	3.27 (2.95)	32	138-142
4 $Pt(S_2N_2)(P(OEt)_3)_2$	23.25 (23.26)	4.78 (4.88)	3.73 (4.52)	47	117-120
5 $Pt(S_2N_2)(P(OMe)_3)_2$	14.23 (13.46)	3.08 (3.39)	4.68 (5.23)	58	123-125
6 $Pt(S_2N_2)(P(OMe)_2Ph)_2$*	29.74 (29.58)	3.38 (3.46)	4.72 (4.18)	62	139-142
7 $Pt(S_2N_2)(P(OMe)Ph_2)_2$	43.22 (43.39)	3.79 (3.64)	4.23 (3.89)	60	160-163

* + 0.5 CH_2Cl_2

4.3. NMR Spectroscopy

The ^{31}P NMR of the complexes **1**-**7** (Figure 24, Table 2) exhibit AX doublets with $^2J_{P\text{-}P}$ couplings together with satellite peaks due to $^1J_{Pt\text{-}P}$ couplings. These couplings enabled assignment of the individual phosphorus resonances. The largest ^1J (^{195}Pt -^{31}P) coupling constant is conventionally assigned to the phosphorus *trans*- to the nitrogen (δ_A) (Figure 23) as this platinum-phosphorus bond is generally shorter than the phosphorus *trans*- to the sulfur (δ_X) and the shorter distance can be associated with the larger coupling constant.[19] This assignment can be justified in terms of π-back-bonding in the platinum-phosphorus bond.

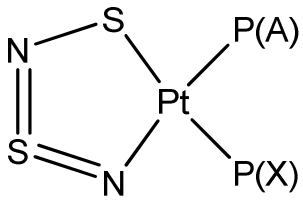

Figure 23: $Pt(S_2N_2)(P(OR)_nR'_{3-n})_2$ showing correct labelling of the phosphorus atoms.

As expected the coupling constants are influenced by the oxygen content of their phosphorus ligands (Table 2). In the starting materials, the greater the oxygen content, the larger the $^1J_{P\text{-}Pt}$ coupling constant is. We found for $[S_2N_2]^{2-}$ complexes that those containing phosphite ligands exhibit much larger coupling constants than the phosphine analogues with increases of up to 50 %. For example, $Pt(S_2N_2)(PPh_3)_2$ gives $^1J_{Pt\text{-}P}$ = 2994 and 2827 Hz and its phosphite equivalent **2** gives $^1J_{Pt\text{-}P}$ = 4634 and 4503 Hz.

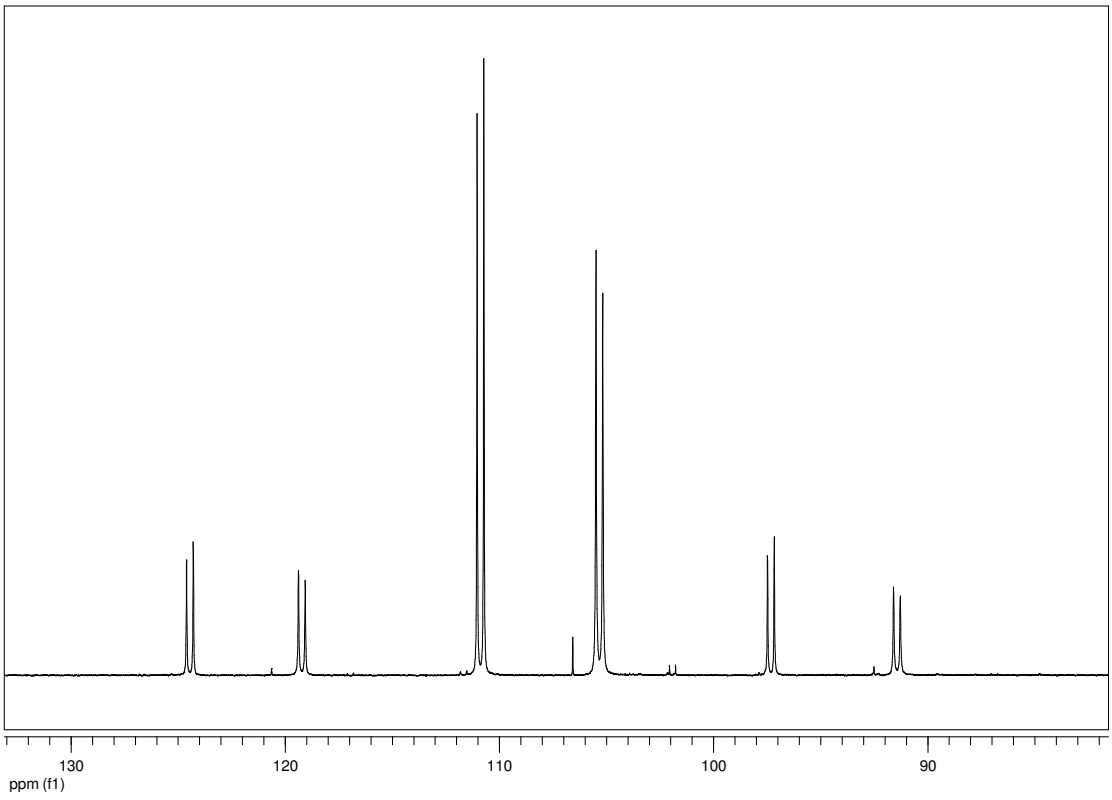

Figure 24: $^{31}P\text{-}\{^1H\}$ NMR spectrum (109 MHz, CH_2Cl_2 solution) of **5**

The effect of replacing phenyl groups of the phosphines with methyl groups has been previously reported,[19] with a decreasing magnitude of the $^1J_{Pt\text{-}P}$ values as more methyl groups are introduced. The effect of replacing phenyl groups in the phosphine with methoxy groups has the opposite effect as the coupling constants increase (Figure 25). As was observed in the trend regarding methyl groups, the variation of ^1J_X appears to be closer to linear than that of ^1J_A.

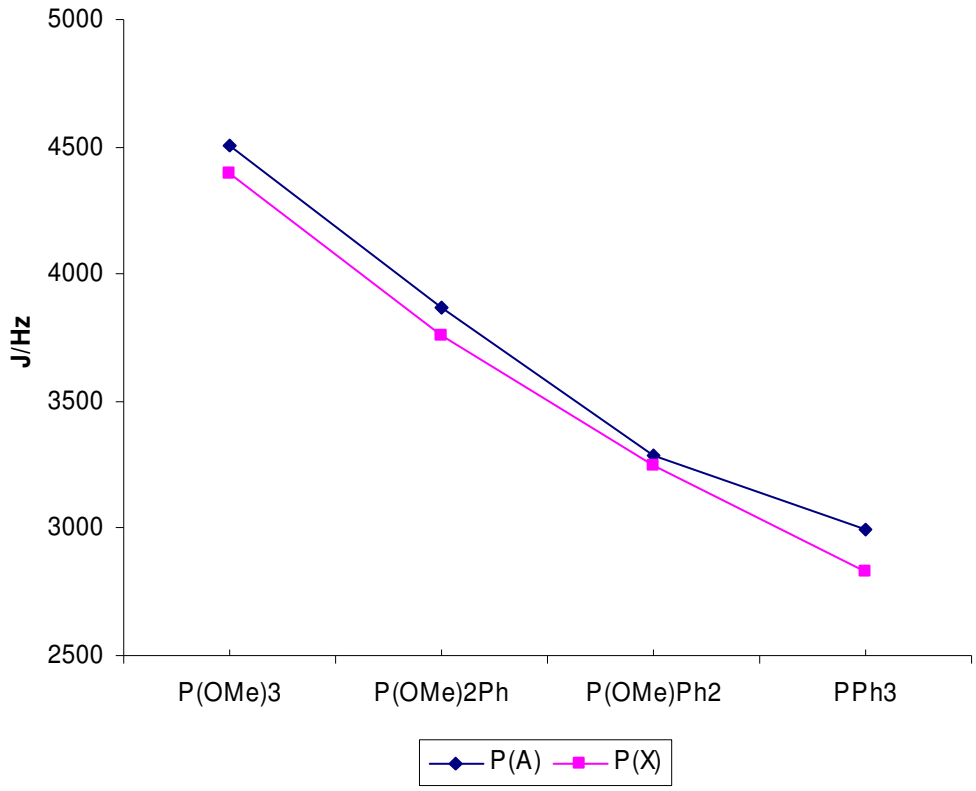

Figure 25: Variation of ^1J_A and ^1J_X in $Pt(S_2N_2)(P(OMe)_nPh_{3-n})_2$ complexes

Comparing the coupling constants of the compounds to those of their dichloride starting materials gives some indication as to the *trans*-influence of the $[S_2N_2]^{2-}$ fragment and the role of π-back-bonding in the platinum-phosphorus bond. The *trans*-influence of a ligand is defined as its ability to weaken the bond *trans* to it.[82] It is

generally accepted that the magnitude of coupling constants is an indication of the s-orbital character of the bond, which can be equated with bond strength. In the starting materials the chlorine atoms exhibit a low *trans*-influence as they are highly electron-withdrawing thus allowing the platinum to accept the lone pair from the phosphorus more readily and produce a stronger Pt-P bond which gives rise to a high coupling constant. This is assisted also by the low π-acidity of chlorides due to their lack of low-lying π-orbitals, which results in less competition for π-back-bonding from the platinum to the phosphorus, further strengthening the Pt-P bond.[77] If this theory is applied to the $[S_2N_2]^{2-}$ complexes, we can see that the *trans*-influence of the $[S_2N_2]^{2-}$ fragment is greater than that of the chlorine atoms as the coupling constants are seen to decrease by over 20 % for both P_A and P_X, indicating weaker Pt-P bonds in both cases. As both the sulfur and the nitrogen atoms are less electron-withdrawing than the chlorine this effect was predictable.

The coupling constant for P_A is higher than that of P_X as the sulfur atom *trans*- to P_X is more π-acidic, *i.e.* more able to accept low-lying d-electrons from the platinum than the nitrogen *trans*- to P_A. This increased competition for π-back-bonding weakens the P_X-Pt bond to a greater extent than the nitrogen atom weakens P_A-Pt.

The effect of the oxygen content on the coupling constant which is observed arises as the greater the phosphite character exhibited by the ligand the more electron-withdrawing it is. As oxygen atoms are very electronegative they pull electrons away from the phosphorus atom thus increasing its π-acidity and subsequently, via the synergistic effect, its ability to donate its lone pair to the platinum.

The $^2J_{P\text{-}P}$ coupling constants are also affected by the increased oxygen content of the phosphorus-containing ligands with the variation on a scale similar to that of the $^1J_{Pt\text{-}P}$ coupling constants. We concluded this could not be explained as an angle effect but as another consequence of the electrical properties of the ligands as the interaction of the two phosphorus atoms through space is negligible.

Table 2: ^{31}P NMR chemical shifts and coupling constants for **1**-**7** and $Pt(S_2N_2)(PPh_3)_2$

Compound	δ_A	δ_X	^1J_A	^1J_X	$^2J_{P\text{-}P}$
1 $Pt(S_2N_2)(PMe_2Ph)_2$	-24.0	-7.4	2812	2737	26
2 $Pt(S_2N_2)(P(OPh)_3)_2$	89.6	96.7	4634	4503	54
3 $Pt(S_2N_2)(P(O^nBu)_3)_2$	102.8	109.0	4470	4334	49
4 $Pt(S_2N_2)(P(OEt)_3)_2$	98.5	105.5	4498	4415	49
5 $Pt(S_2N_2)(P(OMe)_3)_2$	105.3	110.9	4502	4395	51
6 $Pt(S_2N_2)(P(OMe)_2Ph)_2$	120.4	126.2	3864	3761	37
7 $Pt(S_2N_2)(P(OMe)Ph_2)_2$	91.8	104.1	3287	3249	28
$Pt(S_2N_2)(PPh_3)_2$[19]	11.4	23.6	2994	2827	22

The co-ordination shifts of the $[Pt(S_2N_2)(PR_3)]$ (R = alkyl, aryl) relative to their $[PtCl_2(PR_3)_2]$ starting materials are *ca.* –8 ppm for δ_A and *ca.* +7 ppm for δ_X.[19] For the phosphite-containing complexes the chemical shifts also exhibit a relatively constant co-ordination shift compared to their starting materials: δ_A is shifted by *ca.* +31 ppm and δ_X by *ca.* +37 ppm for all the phosphite systems. The magnitude of the co-ordination shift increases with oxygen content as evidenced by the shifts for **6** (+23.2 ppm for δ_A and +29 ppm for δ_X) and **7** (+6.6 ppm for δ_A and +18.9 for δ_X).

4.4. IR Spectroscopy

In their IR spectra (Table 3) the important ν_{SN} vibrations were assigned by analogy with previously reported $[Pt(S_2N_2)(PR_3)_2]$ complexes.[19] However, the presence of the $\nu_{(P\text{-}O\text{-}alkyl)}$ vibration (1050-1030 cm^{-1}) obscures one of the ν_{SN} vibrations, which is normally observed around 1050 cm^{-1} for **4** and **5**, though the band at around 680 cm^{-1} is not obscured as it is in some cases by phosphine absorption in $[Pt(S_2N_2)(PR_3)_2]$. The intensity of the $\nu_{(P\text{-}O\text{-}alkyl)}$ vibration (1050-1030 cm^{-1}) increases with the oxygen content as would be expected. Distinct vibrations due to the P-Ph group (approx. 1440 cm^{-1}) were also observed for **6** and **7**.

Table 3: Selected IR absorptions (cm^{-1}) for **2** and **4**-**7**

Compound	ν_{SN}		ν_{SN}	ν_{PtN}	δ_{SN}	ν_{PtS}
2 $Pt(S_2N_2)(P(OPh)_3)_2$	1052s	687s	618m	491s	380w	357w
4 $Pt(S_2N_2)(P(OEt)_3)_2$	*	686s	618m	469m	370m	355m
5 $Pt(S_2N_2)(P(OMe)_3)_2$	*	682s	615m	467w	372m	354w
6 $Pt(S_2N_2)(P(OMe)_2Ph)_2$	1047s	684m	614m	467m	371m	355m
7 $Pt(S_2N_2)(P(OMe)Ph_2)_2$	1042s	680m	615w	462m	360w	349w

* Band obscured by P-O-Alkyl absorption

4.5. X-ray Crystal Structures

4.5.1. Low-temperature X-ray crystal structure of $Pt(S_2N_2)(PMe_2Ph)_2$

The complex **1** is a known compound and its X-ray crystal structure has been recorded previously.[27] The structure was solved at room temperature and contains and unusual pattern of bond lengths within the ring. In most cases the $[S_2N_2]^{2-}$ fragment consists of one short bond, a short to intermediate length bond and one long bond, increasing in the order N(1)-S(1) < S(1)-N(2) < N(2)-S(2). In the case of **1** however the order observed is N(1)-S(1) < N(2)-S(2) < S(1)-N(2). This could potentially be the result of disorder within the room temperature structure. It was thought that repeating the structure at low temperature might give a more accurate/reliable result.

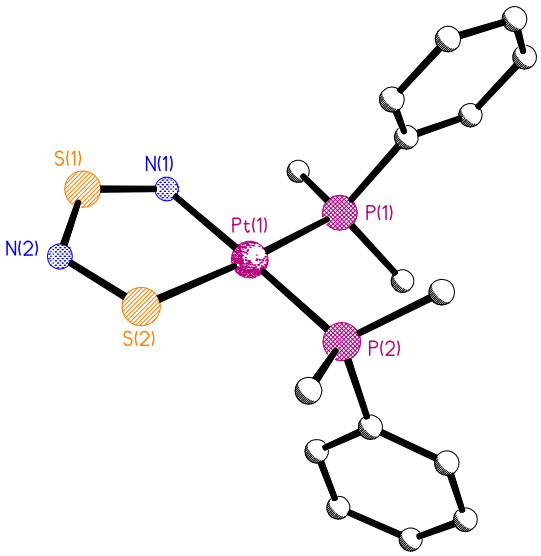

Figure 26: X-ray crystal structure of **1**

The X-ray crystal structure of **1** (Figure 26) was determined at 93 K and refined to a good standard. The difference between the LT and RT structures is not marked, however it can be noted that the bonds coordinated to the platinum centre appear shorter at lower temperature (Table 4). The unusual ordering of the S-N bond lengths within the ring observed in the room temperature structure is retained at low temperature with no significant changes in N(1)-S(1) and S(1)-N(2). A difference of *ca.* 0.05 Å is observed between the two structures in the case of S(2)-N(2) though this lengthening of the bond is not readily rationalised.

Table 4: Selected bond distances (Å) and angles (°) of **1**

	Low Temperature	Room Temperature[27]
Pt-N(1)	2.056(5)	2.081(8)
Pt-S(2)	2.2563(18)	2.270(5)
Pt-P(1)	2.2573(16)	2.271(4)
Pt-P(2)	2.2438(16)	2.265(3)
N(1)-S(1)	1.470(5)	1.466(10)
S(1)-N(2)	1.644(8)	1.660(13)
N(2)-S(2)	1.609(7)	1.560(14)
P(1)-Pt-P(2)	93.92(6)	94.4(1)
N(1)-Pt-S(2)	85.98(15)	85.0(3)
Pt-N(1)-S(1)	117.2(3)	117.3(6)
N(1)-S(1)-N(2)	115.0(3)	113.8(6)
S(1)-N(2)-S(2)	114.7(3)	116.0(9)
N(2)-S(2)-Pt	106.8(2)	107.4(5)

4.5.2. X-ray crystal structures of $Pt(S_2N_2)(P(OR)_3)_2$ Complexes

Of the four phosphite-containing complexes, the X-ray structures of **2**, **4** and **5** were determined (Figure 27, Table 5). Of the structures obtained, all were refined to a good standard except **4**, for which the structure could only be poorly be determined due to a two-fold disorder within the metal sulfur-nitrogen ring (Figure 28).

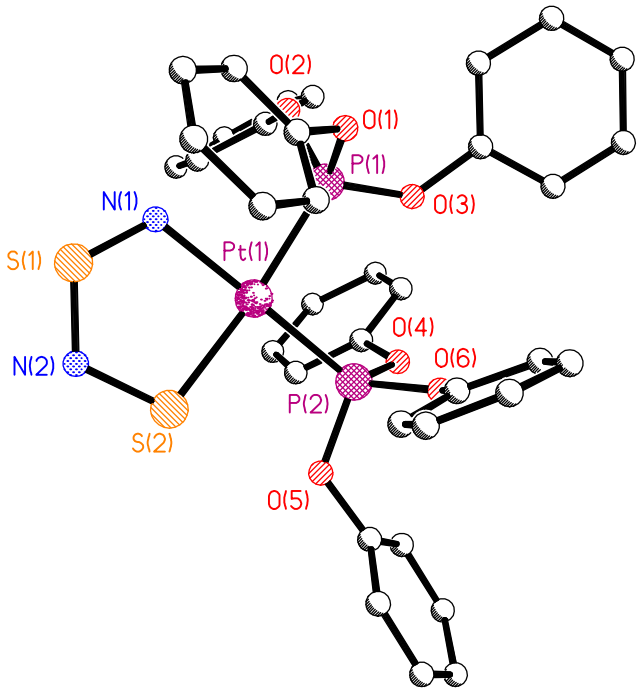

Figure 27: X-ray crystal structure of **2**.
The structure of **5** is not illustrated as it is similar

All of the structures exhibit square planar geometry about platinum. The Pt-P distances lie in the range 2.217(3) Å to 2.246(3) Å. One might anticipate a difference in Pt-P bond length *trans*- to sulfur verses *trans*- to nitrogen and there does appear to be a trend suggesting that Pt-P(2) (*trans*- to nitrogen) is usually shorter (*i.e.* for those where there is a structurally relevant difference, Pt-P(2) is shorter) than Pt-P(1) (*trans*- to sulfur), which is also observed in the phosphine equivalents of **2** and **5**, the two

different structures of $Pt(S_2N_2)(PPh_3)_2$[17, 145] and the structure of $Pt(S_2N_2)(PMe_3)_2$.[19] In general all of the Pt-P distances observed are longer than for the chloride complexes. In addition, the Pt-P bond lengths of **2** and **5** were shorter than in their phosphine equivalents, mirroring the increase in $^1J_{Pt\text{-}P}$ observed in the oxygen containing complexes relative to the phosphine containing complexes. The Pt-N bond lengths are in the range 2.050(17) Å to 2.064(8) Å and the Pt-S bond lengths are in the range 2.291(3) Å to 2.295(3) Å.

Table 5: Selected bond lengths (Å) and angles (°) for **2**, **4** and **5**

	2 $Pt(S_2N_2)(P(OPh)_3)_2$	**4** $Pt(S_2N_2)(P(OEt)_3)_2$	**5** $Pt(S_2N_2)(P(OMe)_3)_2$
Pt-N(1)	2.057(11)	2.050(17)	2.064(8)
Pt-S(2)	2.291(3)	2.293(9)	2.295(3)
Pt-P(1)	2.234(3)	2.237(2)	2.246(3)
Pt-P(2)	2.221(3)	2.239(2)	2.217(3)
N(1)-S(1)	1.541(11)	1.69(2)*	1.544(13)
S(1)-N(2)	1.589(13)	1.46(2)*	1.554(13)
N(2)-S(2)	1.689(12)	1.763(17)*	1.709(11)
P(1)-Pt-P(2)	96.18(11)	93.57(7)	93.89(15)
N(1)-Pt-S(2)	88.5(3)	90.5(5)	87.8(4)
Pt-N(1)-S(1)	114.6(6)	109.5(10)	115.0(7)
N(1)-S(1)-N(2)	116.9(6)	120.6(12)	117.2(6)
S(1)-N(2)-S(2)	116.3(6)	115.2(14)	116.6(7)
N(2)-S(2)-Pt	103.6(4)	103.3(9)	103.4(4)

* Two-fold disorder

As replacing phosphines with phosphites gave rise to a dramatic increase in coupling constants in ^{31}P NMR it was hypothesised that the increase in oxygen

content might also have an effect on the geometry of the metal sulfur-nitrogen ring complexes. Due to the high electronegativity of the oxygen atoms, the electron withdrawing effect on the ring increases which could potentially be observed in the bond orders within the ring. On the whole however this effect was not measurable crystallographically. The bond lengths and angles are comparable to equivalent complexes with phosphine ligands with two short sulfur-nitrogen bonds, which are slightly longer than a typical sulfur-nitrogen double bond (1.45 Å), ranging from 1.541(11) Å to 1.589(13) Å and one long sulfur-nitrogen bond, which corresponds to the length of a typical sulfur-nitrogen single bond (1.69 Å), ranging from 1.689(12) Å to 1.709(11) Å.

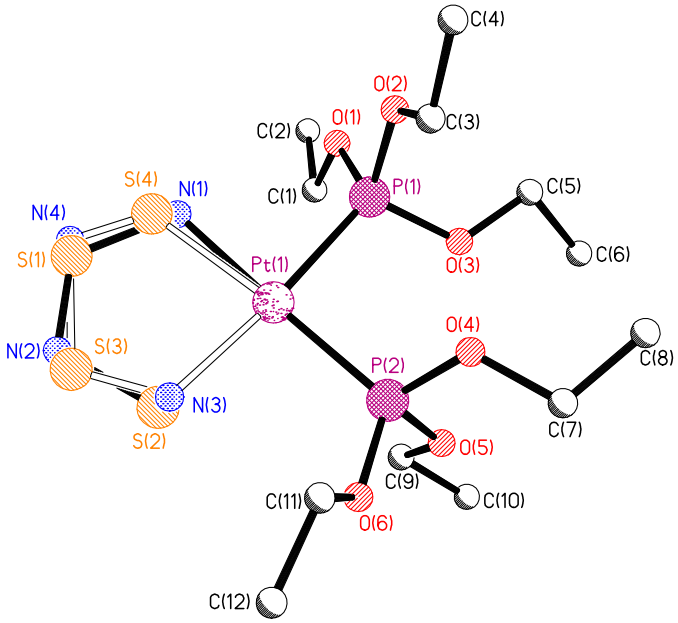

Figure 28: X-ray crystal structure of **4** showing two-fold disorder about the $[S_2N_2]^{2-}$ fragment

Bond angles within the ring were fairly consistent throughout and were comparable to previously reported examples. When compared to the starting materials the bond angle P(1)-Pt-P(2) was observed to be smaller with a range of 96.18(11) Å to

93.57(7) Å whereas the N(1)-Pt-S(2) angles were comparable to the Cl(1)-Pt-Cl(2) angles ranging from 87.8(4) Å to 90.5(5) Å.

4.5.3. X-ray crystal structures of $Pt(S_2N_2)(P(OMe)_nPh_{3-n})_2$

The complexes **5**-**7** and $Pt(S_2N_2)(PPh_3)_2$ form a series of $Pt(S_2N_2)(P(OMe)_nPh_{3-n})_2$ complexes beginning with $P(OMe)_nPh_{3-n} = P(OMe)_3$ and replacing the methoxy groups with phenyls until $P(OMe)_nPh_{3-n} = PPh_3$. Given the trend of decreasing $^1J_{Pt-P}$ coupling constant across this series (Figure 25) it was thought that this trend might manifest itself in the Pt-P bond lengths and the distances within the sulfur-nitrogen metallacycle.

The crystal structures of **6** and **7** (Figure 29, Table 6) were determined and refined to a good standard. All of the structures exhibit square planar geometry about platinum and were consistent with known phosphine complexes and **2**, **4** and **5**, with similar Pt-S(2) distances and bond angles within the ring and about platinum. In the case of **6** however, the Pt-N(1) bond was observed to be significantly shorter than most examples though similar to the tetrachloroform solvate structure of $Pt(S_2N_2)(PPh_3)_2$.[17] Bonding within $[S_2N_2]^{2-}$ fragment for **6** was consistent with the phosphite complexes however there is a small departure from this trend in the case of **7** for which there is one short, one long and one longer intermediate length bond indicating some degree of electron delocalisation. The cause of this is unclear.

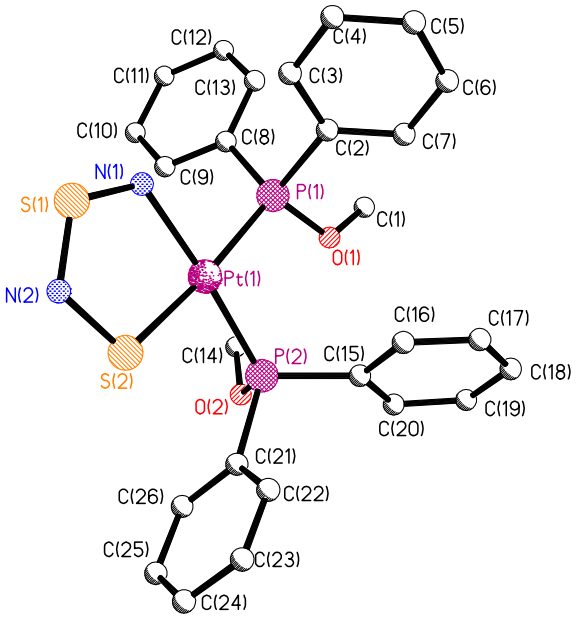

Figure 29: X-ray crystal structure of **7**.
The structure of **6** is not illustrated as it is similar

Comparing the structures of **6** and **7** to those of **5** and $Pt(S_2N_2)(PPh_3)_2$, for which two structures are reported (Table 6),[17, 145] no trends are observed in the bond lengths and angles of the metallacycle. It can be concluded from this that the increased electron-withdrawing effect is not significant enough to act on the ring itself.

Significant trends are observed in the Pt-P bond lengths and P(1)-Pt-P(2) bond angles. The Pt-P bond length is seen to increase in the order $P(OMe)_3 < P(OMe)_2Ph < P(OMe)Ph_2 < PPh_3$ (Figure 30). This increase is *ca.* 0.06 Å for Pt-P(1) and *ca.* 0.04 Å for Pt-P(2). The lengthening of these bonds correlates with the decreases in $^1J_{Pt\text{-}P}$ observed in the ^{31}P NMR spectra for these compounds and can likewise be explained in terms of decreasing π-acceptor ability of the phosphorus ligand weakening and hence lengthening the Pt-P bond.

The P(1)-Pt-P(2) bond angle is also observed to increase, from 93.89(15)° to 98.4(1)° in the order $P(OMe)_3 < P(OMe)_2Ph < P(OMe)Ph_2 < PPh_3$. Although this increase correlates with a decrease in $^2J_{P\text{-}P}$, it is most likely to be a product of the increasing steric bulk of the phosphorus ligand and not a result of any electrical effects.

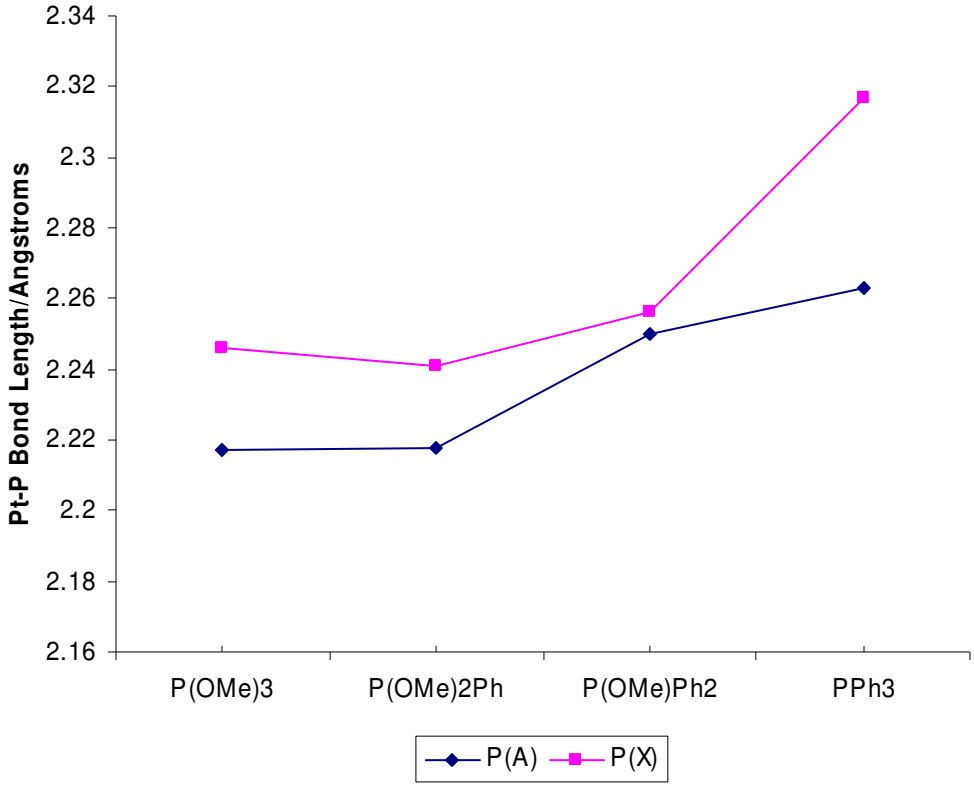

Figure 30: Variation of Pt-P(A) and Pt-P(X) distances in $Pt(S_2N_2)(P(OMe)_nPh_{3-n})_2$ complexes

Table 6: Selected bond lengths (Å) and angles (°) for **5**-**7** and $Pt(S_2N_2)(PPh_3)_2$

	5 $Pt(S_2N_2)(P(OMe)_3)_2$	**6** $Pt(S_2N_2)(P(OMe)_2Ph)_2$	**7** $Pt(S_2N_2)(P(OMe)Ph_2)_2$	$Pt(S_2N_2)(PPh_3)_2 \cdot 4CH_2Cl_2$[17]	$Pt(S_2N_2)(PPh_3)_2 \cdot C_7H_8$[145]
Pt-N(1)	2.064(8)	2.016(4)	2.070(7)	2.018(4)	2.093(13)
Pt-S(2)	2.295(3)	2.2923(15)	2.289(2)	2.288(5)	2.294(6)
Pt-P(1)	2.246(3)	2.2407(15)	2.256(2)	2.317(4)	2.308(5)
Pt-P(2)	2.217(3)	2.2175(15)	2.250(2)	2.263(4)	2.259(3)
N(1)-S(1)	1.544(13)	1.572(5)	1.515(8)	1.546(16)	1.499(16)
S(1)-N(2)	1.554(13)	1.568(5)	1.590(9)	1.567(19)	1.702(15)
N(2)-S(2)	1.709(11)	1.702(5)	1.673(9)	1.682(16)	1.548(12)
P(1)-Pt-P(2)	93.89(15)	95.12(6)	96.14(7)	98.4(1)	97.8(1)
N(1)-Pt-S(2)	87.8(4)	88.78(15)	87.0(2)	87.6(5)	86.8(4)
Pt-N(1)-S(1)	115.0(7)	115.1(3)	115.6(4)	116.2(9)	113.5(7)
N(1)-S(1)-N(2)	117.2(6)	116.7(3)	117.0(4)	116.0(9)	117.5(7)
S(1)-N(2)-S(2)	116.6(7)	115.8(3)	115.6(5)	116.1(11)	113.7(8)
N(2)-S(2)-Pt	103.4(4)	103.60(18)	104.9(3)	104.0(7)	108.4(7)

5. 1-D Disulfur-Dinitrido Complexes

5.1. Introduction

Given the interesting electrical properties of planar platinum-centred stacking arrays, such as Magnus' Green Salt[132] and the Krogmann Salts,[127] and the similar stacking ability of $[Pt(S_2N_2H)(PR_3)_2]^+$ systems,[20, 27] it seemed logical to attempt the preparation of planar $[S_2N_2H]^-$ complexes. Previously reported $[Pt(S_2N_2H)(PR_3)_2][X]$ complexes exhibited stacking arrangements in their X-ray crystal structures however although the $[S_2N_2H]^-$ fragment is planar, the bulky phosphine ligands were shown to hinder close approach of the molecules, thus inhibiting any potential electrical conduction.

The synthesis of completely planar molecules would potentially negate the steric interference observed in previous $[S_2N_2H]^-$ stacking arrays and allow for close approach and electrical conductor properties.

5.2. Synthesis of Planar $[S_2N_2]^{2-}$ or $[S_2N_2H]^-$-containing Complexes

The synthesis of planar $[S_2N_2]^{2-}$ or $[S_2N_2H]^-$ complexes requires that the starting material also be planar in nature. The starting material should preferably contain labile halides to be displaced by the $[S_2N_2]^{2-}$ or $[S_2N_2H]^-$ fragment. To this end the compound M(II)Cl_2(2,2′-bipyridine) (M = Pd or Pt) was selected as a target compound. The 2,2′-bipyridyl ligand (bipy) is planar and its platinum and palladium complexes are planar in nature, forming stacking arrays in their crystal structures where the molecules are nearly superimposed, with a M···M distance of 3.38 Å for M = Pd and 3.45 Å in the case of M = Pt.[150] This is comparable to the interplanar distances observed in Krogmann Salts prior to oxidation.[139]

Synthetic strategies based on liquid ammonia methodologies were not successful, most likely due to the insolubility of the starting materials in ammonia, so we used the metathetical reagent $[^nBu_2Sn(S_2N_2)]_2$. In a typical reaction two equivalents of MCl_2(bipy) was suspended in 250 mL of dry dichloromethane to which one equivalent of the metathetical reagent $[^nBu_2Sn(S_2N_2)]_2$ was added. After stirring for 30 mins a sharp colour-change was observed; pale yellow to red for M = Pd and yellow to purple in the case of M = Pt.

For M = Pd the product $[Pd(S_2N_2H)(bipy)][^nBu_2SnCl_3]$ (**8**) was crystallised by reducing the volume of the solution and precipitating the product *via* addition of hexane. Performing the reaction with the addition of $NaPF_6$ was predicted to yield the

compound $[Pd(S_2N_2H)(bipy)][PF_6]$, however crystals of $[Pd(S_2N_2H)(bipy)][Cl]$ (**9**) were formed instead. The compound $Pd(S_2N_2)(bipy)$ (**10**) was formed when the reaction mixture was evaporated to dryness and the residue washed with methanol. Addition of 1,8-diazabicyclo[5.4.0]undec-7-ene (DBU) to the yellow methanol washings afforded a red solution from which crystals were grown.

For M = Pt the reaction vessels needed to be wrapped in aluminium foil, so as to prevent exposure to sunlight, as the purple reaction mixture was found to turn yellow when exposed to sunlight. This is thought to be the result of radicals formed by the interaction of UV light with dichloromethane reacting with the product to reform the starting material, the presence of which was confirmed with IR spectroscopy. If the reaction mixture is evaporated to dryness and dissolved in methanol, a colour change is not observed, further strengthening the argument that dichloromethane is responsible for the photoactivity of the reaction mixture. Red crystals of $Pt(S_2N_2)(bipy)$ (**11**) were grown *via* slow diffusion of hexane into the reaction mixture. Where HBF_4 was added to the reaction mixture, a brown precipitate, thought to be $[Pt(S_2N_2H)(bipy)][BF_4]$ (**12**), was formed.

Isolation of the products was hampered by the low solubility of both the starting materials and the products. Although some crystals of the desired products were grown a high level of purity was not attained (Table 7). By-products such as the homoleptic $[M(bipy)_2][2X]$ and $^{n}Bu_2SnCl_2(bipy)$ were confirmed by X-ray crystallography and the presence of $^{n}Bu_2SnCl_2$ was observed in all ^{1}H NMR spectra of these products. Separation of these by-products proved extremely difficult.

Table 7: Microanalyses and yields for **8**-**12**

Compound	%C (calc.)	%H (calc.)	%N (calc.)	Yield (%)
8 $[Pd(S_2N_2H)(bipy)][^nBu_2SnCl_3]$	33.56 (31.10)	3.67 (3.92)	7.41 (8.06)	23
9 $[Pd(S_2N_2H)(bipy)][Cl]$*	31.05 (30.56)	2.93 (3.26)	12.51 (12.96)	41
10 $Pd(S_2N_2)(bipy)$§	32.60 (31.74)	2.58 (2.28)	14.09 (14.10)	34
11 $Pt(S_2N_2)(bipy)$	30.32 (27.09)	2.35 (1.82)	11.50 (12.64)	25
12 $[Pt(S_2N_2H)(bipy)][BF_4]$	24.10 (22.61)	1.43 (1.71)	10.06 (10.54)	14

* + MeOH, 0.5 H_2O

§ + 0.5 CH_2Cl_2

5.3. NMR Spectroscopy

Despite the poor solubility of the products and the presence of impurities the ^1H NMR spectrum of **9** was interpreted to a good degree (Figure 31, Table 8). The compound contains 9 different hydrogen environments, 8 of which could be expected to be observed in the aromatic region, compared to the 4 environments observed in the starting material.

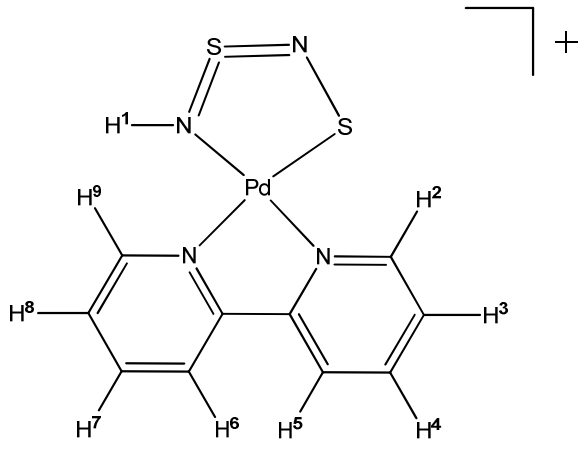

Figure 31: ^1H environments in $[Pd(S_2N_2H)(bipy)]^+$

As would be expected H^{1}, which is bound to the metal-bound nitrogen in the $[S_2N_2H]^-$ fragment, is observed as a very broad single peak between *ca.* 11.4-12.0 ppm. When assigning the aromatic protons it is reasonable to assume that, due to the greater electronegativity of the protonated nitrogen atom on the $[S_2N_2H]^-$ fragment than that of the metal-bound sulfur, the chemical shifts of the hydrogen atoms on the pyridyl group *trans*- to the nitrogen will be observed to be higher than the corresponding hydrogen on the pyridyl group *trans*- to the sulfur. Hence H^{2} is assigned as the doublet with the highest chemical shift (9.51-9.53 ppm), due to its proximity to the bipyridyl nitrogen *trans*- to the metal-bound nitrogen, whereas the corresponding proton on the bipyridyl group *trans*- to the metal-bound sulfur, H^{9}, is assigned to the next doublet, as it will be shifted due to its proximity to the bipyridyl nitrogen, though not as high as H^{1}. The remaining protons were assigned in this fashion.

Table 8: ^{1}H NMR data for **9** $[Pd(S_2N_2H)(bipy)][Cl]$

δ(ppm)	Multiplet	Assignment	Coupling Constant (Hz)
7.39-7.44	dd	1H, H^{7}	
7.65-7.69	dd	1H, H^{4}	
7.98-8.10	m	4H, H^{3}, H^{5}, H^{6}, H^{8}	
8.45-8.47	d	1H, H^{9}	$^{3}J_{H\text{-}H} = 5.5$
9.51-9.53	d	1H, H^{2}	$^{3}J_{H\text{-}H} = 5.2$
11.4-12.0	s	1H, H^{1}	

5.4. X-ray Crystal Structures

Crystals were grown of **8**-**11,** however, only the structure of **9** has been refined to a good standard. The data acquired for **10** and **11** produced severely disordered structures and were good enough only to confirm connectivity. The structure of **8** could be solved to some extent, however the butyl groups on the $^{n}Bu_2SnCl_3$ anion exhibited disorder due to poor crystal and data quality and could not be fully resolved.

.

The structure of **9** (Figure 32, Table 9) contains two crystallographically independent molecules (the second independent molecule is denoted by $\mathbf{9}^1$). Both molecules exhibit square planar geometry about palladium and are almost perfectly planar. Bond distances within the $Pd(S_2N_2H)$ ring differ from those of the previously reported example $[PPh_4][Pd(S_2N_2H)Cl_2]$.[10] In the literature example N(1)-S(1) is 1.577(10) Å, S(1)-N(2) is 1.753(20) Å and N(2)-S(2) is 1.516(16) Å. In the case of **9** the N(1)-S(1) bond is slightly longer (1.612(13) Å), yet is comparable to the N(1)-S(1) bond in $[PPh_4][Pd(S_2N_2H)Cl_2]$. The S(1)-N(2) and N(2)-S(2) bonds however, are observed to be dramatically shorter (1.505(15) Å) and longer (1.680(14) Å) respectively. The S(1)-N(2) bond distance is also seen to differ between the two molecules in the unit cell as S(4)-N(5), the equivalent to S(1)-N(2) in $\mathbf{9}^1$ is observed to be 1.580(15) Å. These discrepancies are not readily explained.

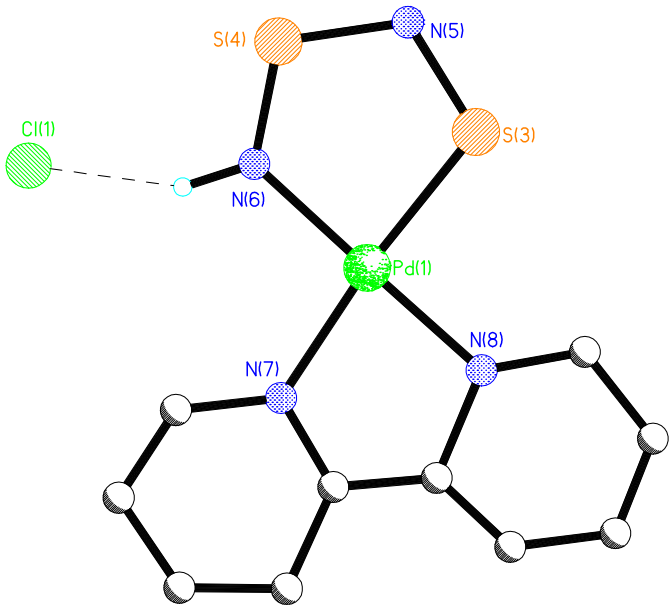

Figure 32: X-ray crystal structure of **9**[1] showing hydrogen bonding to Cl^-
The structure of **9** is not illustrated as it is similar

The protonated, metal-bonded nitrogen atoms were observed to be within 3.2 Å of the chloride anions, suggesting hydrogen bonding between the anion and the proton. The molecules within the unit cell were observed to lie parallel to each other along a one dimensional axis, though they were not superimposed and the palladium atoms were not directly above each other, which would not allow for any d-orbital overlap (Figure 33).

The interplanar distance was 3.45 Å, which is comparable to the starting material however, as the palladium atoms were not perfectly aligned the Pd···Pd distance was observed to be 4.4920(18) Å.

Table 9: Selected bond lengths (Å) and angles (°) for **9** and **9**[1]

	9 [Pd(S_2N_2H)(bipy)][Cl]		**9**[1] [Pd(S_2N_2H)(bipy)][Cl]
Pd(1)-N(1)	2.011(12)	Pd(2)-N(6)	1.998(13)
Pd(1)-S(2)	2.242(4)	Pd(2)-S(3)	2.249(4)
Pd(1)-N(3)	2.021(13)	Pd(2)-N(7)	2.039(12)
Pd(1)-N(4)	2.059(12)	Pd(2)-N(8)	2.115(14)
N(1)-S(1)	1.612(13)	N(6)-S(4)	1.609(14)
S(1)-N(2)	1.505(15)	S(4)-N(5)	1.580(15)
N(2)-S(2)	1.680(14)	N(5)-S(3)	1.686(15)
N(3)-Pd(1)-N(4)	80.4(5)	N(7)-Pd(2)-N(8)	78.3(5)
N(1)-Pd(1)-S(2)	85.2(3)	N(6)-Pd(2)-S(3)	85.8(3)
Pd(1)-N(1)-S(1)	120.1(7)	Pd(2)-N(6)-S(4)	120.5(7)
N(1)-S(1)-N(2)	109.1(7)	N(6)-S(4)-N(5)	110.0(7)
S(1)-N(2)-S(2)	120.4(8)	S(4)-N(5)-S(3)	117.0(8)
N(2)-S(2)-Pd(1)	104.9(4)	N(5)-S(3)-Pd(2)	106.6(5)

This system could be described as a Class II transition metal polymer, where the 1-D axis goes through each metal centre (Figure 19). This implies that there may be a certain amount of ligand-metal interaction between the molecules in the structure, possibly between the d_z^2 orbitals of the palladium atom and the π-orbitals of either the disulfur dinitride or bipyridyl ligand. Although oxidation with bromine in the style of a Krogmann salt may have reduced the interplanar distance it is unlikely to have improved the 1-D electrical conducting properties due to the large Pd···Pd distance observed.

The structure of **8**, which also contained two independent molecules, exhibits a similar bond order within the ring to that observed in **9**. The $[Pd(S_2N_2H)(bipy)]^+$ cations were observed to stack with an interplanar distance of *ca.* 3.67 Å. The Pd···Pd distance was lower than observed for **9** (3.773(3) Å) as the palladium atoms were closer to stacking on top of each other contrary to the findings of a previous study which suggested that the larger the anion the larger the interplanar distance.[27] These distances can only be considered tentatively due to disorder problems within the structure.

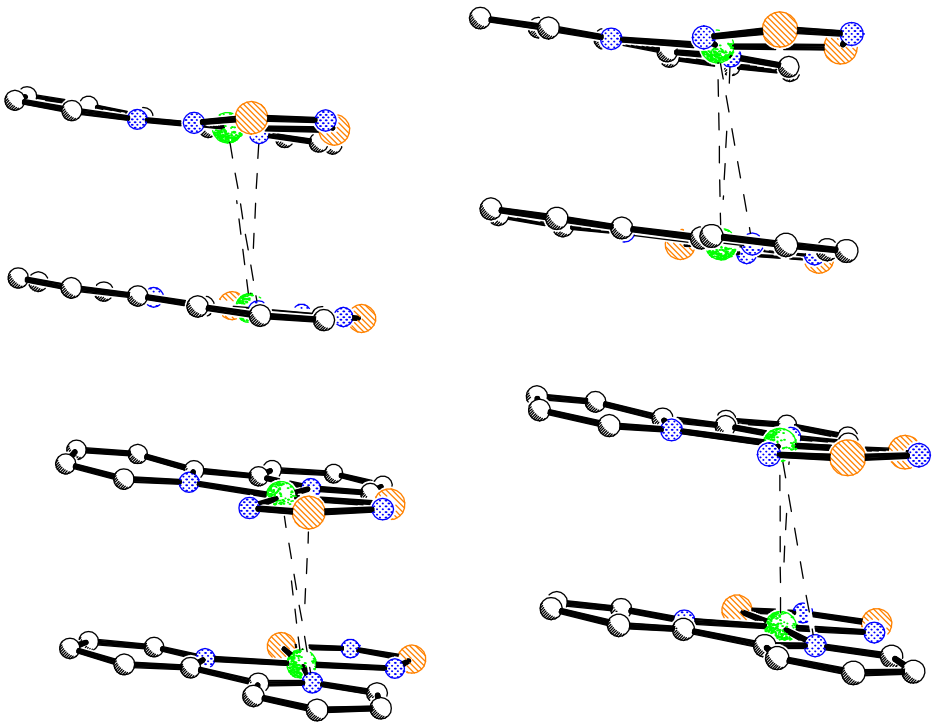

Figure 33: X-ray crystal structure of **9** showing stacking between $[Pd(S_2N_2H)(bipy)]^+$ units

6. Trisulfur-Mononitrido Complexes

6.1. Introduction

Though a great many examples of $[S_2N_2]^{2-}$ and $[S_2N_2H]^-$ containing complexes with coordinating phosphorus ligands have been reported only very few of the type $[M(S_3N)(PR_3)_2][X]$ are known.[151] Much like the $[S_2N_2]^{2-}$ complexes, these examples exclusively contain phosphine ligands, therefore investigations into phosphite, phosphonite and phosphinite complexes containing the S_3N^- ligand could potentially yield interesting results in terms of ^{31}P NMR and X-ray crystallography.

6.2. Synthesis of $[Pt(S_3N)(P(OR)_nR'_{3-n})_2][BF_4]$ Complexes

All previous $[M(S_3N)(PR_3)_2][X]$ complexes were synthesised using the reagent $Hg(S_7N)_2$ which is itself prepared from heptasulfurimide (S_7NH). The preparation of S_7NH and its purification for use as a reagent is very inefficient and, as the resulting compound decomposes to cyclo-octasulfur (S_8) over time, its purity cannot be guaranteed for very long. The use of carcinogenic hexamethylphosphoramide (HMPA) in its preparation is another drawback of S_7NH.

In a typical reaction $Hg(S_7N)_2$ was first prepared *via* reaction of mercuric acetate and S_7NH in acetone. One equivalent of the reagent was then stirred with one equivalent of both $PtCl_2(P(OR)_nR'_{3-n})_2$ ($P(OR)_nR'_{3-n}$ = $P(OMe)_3$, $P(OMe)_2Ph$ or $P(OMe)Ph_2$) and $AgBF_4$. The resulting yellow solution was confirmed to contain the products $[Pt(S_3N)(P(OR)_nR'_{3-n})_2][BF_4]$ (**13**, $P(OR)_nR'_{3-n}$ = $P(OMe)_3$; **14**, $P(OR)_nR'_{3-n}$ = $P(OMe)_2Ph$; **15**, $P(OR)_nR'_{3-n}$ = $P(OMe)Ph_2$) *via* ^{31}P NMR. All attempts to isolate the products for further analysis were unsuccessful.

6.3. NMR Spectroscopy

The $^{31}P\{^1H\}$ NMR spectra of compounds **13**-**15** (Table 10) exhibit AX splittings similar to those observed for the $[S_2N_2]^{2-}$ complexes. There is some confusion regarding the correct assignment of the $^1J_{Pt\text{-}P}$ coupling constants in the known $[Pt(S_3N)(PR_3)_2][PF_6]$ complexes as the Pt-P bond distances were unreliable as an indicator due to disorder in the reported structures. Considering the $[S_3N]^-$ ligand in terms of its *trans*-influence a rational assignment is possible. The lower $^1J_{Pt\text{-}P}$ value at δ_X is assigned to P(2) (Figure 34) by analogy with $[S_2N_2]^{2-}$ complexes **5**-**7**, as these values are closest and both phosphorus atoms are *trans*- to a negatively charged sulfur atom. The ^1J_X value observed in $[S_3N]^-$ complexes is *ca.* 200 Hz lower than that observed in $[S_2N_2]^{2-}$ complexes due to the increased π-acidity of S(1) in the $[S_3N]^-$ complexes possibly due to electron delocalisation along the S(1)-S(2) bond.

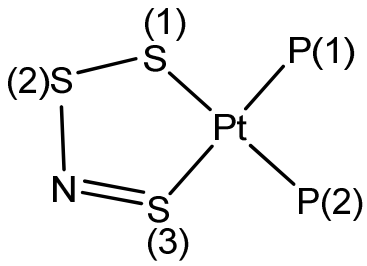

Figure 34: Fragment of $[Pt(S_3N)(P(OR)_nR'_{3-n})_2][X]$ with important atoms labelled

The much higher ^1J value at δ_A is assigned to P(1) *trans*- to the neutral coordinated S(3). As ^1J_A in this case is *ca.* 500 Hz higher than ^1J_X in $[S_2N_2]^{2-}$ complexes it is unlikely to be the result of a phosphorus atom *trans*- to a charged sulfur atom. The higher value is indicative of the lower π-acidity of S(3) which suggests that the orbitals which would be involved in π-back-bonding may be involved in the S(3)=N bond.

Table 10: ^{31}P NMR chemical shifts and coupling constants for **13**-**15** and $[Pt(S_3N)(PPh)_3)_2][PF_6]$

Compound	δ_A	δ_X	^1J_A	^1J_X	$^2J_{P\text{-}P}$
13 $[Pt(S_3N)(P(OMe)_3)_2][BF_4]$	80.8	92.2	4953	4176	38
14 $[Pt(S_3N)(P(OMe)_2Ph)_2][BF_4]$	104.4	114.4	4073	3446	31
15 $[Pt(S_3N)(P(OMe)Ph_2)_2][BF_4]$	89.7	93.7	3579	3045	24
$[Pt(S_3N)(PPh)_3)_2][PF_6]$[151]	7.1	11.4	3120	2566	22

As was observed in the $[S_2N_2]^{2-}$ complexes the decreasing oxygen content of the phosphorus ligands was accompanied by a decrease in coupling constants (Figure 35). This was again indicative of the decreasing π-acidity of the phosphorus ligands in the order $P(OMe)_3 > P(OMe)_2Ph > P(OMe)Ph_2 > PPh_3$. It can be speculated that this trend indicates an increasing Pt-P bond length however as no crystal data was obtained this cannot be known for certain.

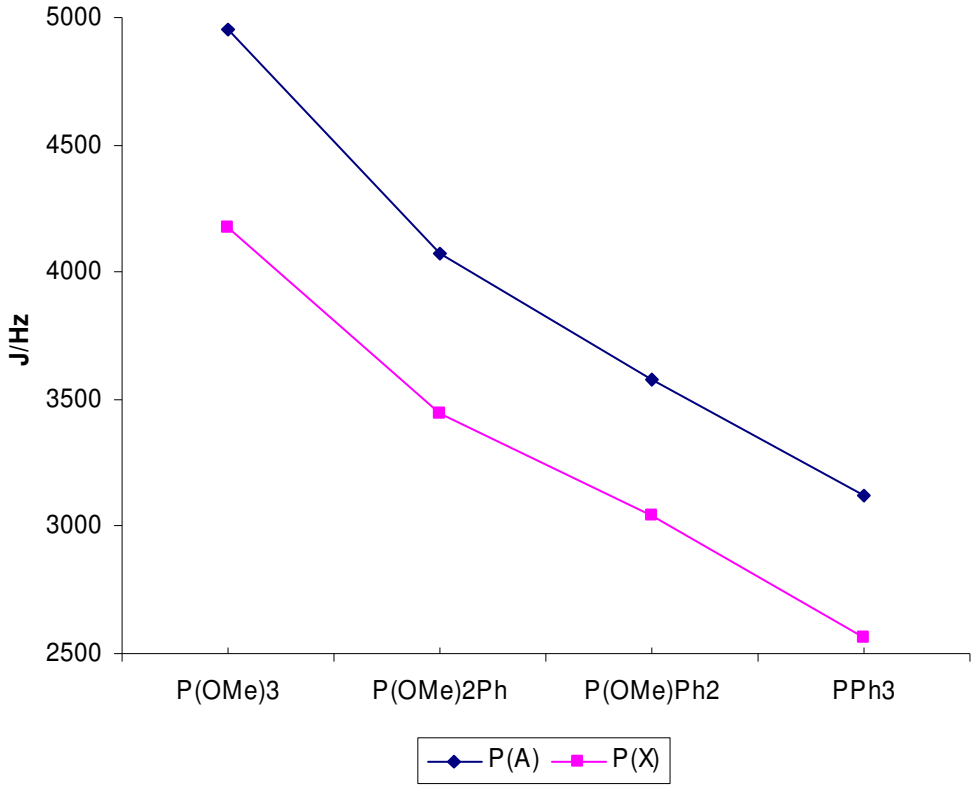

Figure 35: Variation of $^{1}J_{A}$ and $^{1}J_{X}$ in $[Pt(S_3N)(P(OMe)_nPh_{3-n})_2][X]$ complexes

CHAPTER 3: 5-membered Selenium-containing Metal-Chalcogen-Nitrogen Complexes

7. Monoselenium-Monosulfur-Dinitrido Complexes

7.1. Introduction

In addition to complexes of the type $Pt(S_2N_2)(PR_3)_2$, a number of selenium-substituted analogues have been investigated.[45-48] Some of the chemistry involved is analogous although given the limited number of stable selenium-containing heterocycles and their general insolubility fewer examples exist relative to the sulfur analogues. Mixed-chalcogen ligands of the type $[SeSN_2]^{2-}$ can be synthesised using liquid ammonia as a solvent and nitrogen-donor.[42, 43] In the same way that $[S_4N_3]Cl$ and $[S_3N_2Cl]Cl$ can be used to produce complexes containing $[S_2N_2]^{2-}$ ligands,[28] $[Se_2SN_2]_2Cl_2$ or a combination of $SeCl_4$ and $[S_4N_3]Cl$ will react with $PtCl_2(PR_3)_2$ to produce $[SeSN_2]^{2-}$ complexes of the type $Pt(SeSN_2)(PR_3)_2$. Successful structural analysis has yet to be performed on these compounds. As yet only one $[SeSN_2]^{2-}$ containing complex, $Pt(SeSN_2)(PMe_2Ph)_2$, has been analysed using X-ray crystallography and this example was found to exhibit a two-fold disorder about the ring. In this chapter the syntheses of three novel $Pt(SeSN_2)(P(OR)_nR'_{3-n})_2$ complexes, which have been characterised by ^{31}P NMR spectroscopy, IR spectroscopy, elemental

analysis and X-ray crystallography are reported, as well as the X-ray crystal structure and ^{31}P NMR spectrum of the previously reported compound $Pt(SeSN_2)(PPh)_3)_2$.

7.2. Synthesis of $Pt(SeSN_2)(P(OR)_nR'_{3-n})_2$ Complexes

The starting materials *cis*-$[PtCl_2(P(OR)_nR'_{3-n})_2]$ ($(P(OR)_nR'_{3-n})$ = $P(OMe)_3$, $P(OMe)_2Ph$ or $P(OMe)Ph_2$) were prepared from $[PtCl_2$(cyclo-octa-1,5-diene)$]$[69] and two equivalents of the phosphite, phosphonite or phosphinite in dichloromethane. *cis*-$PtCl_2(PPh_3)_2$ was prepared *via* reaction of $K_2[PtCl_4]$ with PPh_3 in a solution of water and ethanol.[71] The suitability of these starting materials for reactions in liquid ammonia was established in Chapter 2. The use of $[Se_2SN_2]_2Cl_2$ as a reagent was dismissed in order to bypass the time-consuming preparation of $[Se_2SN_2]_2Cl_2$.[152] Instead the combination of $[S_4N_3]Cl$ and $SeCl_4$ in the ratio of 1:5, as employed by previous studies,[43] was used to generate the appropriate anion(s) *in situ*.

In a typical reaction liquid ammonia (30 mL) was condensed using a condenser filled with dry ice and acetone into a Schlenk tube in a dry ice/acetone bath. To this $[S_4N_3]Cl$ (0.78 mmol) and $SeCl_4$ (3.9 mmol) were added to produce a dark red solution. Over the course of 30 min the solution became pale orange in colour. *cis*-$[PtCl_2(P(OR)_nR'_{3-n})_2]$ (0.5 mmol) was then added and after stirring the reaction mixture at -78 °C for 3 h the solution was allowed to warm to RT and the ammonia was evaporated under a stream of nitrogen. The resulting dark brown residue was dried *in vacuo*, then dissolved in dichloromethane (10 mL) and filtered through celite. The product was purified by means of column chromatography using a silica column

and 90 % CH_2Cl_2-10 % MeOH as the eluent. The products $[Pt(SeSN_2)(P(OR)_nR'_{3-n})_2]$ (**16**, $(P(OR)_nR'_{3-n}) = P(OMe)_3$; **17**, $(P(OR)_nR'_{3-n}) = P(OMe)_2Ph$; **18,** $(P(OR)_nR'_{3-n}) = P(OMe)_2Ph$; **19**, $(P(OR)_nR'_{3-n}) = PPh_3$) were precipitated via slow addition of hexane. Isolated yields were 50-75 % (Table 11). Crystals suitable for X-ray crystallography were grown by slow diffusion of hexane into a solution of the complex in dichloromethane.

Table 11: Microanalyses, yields and melting points for **16**-**18**

Compound	%C (calc.)	%H (calc.)	%N (calc.)	Yield (%)	MP (°C)
16 $Pt(SeSN_2)(P(OMe)_3)_2$	12.76 (12.37)	2.70 (3.12)	4.94 (4.81)	76	132-134
17 $Pt(SeSN_2)(P(OMe)_2Ph)_2$*	27.38 (27.64)	2.82 (3.23)	4.71 (3.91)	51	184-187
18 $Pt(SeSN_2)(P(OMe)Ph_2)_2$*	39.42 (39.34)	2.96 (3.36)	4.14 (3.46)	63	146-149

* + 0.5 CH_2Cl_2

The reaction was observed to produce trace amounts of the compound tetraselenium tetranitride (Se_4N_4), which is highly explosive and more sensitive to mechanical or heat shock than S_4N_4. Due to its low solubility, Se_4N_4 could be removed by filtering through celite and decomposing the residue with aqueous NaOH, though great care needed to be taken to avoid detonation.

The combination of $[S_4N_3]Cl$ and $SeCl_4$ appears to produce the appropriate anion *in situ*, though the exact nature of the species in the liquid ammonia solution has not been determined. Previously, studies have shown by ^{14}N NMR[32, 153] that dissolution of $[S_4N_3]Cl$ in liquid ammonia results in formation of $[S_3N_3]^-$. The presence of $[S_3N_3]^-$ in the liquid ammonia solution was confirmed by trace amounts of $[Pt(S_2N_2)(P(OR)_nR'_{3-n})_2]$ detected in the ^{31}P NMR of the residue. It's involvement in

the formation of $[SeSN_2]^{2-}$ can only be speculated about though it is reasonable to suggest that a partially selenated analogue may also be formed. It is also possible that the $[S_3N_3]^-$ species is in equilibrium with a range of chain SN anions which can undergo chalcogen exchange to give mixed SeSN anions. The formation of the $PtSeSN_2$ rings with selenium always platinum bound may suggest that the SeSN anions have terminal selenium atoms. Certainly we would expect that SeNSN would be a more stable isomer than SNSeN. Furthermore SeNSN could be readily formed by chain lengthening of the well know $[NSN]^{2-}$ dianion.[154]

7.3. NMR Spectroscopy

The ^{31}P NMR of the complexes **16**-**19** (Table 12) exhibit AX doublets with $^2J_{P\text{-}P}$ couplings together with satellites due to $^1J_{Pt\text{-}P}$ and $^2J_{P\text{-}Se(trans)}$ couplings. $^2J_{P\text{-}Se(cis)}$ couplings were not observed. By analogy with phosphine complexes, the largest $^1J_{Pt\text{-}P}$ coupling constant is assigned to the phosphorus *trans*- to the nitrogen (δ_A) as this platinum-phosphorus bond is generally the shorter of the two and the shorter distance can be associated with the larger coupling constant. This assignment can be justified in terms of π-back-bonding in the platinum-phosphorus bond.

When compared with $[S_2N_2]^{2-}$ complexes (Table 2), the $^1J_{Pt\text{-}P}$ coupling constants for the phosphorus *trans*- to nitrogen (δ_A) are observed to be of a similar magnitude and the coupling constant for the phosphorus *trans*- to selenium (δ_x) is seen to be *ca.* 100-200 Hz greater than for the phosphorus *trans*- to sulfur. This assignment can be justified in terms of π-back-bonding in the platinum-phosphorus bond and the *trans*-

influence of the $[SeSN_2]^{2-}$. The *trans*-influence of selenium in the $[SeSN_2]^{2-}$ fragment can hence be said to be less than that of the sulfur in the $[S_2N_2]^{2-}$ fragment as it produces a higher $^1J_{Pt\text{-}P}$ value, which is indicative of a stronger Pt-P_X bond. This is a result of the lower π-acidity of the selenium atom compared to that of the sulfur atom.

By comparing the ^{31}P NMR spectra of **16**-**19** the effect of increased oxygen content of the phosphorus ligands can be observed. Across the series $P(OMe)_3$ to PPh_3 where methoxy groups are replaced by phenyl groups we observe a marked decrease in the magnitude of $^1J_{Pt\text{-}P}$ (Figure 36). This is due to the decreasing electron-withdrawing ability of the groups on the phosphorus ligand as was observed in the analogous $[S_2N_2]^{2-}$ (Figure 25) and $[S_3N]^-$ (Figure 35) complexes.

Table 12: ^{31}P NMR chemical shifts and coupling constants for **16**-**19**

Compound	δ_A	δ_X	^1J_A	^1J_X	$^2J_{P\text{-}P}$	$^2J_{P\text{-}Se(trans)}$
16 $Pt(SeSN_2)(P(OMe)_3)_2$	106.0	108.1	4530	4571	49	94
17 $Pt(SeSN_2)(P(OMe)_2Ph)_2$	122.9	124.8	3868	3900	33	75
18 $Pt(SeSN_2)(P(OMe)Ph_2)_2$	89.3	103.1	3309	3391	26	66
19 $Pt(SeSN_2)(PPh_3)_2$	7.2	22.6	2995	2956	21	54

Similarly the $^2J_{P\text{-}P}$ and $^2J_{P\text{-}Se(trans)}$ coupling constants are also affected by the increased oxygen content of the phosphorus-containing ligands. The $^2J_{P\text{-}P}$ values, which were observed to be similar to those observed in $[S_2N_2]^{2-}$ complexes, decrease from 49 Hz for **16** to 21 Hz for **19** presumably reflecting the relative Pt-P bond strengths in this series. Similarly the $^2J_{P\text{-}Se(trans)}$ decreases from 94 to 54 Hz. No *cis*-

selenium satellites were observed and given the small magnitudes of previously reported $^{2}J_{\text{P-Se}(cis)}$ values this is understandable[155].

The coordination shifts for **16**-**19** relative to their starting materials were of a similar magnitude to those observed for the $[S_2N_2]^{2-}$ complexes decreasing in the same order; $P(OMe)_3 > P(OMe)_2Ph > P(OMe)Ph_2 > PPh_3$. The coordination shift from $[SeSN_2]^{2-}$ to $[S_2N_2]^{2-}$ was in the order of 2-3 ppm and was hence considered negligible.

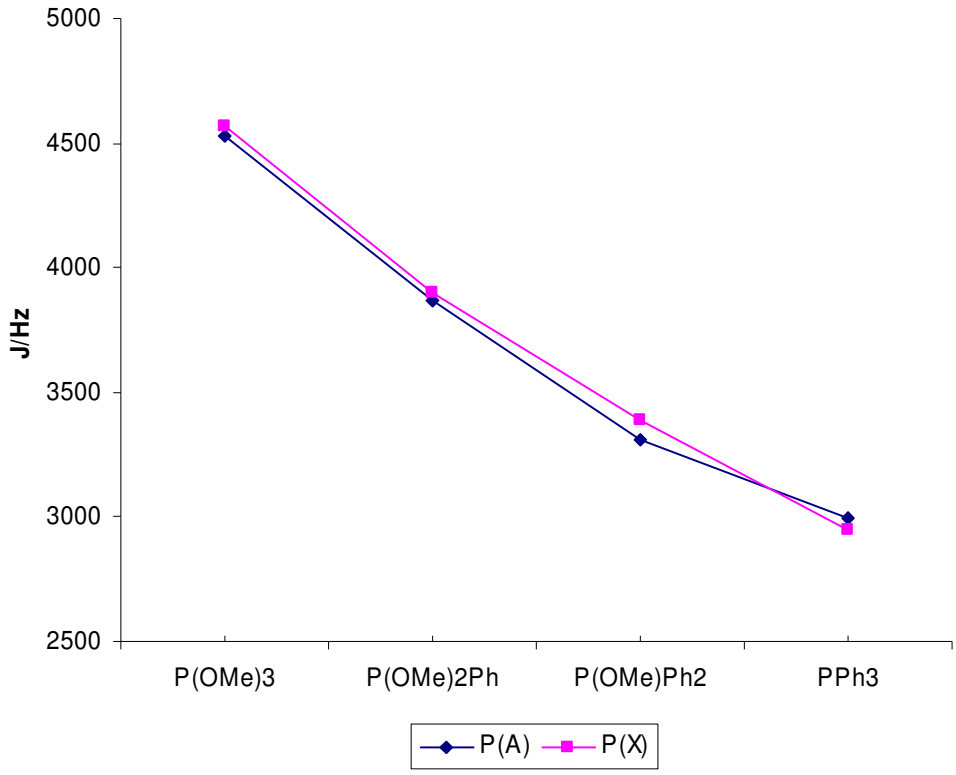

Figure 36: Variation of $^{1}J_{A}$ and $^{1}J_{X}$ in $Pt(SeSN_2)(P(OMe)_nPh_{3-n})_2$ complexes

7.4. IR Spectroscopy

In the IR spectra of **16**-**19** (Table 1) the characteristic vibrations of the $[SeSN_2]^{2-}$ fragment were assigned by analogy with previously reported $[Pt(SeSN_2)(PR_3)_2]$ complexes.[43] In the case of **18** the ν_{SN} vibration typically observed at *ca.* 1070 cm^{-1} was slightly lower than expected (1059 cm^{-1}). The corresponding stretch observed in $[S_2N_2]^{2-}$ complexes is observed at *ca.* 1045 cm^{-1}. Vibrations indicative of ν_{PtSe} were not observed and are likely to be very low in frequency compared to the ν_{PtS} stretch in $[S_2N_2]^{2-}$ complexes (*ca.* 350 cm^{-1}) due to the larger mass of selenium compared to sulfur. The intensity of the $\nu_{(P\text{-}O\text{-}alkyl)}$ vibration (1050-1030 cm^{-1}) increases with the oxygen content as would be expected. Distinct vibrations due to the P-Ph group (approx. 1440 cm^{-1}) were also observed for **17** and **18**.

Table 13: Selected IR absorptions (cm^{-1}) for **16**-**19**

Compound	ν_{SN}		ν_{SeN}	ν_{PtN}	δ_{SN}
16 $Pt(SeSN_2)(P(OMe)_3)_2$	1068s	633m	541m	401w	357w
17 $Pt(SeSN_2)(P(OMe)_2Ph)_2$	1071s	634m	556s	402m	357m
18 $Pt(SeSN_2)(P(OMe)Ph_2)_2$	1059s	634m	542s	402w	355w
19 $Pt(SeSN_2)(PPh)_3)_2$[43]	1067s	638m	541m	400w	360w

7.5. X-ray Crystal Structures

The structures of **16**-**19** were determined and refined to a good standard (Figure 37, Table 14). All of the structures exhibit square planar geometry about platinum.

Unlike the previously reported structure none of the structures exhibited disorder and only **18** was observed to be isomorphous to its $[S_2N_2]^{2-}$ analogue.

Of the bonds within the $Pt(SeSN_2)$ ring, the bonds involving N(1) are observed to be most sensitive to the nature of the phosphorus ligand. Pt-N(1) increases in the order $P(OMe)_3 < P(OMe)_2Ph < P(OMe)Ph_2 < PPh_3$ from 2.041(9) Å to 2.095(4) Å and N(1)-S(1) decreases in length from 1.532(9) Å to 1.480(7) Å in the order $PPh_3 > P(OMe)Ph_2 > P(OMe)_2Ph > P(OMe)_3$. The remaining three bonds appear less sensitive to the phosphorus ligand and do not exhibit any distinguishable trend (S(1) - N(2) ranges from 1.547(16) Å to 1.572(6) Å and N(2)-Se(1) ranges from 1.819(5) Å to 1.858(15) Å). The Pt-Se bond lengths are in the range 2.3818(9) Å to 2.4099(5) Å.

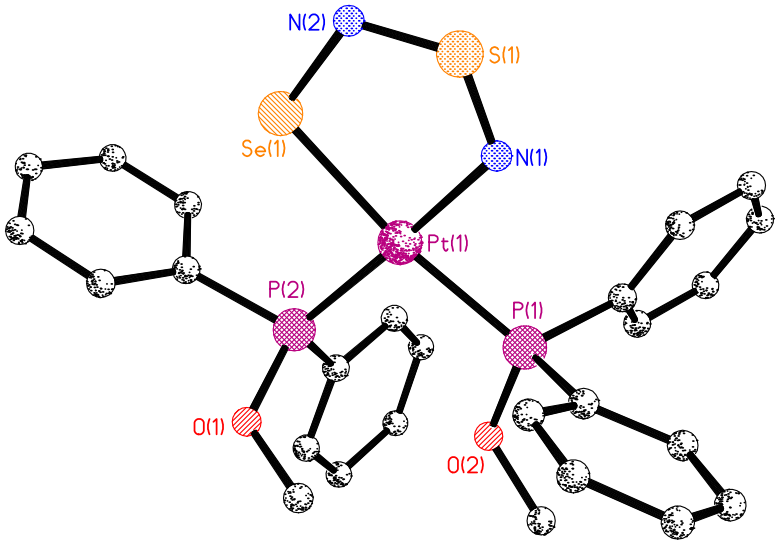

Figure 37: X-ray crystal structure of **18**.
The structures of **16**, **17** and **19** are not illustrated as they are similar

The Pt-P distances lie in the range 2.214(2) Å to 2.3069(17) Å increasing in the order $P(OMe)_3 < P(OMe)_2Ph < P(OMe)Ph_2 < PPh_3$ with Pt-P(1) increasing by *ca.*

0.05 Å and Pt-P(2) by *ca.* 0.06 Å (Figure 38). This can be correlated with the magnitude of $^{1}J_{Pt\text{-}P}$, which is itself a crude measure of bond strength, and reflects the trend observed in the $Pt(S_2N_2)(P(OMe)_nPh_{3-n})_2$ complexes (Figure 30).

When compared to the $[S_2N_2]^{2-}$ analogues the P(1)-Pt-P(2) bond angle is observed to be similar with a range of 94.83(9)° to 97.84(5)° with an increase in the order $P(OMe)_3 < P(OMe)_2Ph < P(OMe)Ph_2 < PPh_3$ being observed. Although this is accompanied by an increase in the magnitude of $^{2}J_{P\text{-}P}$ it is more likely to be the result of the increasing steric bulk of the phosphorus ligand. Similarly the N(1)-Pt-Se angles, which are comparable to the N(1)-Pt-S(2) angles of $Pt(S_2N_2)(P(OMe)_nPh_{3-n})_2$ complexes with a range of 86.31(18)° to 88.0(2)°, decrease as the P(1)-Pt-P(2) bond angle increases reflecting again the increased steric bulk of the phosphorus ligands. The P(2)-Pt-Se(1) bond angle also exhibits a trend increasing from 170.74(3)° to 174.37(3)° in the order $PPh_3 < P(OMe)Ph_2 < P(OMe)_2Ph < P(OMe)_3$ reflecting the decrease in $^{2}J_{P\text{-}Se(\textit{trans})}$, although this too can be attributed to steric effects. A similar trend in the N(1)-Pt-Se(1) angle is not observed.

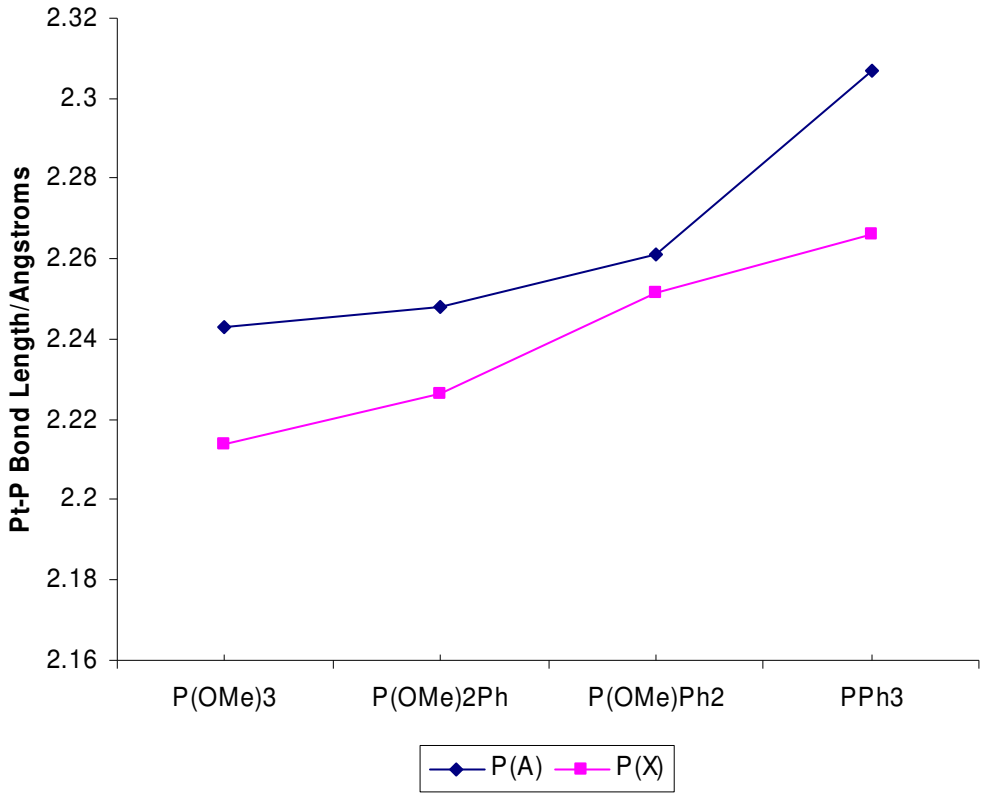

Figure 38: Variation of Pt-P(A) and Pt-P(X) distances in $Pt(SeSN_2)(P(OMe)_nPh_{3-n})_2$ complexes

Table 14: Selected bond lengths (Å) and angles (°) for **16**-**19**

	16 $Pt(SeSN_2)(P(OMe)_3)_2$	**17** $Pt(SeSN_2)(P(OMe)_2Ph)_2$	**18** $Pt(SeSN_2)(P(OMe)Ph_2)_2$	**19** $Pt(SeSN_2)(PPh_3)_2 \cdot 2H_2O$
Pt-N(1)	2.041(9)	2.065(4)	2.074(13)	2.095(4)
Pt-Se(1)	2.3874(11)	2.4099(5)	2.3987(16)	2.3818(9)
Pt-P(1)	2.214(2)	2.2266(13)	2.2517(18)	2.2664(12)
Pt-P(2)	2.243(2)	2.2480(14)	2.2609(16)	2.3069(17)
N(1)-S(1)	1.532(9)	1.523(4)	1.496(15)	1.480(7)
S(1)-N(2)	1.571(7)	1.564(5)	1.547(16)	1.572(6)
N(2)- Se(1)	1.826(9)	1.858(4)	1.858(15)	1.819(5)
P(1)-Pt-P(2)	94.83(9)	94.94(5)	96.29(14)	97.84(5)
P(1)-Pt-N(1)	179.4(2)	173.80(11)	175.32(16)	176.85(18)
P(2)-Pt-Se(1)	174.37(3)	173.45(7)	172.49(4)	170.74(3)
N(1)-Pt- Se(1)	88.0(2)	87.87(12)	86.7(3)	86.31(18)
Pt-N(1)-S(1)	117.9(4)	117.8(2)	119.1(7)	118.5(2)
N(1)-S(1)-N(2)	118.4(4)	119.5(2)	118.8(7)	118.9(2)
S(1)-N(2)- Se(1)	115.0(5)	114.8(2)	115.1(8)	114.8(4)
N(2)- Se(1)-Pt	100.7(2)	100.01(15)	100.2(4)	101.5(2)

Chapter 4: Correlating Pt-P Bond lengths and Pt-P Coupling Constants

8. $MX_2(P(OR)_nR'_{3-n})_2$ Complexes

8.1. Introduction

As a consequence of their interesting reactivity and since the discovery of the anti-cancer action of *cis*-platin[156] the study of square planar platinum complexes has been of great interest. Platinum complexes containing phosphorus ligands are of particular interest as their ^{31}P NMR spectra contain ^{195}Pt satellite peaks which allow the ^{31}P-^{195}Pt coupling constant to be measured giving insight into the nature of bonding around the platinum centre.[157] Previous studies have shown there to be a crude correlation between the P-Pt bond length and the ^{31}P-^{195}Pt coupling constant.[83, 125, 126] Compounds of the type $MX_2(P(OR)_nR'_{3-n})_2$ are relatively well known and their use as starting materials and in catalysis is well documented. Despite this few crystal structures have been reported, especially where X = Br or I and there are even fewer examples for which both crystallographic and ^{31}P NMR data are available. To redress this, this chapter reports the ^{31}P NMR spectra and X-ray crystal structures of a number of $MX_2(P(OR)_nR'_{3-n})_2$ complexes with an aim to investigate further the correlation between the P-Pt bond length and $^1J_{Pt\text{-}P}$.

8.2. Synthesis of $MX_2(P(OR)_nR'_{3-n})_2$ Complexes

8.2.1. Synthesis of *cis*-$PtCl_2(P(OR)_nR'_{3-n})_2$ complexes

cis-$MX_2(P(OR)_nR'_{3-n})_2$ complexes where M = Pt and X = Cl were prepared *via* the addition of the relevant phosphorus ligand to $PtCl_2(COD)$ in dichloromethane (Equation 22).[69] The choice of $PtCl_2(COD)$ was based on its relatively simple preparation.[148] In a typical reaction 1 g (2.7 mmol) of $PtCl_2(COD)$ was dissolved in the minimum volume of dichloromethane to which two equivalents (5.3 mmol) of the phosphine, phosphinite, phosphonite or phosphite was added. After stirring for 0.5 h the solution no longer contained a peak due to the free ligand in its ^{31}P NMR spectrum. The product *cis*-$PtCl_2(P(OR)_nR'_{3-n})_2$ (**20**, $P(OR)_nR'_{3-n} = P(O^iPr)_3$; **21**, $P(OR)_nR'_{3-n} = P(OEt)_3$; **22**, $P(OR)_nR'_{3-n} = P(OMe)_3$; **23**, $P(OR)_nR'_{3-n} = P(OMe)_2Ph$; **24**, $P(OR)_nR'_{3-n} = P(OMe)Ph_2$) were precipitated via slow addition of hexane. Isolated yields were 40-95 % (Table 16).

A different method was used in the preparation of *cis*-$PtCl_2(PPh_3)_2$ (**25**) whereby a solution of potassium tetrachloroplatinate in water was added to a solution of PPh_3 in ethanol, after which the resulting solution was refluxed until the product precipitated as a white solid.[71] The yield for this reaction was 86 %. In all cases crystals suitable for X-ray crystallography were grown by slow diffusion of hexane into a solution of the complex in dichloromethane. $^{31}P\{^1H\}$ NMR data was collected for **20**-**25**, though as these compounds have been reported previously no further characterisation was carried out.[70, 71, 93, 158, 159]

8.2.2. Synthesis of $PtBr_2(P(OR)_nR'_{3-n})_2$ and $PtI_2(P(OR)_nR'_{3-n})_2$ complexes

cis-$MX_2(P(OR)_nR'_{3-n})_2$ complexes where M = Pt and X = Br or I were prepared *via* the addition of the relevant phosphorus ligand to *trans*-$PtX_2(PhCN)_2$ in acetone (Equation 25).[70] *trans*-$PtX_2(PhCN)_2$ where X = Br or I could be easily prepared in good yield *via* the addition of benzonitrile to a solution of potassium tetrachloroplatinate and the relevant potassium halide in water (Equation 24).

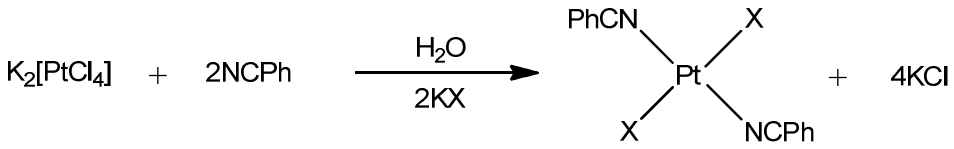

Equation 24

In a typical reaction a suspension of 1 g of *trans*-$PtX_2(PhCN)_2$ was vigorously stirred in 40 mL of acetone to which two equivalents of the relevant phosphite, phosphonite, phosphinite or phosphine was added. After stirring for 30 mins a colour change was observed. For X = Br the orange-yellow suspension becomes a colourless solution, except where $P(OR)_nR'_{3-n} = PPh_3$ where a yellow suspension is afforded. For X = I the orange-brown suspension becomes a yellow solution in all cases.

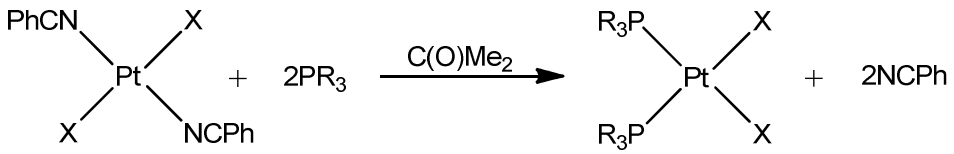

Equation 25

The products *cis*-$PtBr_2(P(OR)_nR'_{3-n})_2$ (**26**, $P(OR)_nR'_{3-n}$ = $P(OMe)_3$; **27**, $P(OR)_nR'_{3-n}$ = $P(OMe)_2Ph$; **28**, $P(OR)_nR'_{3-n}$ = $P(OMe)Ph_2$; **29**, $P(OR)_nR'_{3-n}$ = PPh_3) and *cis*-$PtI_2(P(OR)_nR'_{3-n})_2$ (**30**, $P(OR)_nR'_{3-n}$ = $P(OMe)_3$; **31**, $P(OR)_nR'_{3-n}$ = $P(OMe)_2Ph$; **32**, $P(OR)_nR'_{3-n}$ = $P(OMe)Ph_2$) were precipitated *via* addition of diethyl ether. Isolated yields were 30-95 % (Table 16). *cis*-$PtI_2(PPh_3)_2$ (**33**) was prepared *via* metathesis of *cis*-$PtCl_2(PPh_3)_2$ with excess sodium iodide in an equivolume mixture of water, ethanol, acetone and chloroform.[74] The yield of this reaction was 81 %. Crystals suitable for X-ray crystallography were grown by slow diffusion of hexane into a solution of the complex in dichloromethane, except for **29**, for which crystals were grown by slow diffusion of hexane into a solution of the complex in chloroform.

As the solubility of the products in acetone decreases in the order $P(OMe)_3$ > $P(OMe)_2Ph$ > $P(OMe)Ph_2$ > PPh_3 it was noted that a decreasing volume of diethyl ether is required to precipitate each of the products ranging from 50 mL for $P(OMe)_3$ to none required for PPh_3. For **29** a mixture of both *cis*- and *trans*- isomers is afforded. Although *trans*-$PtBr_2(PPh_3)_2$ (**29a**) was not visible in the ^{31}P NMR spectrum its presence was confirmed by the yellow colour of the product and *via* X-ray crystallography. **33** could not be prepared from *trans*-$PtI_2(PhCN)_2$, instead *trans*-$PtI_2(PPh_3)_2$ (**33a**) was isolated.

Table 15: Microanalyses, yields and melting points for **31** and **32**

Compound	%C (calc.)	%H (calc.)	Yield (%)	MP (°C)
31 *cis*-$PtI_2(P(OMe)_2Ph)_2$	24.65 (24.35)	2.51 (2.81)	52	172-174
32 *cis*-$PtI_2(P(OMe)Ph_2)_2$	35.52 (35.42)	2.66 (2.97)	93	182-186

All products were characterised using ^{31}P NMR. As **31** and **32** had not previously been reported they were further characterised by ^{1}H NMR, IR spectroscopy and microanalysis (Table 15). As they had been previously reported, further characterisation for **26**-**30** and **33** was deemed unnecessary.[70, 74, 93]

8.2.3. Synthesis of *cis*-$PdCl_2(P(OR)_nR'_{3-n})_2$ complexes

cis-$MX_2(P(OR)_nR'_{3-n})_2$ complexes, where M = Pd and X = Cl, were prepared in the same way as their platinum analogues *via* the addition of the relevant phosphorus ligand to $PdCl_2(COD)$ in dichloromethane. The reaction was carried out in exactly the same way as for *cis*-$PtCl_2(P(OR)_nR'_{3-n})_2$. The product *cis*-$PdCl_2(P(OR)_nR'_{3-n})_2$ (**34**, $P(OR)_nR'_{3-n}$ = $P(OMe)_3$; **35**, $P(OR)_nR'_{3-n}$ = $P(OMe)_2Ph$) were isolated in good yield (65-80 % (Table 16)) and crystals suitable for X-ray crystallography were grown *via* slow diffusion of hexane into a solution of the complex in dichloromethane. The complexes were also characterised by ^{31}P NMR with further characterisation deemed unnecessary as they are known compounds.[93, 160]

8.3. NMR Spectroscopy

All the $^{31}P\{^{1}H\}$ NMR spectra exhibit singlets together with satellites due to $^{1}J_{Pt-P}$ couplings for **20**-**33** (Table 16). In **22**-**33**, for each of the three halides the coupling constant is observed to decrease in the order $P(OMe)_3 > P(OMe)_2Ph > P(OMe)Ph_2 > PPh_3$ as the electron-withdrawing and π-acceptor abilities of the phosphorus ligand decreases (Figure 39). In addition to this, for each of the four types of phosphorus ligand the coupling constant decreases in the order Cl > Br > I as the degree of π-

back-bonding between the platinum and the halide, and hence the halide's ability to compete with the phosphorus for the electron back-donation, increases. This can be interpreted as an increase in the *trans*-influence of the halides, as the coupling constant is an indication of bond strength and *trans*-influence is defined as the ability of a ligand to weaken the bond *trans*- to it.[76] The chemical shifts are also seen to decrease in the order Cl > Br > I with the exception of the complexes containing $P(OMe)_3$ where the opposite is observed.

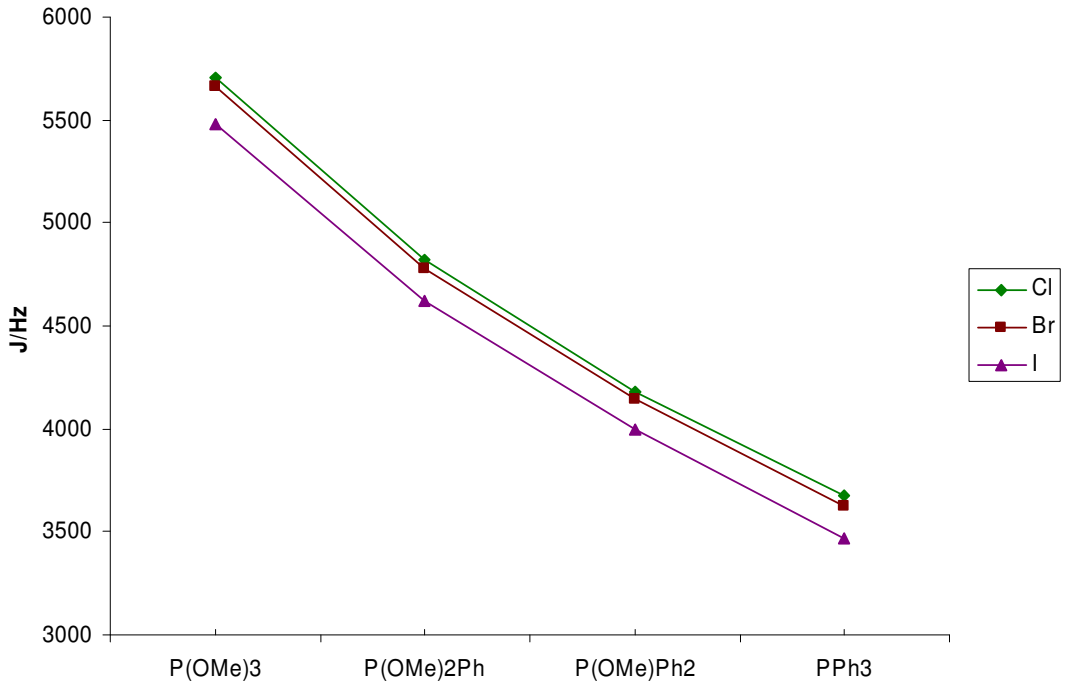

Figure 39: Variation of $^{1}J_{Pt\text{-}P}$ in $[PtCl_2(P(OMe)_nPh_{3-n})_2]$ complexes

The coupling constants for **20**-**22** are all of a similar magnitude reflecting higher *trans*-influence of the phosphite ligand compared to the *trans*-influence of the chlorine atom in these complexes. The slightly higher $^{1}J_{Pt\text{-}P}$ value for **20** compared to **21** to **22** is due to the more electron electron-withdrawing isopropyl group compared to the ethyl and methyl groups. The large difference in $^{1}J_{Pt\text{-}P}$ between **33** and **33a** (*ca.*

1000 Hz) is characteristic of that seen between *cis*- and *trans*- isomers of $PtX_2(PR_3)_2$ due to the greater *trans*-influence of the phosphorus ligand compared to the halide (Figure 16). The ^{31}P chemical shifts of the palladium-centred compounds **34** and **35** were observed to be shifted higher than those of their platinum analogues, which is comparable to published results.[93]

Table 16: ^{31}P NMR chemical shifts, coupling constants and isolated yields for **20**-**35**

Compound	δ_{ppm}	$J_{Pt\text{-}P}$(Hz)	Yield (%)
20 *cis*-$PtCl_2(P(O^iPr)_3)_2$	61.7	5812	94
21 *cis*-$PtCl_2(P(OEt)_3)_2$	68.1	5697	57
22 *cis*-$PtCl_2(P(OMe)_3)_2$	73.7	5707	75
23 *cis*-$PtCl_2(P(OMe)_2Ph)_2$	97.2	4819	37
24 *cis*-$PtCl_2(P(OMe)Ph_2)_2$	85.2	4183	90
25 *cis*-$PtCl_2(PPh_3)_2$	14.5	3679	86
26 *cis*-$PtBr_2(P(OMe)_3)_2$	75.2	5662	35
27 *cis*-$PtBr_2(P(OMe)_2Ph)_2$	97.0	4777	65
28 *cis*-$PtBr_2(P(OMe)Ph_2)_2$	84.9	4141	79
29 *cis*-$PtBr_2(PPh_3)_2$	14.0	3627	92
30 *cis*-$PtI_2(P(OMe)_3)_2$	77.6	5477	29
31 *cis*-$PtI_2(P(OMe)_2Ph)_2$	96.4	4618	52
32 *cis*-$PtI_2(P(OMe)Ph_2)_2$	83.5	3995	93
33 *cis*-$PtI_2(PPh_3)_2$	11.6	3472	81
33a *trans*-$PtI_2(PPh_3)_2$	12.6	2491	69
34 *cis*-$PdCl_2(P(OMe)_3)_2$	97.9		78
35 *cis*-$PdCl_2(P(OMe)_2Ph)_2$	125.8		68

The ^1H NMR of **31** and **32** exhibited a doublet and a multiplet corresponding to the methyl and phenyl groups on the phosphorus ligand respectively (Table 17). The

chemical shifts observed were comparable to the dichloride and dibromide analogues.[93]

Table 17: ^{1}H NMR data for **31** and **32**

Compound	δ(ppm)	Multiplet	Assignment	Coupling Constant (Hz)
31 *cis*-$PtI_2(P(OMe)_2Ph)_2$	3.66	d	12H, methyl	$^{3}J_{P\text{-}H} = 12.9$
	7.41-7.77	m	10H, phenyl	
32 *cis*-$PtI_2(P(OMe)Ph_2)_2$	3.31	d	6H, methyl	$^{3}J_{P\text{-}H} = 12.4$
	7.36-7.79	m	20H, phenyl	

8.4. X-ray Crystal Structures

The X-ray structures of the *cis*-$PtCl_2(P(OR)_nR'_{3-n})_2$ complexes **20**, **23**, and **24** were determined and refined to a good standard (Figure 40, Table 18). Though the structure of **21** could be solved to some extent, it was observed to be disordered. The structures of **22** and **25** have been reported previously.[83, 99]

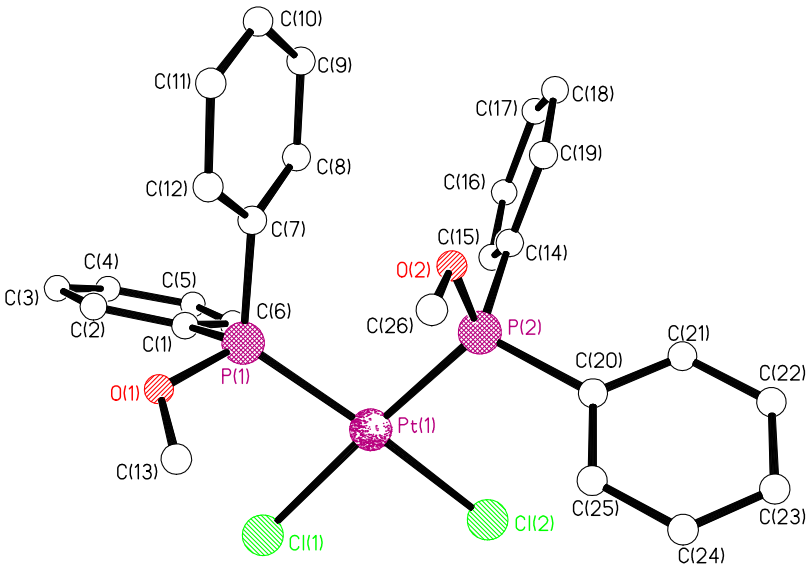

Figure 40: X-ray crystal structure of **24**.
The structures of **20**-**23** and **25** are not illustrated as they are similar

Table 18: Selected bond lengths (Å) and angles (°) for **20**-**25**

	20 *cis*-$PtCl_2(P(O^iPr)_3)_2$[161]	**21** *cis*-$PtCl_2(P(OEt)_3)_2$
Pt-Cl(1)	2.3548(7)	2.360(9)
Pt-Cl(2)	2.3547(9)	2.344(9)
Pt-P(1)	2.2176(7)	2.226(9)
Pt-P(2)	2.2117(8)	2.221(11)
P(1)-Pt-P(2)	96.99(3)	92.1(4)
Cl(1)-Pt-Cl(2)	87.18(2)	88.3(3)
	22 *cis*-$PtCl_2(P(OMe)_3)_2$[83]	**23** *cis*-$PtCl_2(P(OMe)_2Ph)_2$[162]
Pt-Cl(1)	2.384(4)	2.3625(9)
Pt-Cl(2)	2.408(4)	2.3625(9)
Pt-P(1)	2.192(3)	2.2193(9)
Pt-P(2)	2.155(3)	2.2193(9)
P(1)-Pt-P(2)	95.5(1)	101.16(3)
Cl(1)-Pt-Cl(2)	85.8(1)	89.08(3)
	24 *cis*-$PtCl_2(P(OMe)Ph_2)_2$[163]	**25** *cis*-$PtCl_2(PPh_3)_2$[99]
Pt-Cl(1)	2.3693(12)	2.3632(8)
Pt-Cl(2)	2.3533(12)	2.3294(9)
Pt-P(1)	2.2272(11)	2.2713(9)
Pt-P(2)	2.2279(12)	2.2515(8)
P(1)-Pt-P(2)	98.14(4)	99.12(3)
Cl(1)-Pt-Cl(2)	89.37(4)	87.56(3)

The structures were comparable to the previously published structures. All of the structures exhibit square planar geometry about the platinum. The Pt-Cl distances lie within the range 2.344(9) Å to 2.408(4) Å and exhibit no significant trend. The Pt-P bond lengths are within the range 2.155(3) Å to 2.2713(9) Å with the shorter distances being associated with complexes for which $^1J_{Pt\text{-}P}$ is greater. The bond angles P(1)-Pt-

(P2) and Cl(1)-Pt-Cl(2) lie in the ranges 92.1(4)° to 101.16(3)° and 85.8(1)° to 89.37(4)° respectively. When **23** and **24** were compared to the previously reported crystallographic data for **22** and **25** the Pt-P bond lengths were seen to increase in the order $P(OMe)_3 < P(OMe)_2Ph < P(OMe)Ph_2 < PPh_3$. No significant trends in the bond angles were observed.

The X-ray crystal structures of the dibromide complexes **26**-**29** and **29a** were determined and refined to a good standard (Figure 41, Table 19). All of the structures exhibit square planar geometry about the platinum and were observed to be isostructural to their dichloride analogues. Both **29** and **29a** were crystallised as chloroform solvates which is not uncommon for complexes of this type which contain triphenylphosphine.[17, 145] The structure for **29a** has previously been reported as a dichloromethane solvate.[164]

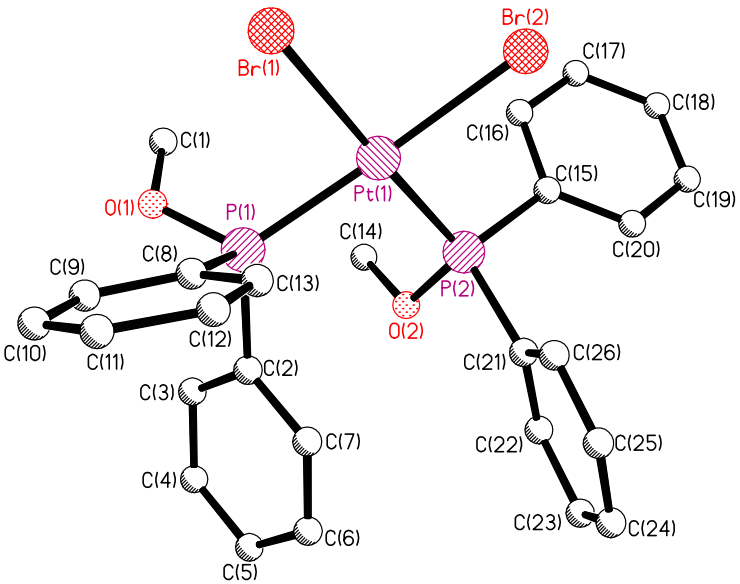

Figure 41: X-ray crystal structure of **28**.
The structures of **26**, **27**, **29** and **29a** are not illustrated as they are similar

Table 19: Selected bond lengths (Å) and angles (°) for **26**-**29** and **29a**

	26 *cis*-$PtBr_2(P(OMe)_3)_2$	**27** *cis*-$PtBr_2(P(OMe)_2Ph)_2$
Pt-Br(1)	2.4742(11)	2.4933(5)
Pt-Br(2)	2.4753(11)	2.4762(4)
Pt-P(1)	2.217(2)	2.2161(9)
Pt-P(2)	2.207(2)	2.2248(12)
P(1)-Pt-P(2)	93.74(9)	93.76(4)
Br(1)-Pt-Br(2)	88.54(3)	89.209(16)
	28 *cis*-$PtBr_2(P(OMe)Ph_2)_2$	**29** *cis*-$PtBr_2(PPh_3)_2{\cdot}CHCl_3$
Pt-Br(1)	2.4895(4)	2.4696(4)
Pt-Br(2)	2.4828(5)	2.4859(5)
Pt-P(1)	2.2400(11)	2.2625(13)
Pt-P(2)	2.2424(11)	2.2685(10)
P(1)-Pt-P(2)	98.41(4)	97.55(4)
Br(1)-Pt-Br(2)	89.265(17)	86.000(18)
	29a *trans*-$PtBr_2(PPh_3)_2{\cdot}CHCl_3$	**29a** *trans*-$PtBr_2(PPh_3)_2{\cdot}CH_2Cl_2$[164]
Pt-Br(1)	2.4417(3)	2.4346(13)
Pt-P(1)	2.3245(9)	2.313(3)
P(1)-Pt-Br(1)	92.30(2)	93.01(9)
P(1a)-Pt-Br(1)	87.69(2)	86.99(9)

In **26**-**29** the Pt-Br distances lie within the range 2.4696(4) Å to 2.4933(5) Å and exhibit no significant trend. The Pt-P bond lengths are within the range 2.207(2) Å to 2.2685(10) Å and, as was observed in the dichloride analogues, were seen to increase in the order $P(OMe)_3 < P(OMe)_2Ph < P(OMe)Ph_2 < PPh_3$. The bond angles P(1)-Pt-P(2) and Br(1)-Pt-Br(2) lie in the ranges 93.74(9)° to 98.41(4)° and 86.000(18)° to 89.265(17)° respectively with no significant trends apparent.

The X-ray crystal structures of the diiodide complexes **30**-**33** (Figure 42, Table 20) were also determined and observed to be isostructural, though not necessarily isomorphous, to the dichloride and dibromide structures. The structure of **33a** was observed to be a dichloromethane solvate which was found to be similar to a published example and will not be discussed here.[111]

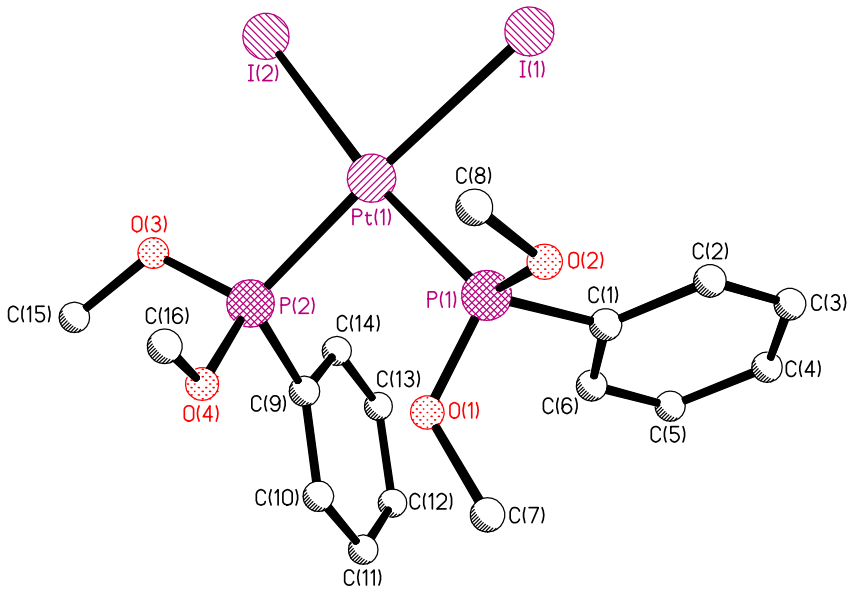

Figure 42: X-ray crystal structure of **32**.
The structures of **30**, **31** and **33** are not illustrated as they are similar

Similar trends in bond lengths and angles as those observed for the dichlorides and dibromides were also evident and the structure of **31** was observed to be essentially isomorphous to that of **27**. Significantly the Pt-P bond lengths (2.2214(14) Å to 2.295(2) Å) increase in the order $P(OMe)_3 < P(OMe)_2Ph < P(OMe)Ph_2 < PPh_3$. The Pt-I distances are in the range 2.6448(5) Å to 2.6814(5) Å and the bond angles P(1)-Pt-(P2) and Br(1)-Pt-Br(2) lie in the ranges from 94.56(5)° to 97.47(7)° and 87.456(18)° to 88.979(13)° respectively with the latter decreasing in the order $P(OMe)_3 > P(OMe)_2Ph > P(OMe)Ph_2 > PPh_3$.

Table 20: Selected bond lengths (Å) and angles (°) for **30**-**33**.

	30 *cis*-$PtI_2(P(OMe)_3)_2$	**31** *cis*-$PtI_2(P(OMe)_2Ph)_2$
Pt-I(1)	2.6587(4)	2.6608(5)
Pt-I(2)	2.6571(4)	2.6569(4)
Pt-P(1)	2.2214(14)	2.2360(14)
Pt-P(2)	2.2248(16)	2.244(2)
P(1)-Pt-P(2)	94.56(5)	93.84(6)
I(1)-Pt-I(2)	88.979(13)	88.836(17)
	32 *cis*-$PtI_2(P(OMe)Ph_2)_2$	**33** *cis*-$PtI_2(PPh_3)_2 \cdot H_2O$
Pt-I(1)	2.6814(5)	2.6647(6)
Pt-I(2)	2.6533(5)	2.6448(5)
Pt-P(1)	2.2481(19)	2.295(2)
Pt-P(2)	2.2518(19)	2.277(2)
P(1)-Pt-P(2)	93.01(7)	97.47(7)
I(1)-Pt-I(2)	88.003(17)	87.456(18)

The X-ray crystal structures of **34** and **35** (Figure 43, Table 21) were determined and refined to a good standard. Both structures were observed to be both isostructural and isomorphous to their platinum-centred analogues **22** and **23**. Interestingly, the Pd-P bond lengths are observed to be longer than in the platinum analogues. As both Pt(II) and Pd(II) have the same ionic radius (86 pm) this is likely due to a weaker interaction between palladium and phosphorus than between platinum and phosphorus. Conversely, the Pd-Cl bond lengths are observed to be shorter than in the platinum analogues suggesting that a stronger interaction between the chlorine and the palladium atoms may be the cause of the increased Pd-P distance in **34** and **35**.

Table 21: Selected bond lengths (Å) and angles (°) for **34**-**35**.

	34 *cis*-$PdCl_2(P(OMe)_3)_2$[165]	**35** *cis*-$PdCl_2(P(OMe)_2Ph)_2$[166]
Pd-Cl(1)	2.356(2)	2.3515(5)
Pd-Cl(2)	2.358(2)	2.3515(5)
Pd-P(1)	2.241(2)	2.2300(6)
Pd-P(2)	2.233(2)	2.2300(6)
P(1)-Pd-P(2)	92.38(8)	100.88(2)
Cl(1)-Pd-Cl(2)	89.71(8)	91.49(2)

Due to the extremely hygroscopic nature of *cis*-$PdCl_2(PPh_3)_2$ crystals could not easily be grown for X-ray crystallography. The structure of *cis*-$PdCl_2(P(OMe)Ph_2)_2$ has been reported previously however the phenyl rings exhibited librational effects.[120] Comparing this structure with those of **34** and **35** there is no trend in Pd-P bond length comparable to the trend observed in Pt-P distances in the platinum analogues.

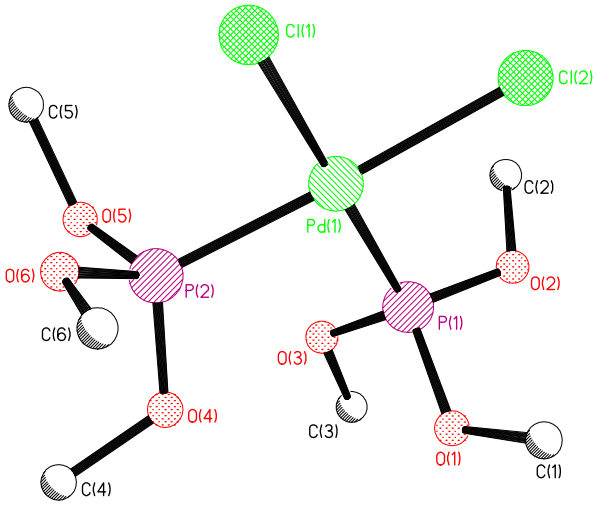

Figure 43: X-ray crystal structure of **34**

Comparing the structures of compounds **22**-**33** it can be seen that for each of the halides the Pt-P bond length is seen to increase in the order $P(OMe)_3 < P(OMe)_2Ph < P(OMe)Ph_2 < PPh_3$ with the PPh_3 complexes having Pt-P bond lengths *ca.* 0.06 Å longer than the $P(OMe)_3$ complexes (Figure 44). For each of the phosphorus ligands the Pt-P bond length increases in the order Cl < Br < I with Pt-P bond lengths in the iodide complexes being *ca.* 0.03 Å longer than their dichloride equivalents. These two effects are in accord with the π-acidity of the phosphorus ligands increasing as the oxygen content rises and as the heavier halogens are better π-acceptors, the phosphorus *trans*- to iodine is less strongly bound than phosphorus *trans*- to chloride.

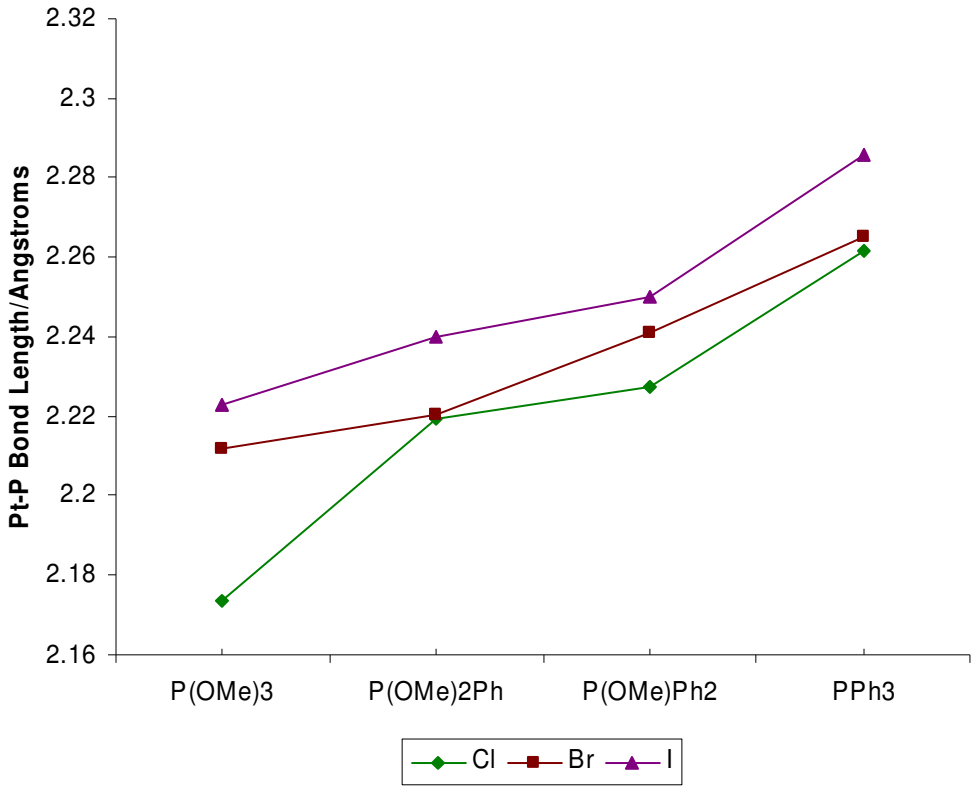

Figure 44: Variation of Pt-P distances in $PtX_2(P(OMe)_nPh_{3-n})_2$ complexes

During the course of this work structures for *cis*-$PtBr_2(PPh_3)_2$ and *cis*-$PtI_2(PPh_3)_2 \cdot H_2O$ were reported,[167] though these structures differed from those

reported here as **29** is observed to be a chloroform solvate and **33** is a low-temperature structure where the reported structure was measured at room temperature.

8.5. Correlating Pt-P Bond Lengths and Pt-P Coupling Constants

When considering the magnitude of the $^{1}J_{\text{Pt-P}}$ coupling constant the s-character of the orbitals involved in the Pt-P bond is usually considered to be the most important variable.

$$^{1}J_{(M-P)} = \gamma_M \gamma_P \frac{64\pi^2}{9} \beta^2 \frac{\left|S_M(0)\right|^2}{\Delta E} \left|S_P(0)\right|^2 (P'_{S_M S_P})^2$$

Equation 26

Thus, to a good approximation, the coupling constant is given by Equation 26.[125] In Equation 26 the s-characters of the orbitals is contained in the M.O. bond order between the s-orbitals $(P'_{S_M S_P})^2$. The valance state s-orbital basis functions are given by the expressions $\left|S_P(0)\right|$ and $\left|S_M(0)\right|$, ΔE is the average excitation energy and γ_M and γ_P the magnetogyric constants for each nucleus. As is evident the principles involved are complex however for a given phosphorus ligand and metal centre $\left|S_P(0)\right|$ and $\left|S_M(0)\right|$ should remain relatively constant leaving $(P'_{S_M S_P})^2$ as the dominating factor in the magnitude of $^{1}J_{\text{Pt-P}}$.

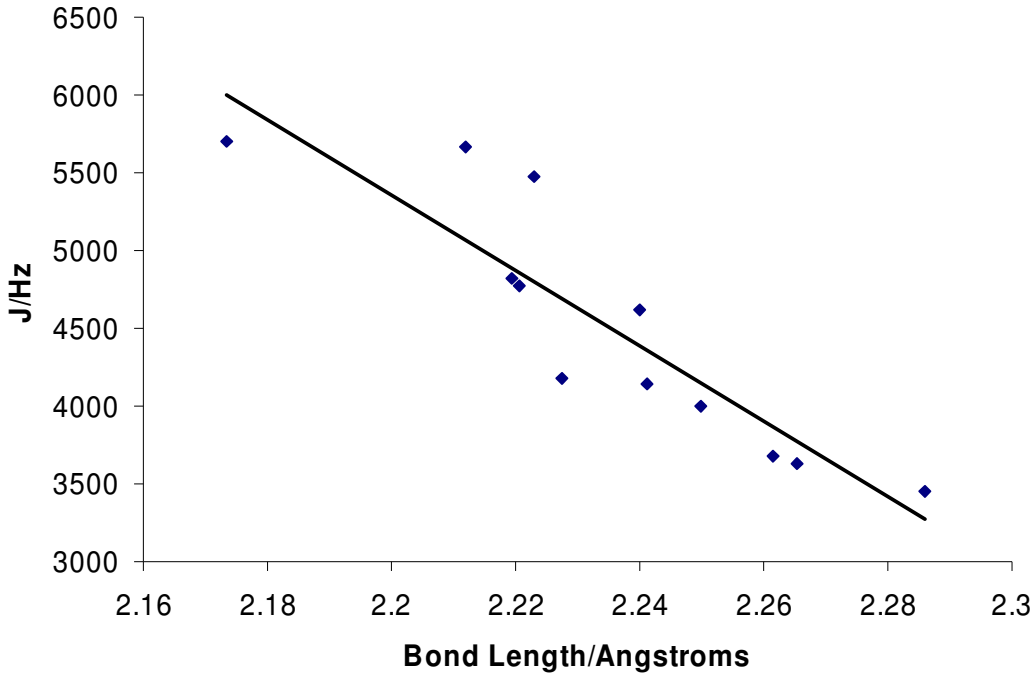

Figure 45: Correlation of $^{1}J_{Pt\text{-}P}$ with Pt-P bond length in **22**-**33**

We found that as the bond length increases the coupling constant decreases. The correlation between these two measurements in **22**-**33** is rather good (Figure 45). We did consider that another way of gauging the s-character and hence the strength of the bond would be to look at the R-P-R, R-P-O and O-P-O bond angles in these complexes with larger values indicating a move towards more ideal sp^3 hybridisation however we did not observe any correlation in this regard. It thus appears that in a narrow series of complexes the coupling constant could be used as a good indicator of bond length (Equation 27).

$$l_{(Pt-P)} = 2.421 - \frac{J}{24255}$$

Equation 27

To further test the principle we compared Pt-P bond lengths and $^{1}J_{Pt\text{-}P}$ coupling constants for **1**, **2**, **4**-**7** and **16**-**19** along with all characterised $Pt(E_2N_2)(PR_3)_2$[17, 19, 27, 42, 43, 147] as well as their protonated equivalents, corresponding *cis*- and *trans*-dihalides[85-89, 92, 97, 98, 100-112, 161, 168] and $Pt(NSO)_2(PR_3)_2$ complexes (Figure 46).[34, 35]

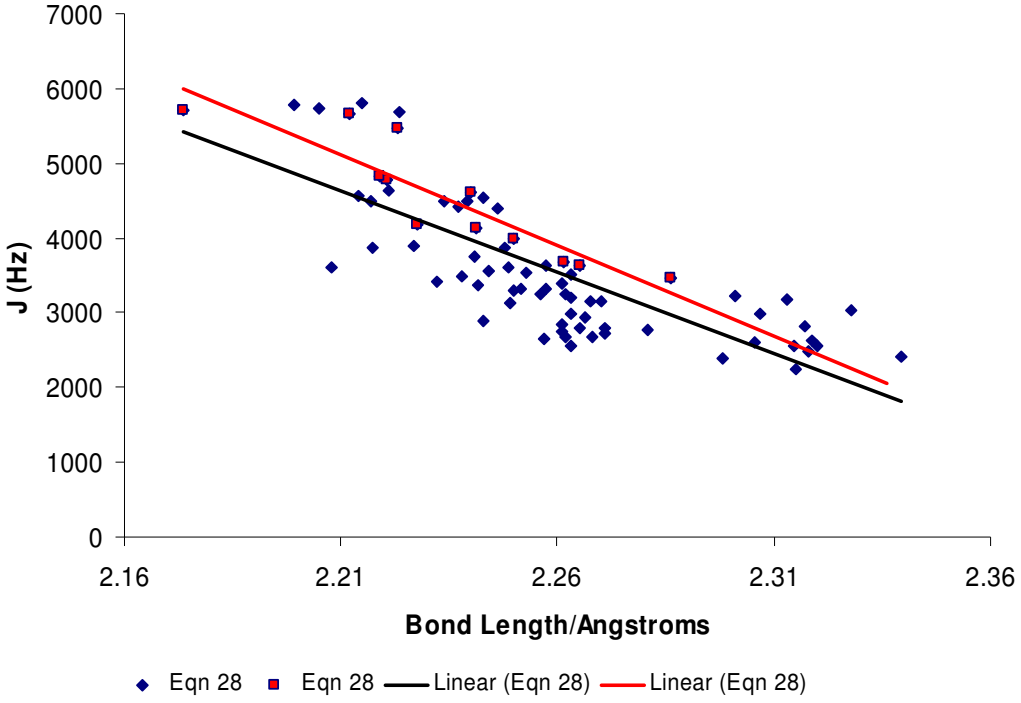

Figure 46: Correlation of $^{1}J_{Pt\text{-}P}$ with Pt-P bond length in large range of Platinum-Phosphorus complexes

The correlation observed is poor though very generally, the larger the coupling constant the shorter the Pt-P bond length. As can be seen in Figure 46, the correlation is not necessarily linear, since at the extremes significant energetic stabilisation is needed in order to influence bond length and the magnitude of coupling constants is a better measure of s orbital overlap than of absolute bond length.

$$l_{(Pt-P)} = 2.422 - \frac{J}{21827}$$

Equation 28

Using Equation 28 we were able to test the accuracy of the correlation as an indicator of bond length on a selection of compounds (Table 22). It is interesting to note that in most cases Equation 27 tends to give a more accurate result than Equation 28 the former being on average within 0.015 Å of the observed distance and the latter within 0.02 Å. The accuracy of Equation 28 could potentially be improved with a more extensive literature search. There have been previous reports[83, 125, 126] which show a similar trend on a much smaller scale in a series of bis(phosphine) Pt(I) and Pt(II) dihalides.

Table 22: Coupling constants and bond lengths calculated and observed for selected compounds

Compound	$^1J_{Pt\text{-}P}$ (Hz)	$l_{Pt\text{-}P}$ (Å)	Eqn 2 (Å)	Eqn 3 (Å)
$[Pt(9S3)(PPh_3)Cl]PF_6$[169]	3387	2.2838(8)	2.281	2.266
$[Pt(10S3)(PPh_3)Cl]PF_6$[169]	3438	2.285(2)	2.279	2.264
$[Pt(PMe_3)_2\{CS_3\}]$[170]	2969	2.265	2.298	2.285
$[Pt(PPh_3)_2\{CS_3\}]$[170]	3145	2.2915	2.29	2.278
$[Pt(dppp)_2\{CS_3\}]$[170]	2881	2.263	2.302	2.289
$[Pt(Se_2naph)(P(OPh)_3)_2]$[171]	4711	2.231	2.227	2.208

Chapter 5: Metal λ^6-Sulfanenitrile Complexes

9. Metal-ndsdsd Complexes

9.1. Introduction

λ^6-sulfanenitriles have been reported to form metal complexes with the transition metals cobalt, nickel and copper.[67, 68] The function of bis[(nitrilo(diphenyl)-λ^6-sulfanyl)](diphenyl)-λ^6-sulfanediimide ($Ph_2S(=N\text{-}(Ph_2)S\equiv N)_2$, ndsdsd) as a chelating ligand is of interest as it forms an eight-membered metal-sulfur-nitrogen ring with all reported examples adopting the twist-boat conformation. Further studies into this ligand are necessary to establish its *trans*-influence, increase the number of metal centres it has been observed to coordinate to and determine whether other conformations of the ring are possible.

9.2. Synthesis of Metal-ndsdsd Complexes

The compound ndsdsd was prepared *via* the literature method by the Fujii group at Nihon University, Japan (Equation 20).[66] Complexes of the type $M(II)Cl_2(ndsdsd)$ and $[M(II)(ndsdsd)_2][2Cl]$ have been reported as being synthesised rather simply by adding the ligand to a solution of $M(II)Cl_2$ in methanol. In this work dichloromethane was used as the solvent for reactions involving ndsdsd as, given the hygroscopic

nature of the ligand, it was thought that a dry solvent would be preferable for reactions and dry dichloromethane was more readily available than dry methanol.

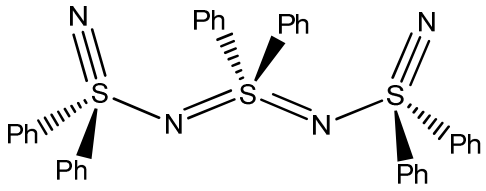

Figure 47: ndsdsd

In a typical reaction an equimolar amount of ndsdsd (Figure 47) and a metal halide, often with another ligand attached were stirred together in dichloromethane for *ca.* 1 h. The resulting solution was then reduced in volume and crystallised *via* slow addition of hexane. In the reaction of ndsdsd with $PtCl_2$(COD) it was thought that ndsdsd would displace the labile COD (in much the same way as it is displaced to produce bis(phosphine)platinum dichloride (Equation 22)) to produce $PtCl_2$(ndsdsd). Contrary to expectation the complex [Pt(ndsdsd)(COD)][2Cl] (**36**) was isolated in 75 % yield and was characterised using X-ray crystallography and elemental analysis (Table 23). An analogous reaction using $PdCl_2$(COD) as a starting material failed to yield any satisfactory results beyond an extremely poor crystal structure of $PdCl_2$(ndsdsd). This indicates an unusual discrepancy between the chemistry of palladium and platinum.

Many attempts to prepare complexes of the type Pt(ndsdsd)$(PR_3)_2$ were attempted, though most produced no reaction. Addition of ndsdsd to a solution of *cis*-$PtCl_2(P(OMe)Ph_2)_2$ in dichloromethane produced no significant changes in the ^{31}P NMR spectrum suggesting that the ligand had failed to react. Repeating the reaction

with *cis*-$PtCl_2(PMe_2Ph)_2$ and *cis*-$PtCl_2(P(OMe)_2Ph)_2$ also failed to produce the desired ndsdsd complex. When ndsdsd was added to a solution of *cis*-$PtCl_2(P(OMe)Ph_2)_2$ in dichloromethane a coordination shift of *ca.* 34 ppm was observed in the ^{31}P NMR spectrum, though this could not be confirmed as the product $[Pd(ndsdsd)(P(OMe)Ph_2)_2][2Cl]$ as it could not be isolated for further analysis. Further attempts using **36** as a starting material in an effort to displace COD with two equivalents of a phosphine (PEt_3) or phosphite ($P(OMe)_3$) also proved unsuccessful. Addition of ndsdsd to a solution of *cis*-$PtCl_2(P(OMe)_3)_2$ in wet dichloromethane did produce the complex $[Pt(ndsdsd)(P(OMe)_3)(P(O)(OMe)_2)][Cl]$ (**37**) in 77 % yield and was further characterised using ^{31}P NMR, elemental analysis and X-ray crystallography. The presence of water may be the cause of the dealkylation of one of the trimethyl phosphite ligands to form a phosphonate. The failure of other complexes containing larger phosphorus ligands to react may be due to steric hindrance. The relatively small steric bulk and cone angle (107°) of $P(OMe)_3$ may have decreased this effect allowing ndsdsd to form the complex.

Addition of ndsdsd to a solution of $PdCl_2(PhCN)_2$ in dichloromethane yields a homoleptic $[Pd(ndsdsd)_2]^{2+}$ cation and a $[Pd_2Cl_6]^{2-}$ anion (**38**) in 44 % yield which was characterised *via* X-ray crystallography, IR spectroscopy and elemental analysis. Repeating this reaction with $PtCl_2(PhCN)_2$ failed to produce a platinum analogue of this complex. A second palladium-centred complex, [Pd(ndsdsd)(bipy)][2Cl] (**39**) was produced *via* reaction of $PdCl_2$(bipy) with ndsdsd in dichloromethane and characterised using X-ray crystallography, IR spectroscopy and elemental analysis.

Table 23: Microanalyses and yields for **36**-**41**

Compound	%C (calc.)	%H (calc.)	%N (calc.)	Yield (%)
36·CH_2Cl_2	49.98 (50.33)	4.49 (4.13)	5.29 (5.21)	75
37·CH_2Cl_2	43.25 (43.36)	3.79 (4.07)	4.69 (4.82)	77
38·0.5CH_2Cl_2	48.48 (48.27)	3.39 (3.41)	6.15 (6.21)	44
39·CH_2Cl_2·2H_2O	52.94 (52.79)	3.72 (4.15)	8.01 (7.86)	82
40	37.01 (35.40)	1.85 (2.48)	4.63 (4.59)	63
41	41.59 (42.07)	2.32 (2.94)	5.45 (4.96)	90

The gold-centred complexes $[AuCl_2(ndsdsd)][AuCl_4]$ (**40**) and $[AuCl_2(ndsdsd)][PF_6]$ (**41**) could also be produced upon addition of ndsdsd to a solution of $AuCl_3$ in dichloromethane. For **41** the reaction was performed in the presence of $NaPF_6$. **40** and **41** were isolated in good yield (63 and 90 % respectively) and characterised using IR spectroscopy and elemental analysis. Crystals of **40** were grown and analysed using X-ray crystallography, however crystals of **41** could not be grown, therefore **41** was further characterised using ^{31}P and ^{1}H NMR.

Attempts were also made to coordinate the ligand to rhodium and molybdenum centres using $RhCl_3$ and $Mo(pip)_2(CO)_4$ as starting materials, though as large crops of ndsdsd crystals were yielded from these examples and no spectroscopic evidence for the coordinated ligand was observed, it was concluded that there was no reaction despite a colour-change being observed in both cases.

9.3. Spectroscopic Analysis

The IR spectra **37**-**41** were found to exhibit similar frequencies to the previously published examples.[68] The characteristic IR band attributed to the terminal S-N usually observed in the range 1285-1261 cm^{-1} was evident in all complexes. This is thought to be a result of the S≡N vibration observed at 1313 cm^{-1} in the free ligand shifting to a lower frequency upon complexation. A weak vibration between 1306-1310 cm^{-1} is observed in all the complexes suggesting that the solid may still contain trace amounts of the free ligand. A vibration typically associated with phenyl groups at *ca.* 1445 cm^{-1} is also observed in **37**-**41**.

The ^{1}H and ^{31}P NMR spectra of **41** were also measured as no crystal data was available. The ^{1}H NMR exhibited four distinct multiplets similar to those observed in the free ligand. On the whole the chemical shifts were observed to be slightly higher than those in the free ligand suggesting that complexation had indeed occurred. Though the number of hydrogen atoms indicated by each multiplet could be calculated *via* integration, a precise assignment was difficult (Table 24).

Table 24: ^{1}H NMR data for **41** $[AuCl_2(ndsdsd)][PF_6]$

δ(ppm)	Multiplet	Assignment
7.44-7.55	m	12H
7.60-7.64	m	6H
7.79-7.82	m	4H
7.94-7.97	m	8H

The ^{31}P NMR exhibited a septuplet at -143.7 ppm characteristic of the $[PF_6]^-$ anion. This was similar to the spectrum of $NaPF_6$ and gave no indication as to formation of the complex.

The ^{31}P NMR spectrum of **37** exhibits an AX splitting with $^2J_{Pt\text{-}P}$ couplings and satellite peaks due to $^1J_{Pt\text{-}P}$ couplings. The spectrum was assigned by analogy with compounds of the type $[Pt(P(OMe)_3)_n(P(O)(OMe)_2)_{4-n}]^{n-2+}$.[172] The peak at δ = 84.2 ppm was assigned to the phosphorus in the $P(OMe)_3$ ligand (δ_A) as ^1J_A (6207 Hz) was observed to be much higher in value than $^1J_{Pt\text{-}P}$ for the phosphorus *trans*- to nitrogen in compounds **5** and **16**. Where in **5** and **16** $P(OMe)_3$ was *trans*- to a negatively-charged nitrogen atom, in the case of **37** $P(OMe)_3$ is *trans*- to a neutral nitrogen atom which accounts for the significantly higher (*ca.* 1700 Hz) $^1J_{Pt\text{-}P}$ value. It can hence be inferred that the π-acidity and by extension the *trans*-influence of the terminal nitrogen atoms of ndsdsd is much lower compared to the nitrogen in $[S_2N_2]^-$.

The peak at δ = 31.4 ppm was assigned to the phosphorus *trans*- to the $[P(O)(OMe)_2]^-$ ligand (δ_X). The $^1J_{Pt\text{-}P}$ value observed (4812 Hz) indicates a weaker Pt-P bond between the negatively-charged phosphorus atom and the platinum centre due to the decreased π-acidity of $[P(O)(OMe)_2]^-$ compared to $P(OMe)_3$. The value of $^2J_{P\text{-}P}$ for **37** (40 Hz) was found to be similar to that of **13**.

9.4. X-ray Crystal Structures

The X-ray crystal structures of **36**-**41** (Figure 48, Table 25 & 26) were determined and refined to as good a standard as was possible. Generally the quality of the crystals of ndsdsd complexes was poor and, as the complexes were hygroscopic, there was often water and solvent within the structure.

All structures exhibited square-planar geometry about the metal. The structures of **38** and **40** contain metal-centred counter-ions which also exhibited square planar geometry about the metal. For all the structures the S-N bond lengths within the ring suggest that the N≡S-N=S=N-S≡N bond order of the free ligand has been maintained. N(1)-S(1) and N(4)-S(3), which correspond to the triply-bonded nitrogen atom range between 1.450(12) Å and 1.507(9) Å, comparable to the terminal S≡N bond length of ndsdsd (1.457(2) Å).[66] The single bonds, N(2)-S(1) and N(3)-S(3), range from 1.639(9) Å to 1.684(14) Å, slightly shorter than the typical value for S-N bonds (1.69 Å), and N(2)-S(2) and N(3)-S(2) range between 1.53(2) Å and 1.575(10) Å, slightly longer than the typical value for an S=N bond (1.52 Å).

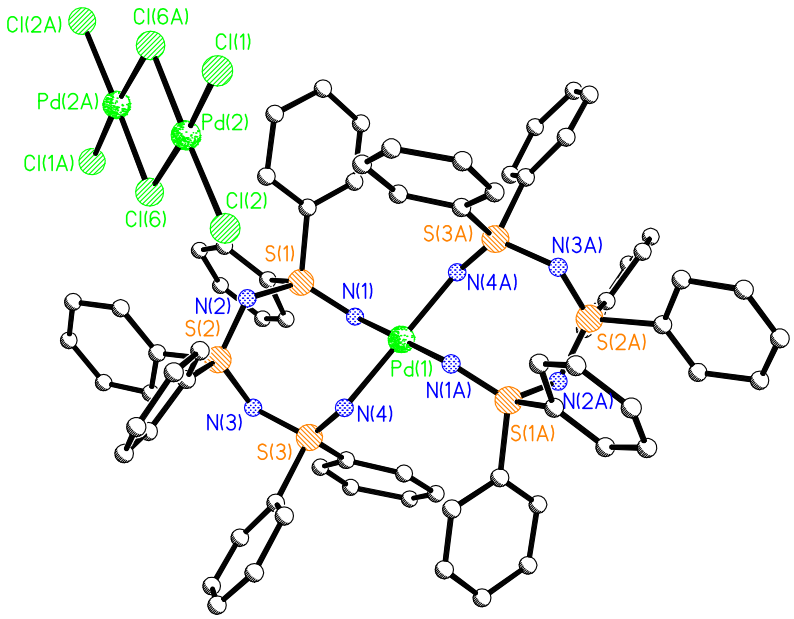

Figure 48: X-ray crystal structure of **38**

The structures of **36**-**38** and **40** exhibit the twist-boat (Figure 49) conformation observed in the previously published examples and comparable bond angles within the ring with the exception of **37** for which a larger than usual M-N(1)-S(1) bond angle was observed.[68] In a typical example, it can be seen that S(1) and S(3) are on opposite sides of the plane containing the N(1)-M-N(4) bond angle. This unusual conformation is no doubt the result of the inconsistent bond order within the ring compared to the more consistant bond order in tetrasulfur tetranitride which adopts a more symmetrical crown conformation,[3] as well as the steric bulk of and the π-stacking observed between the phenyl groups.

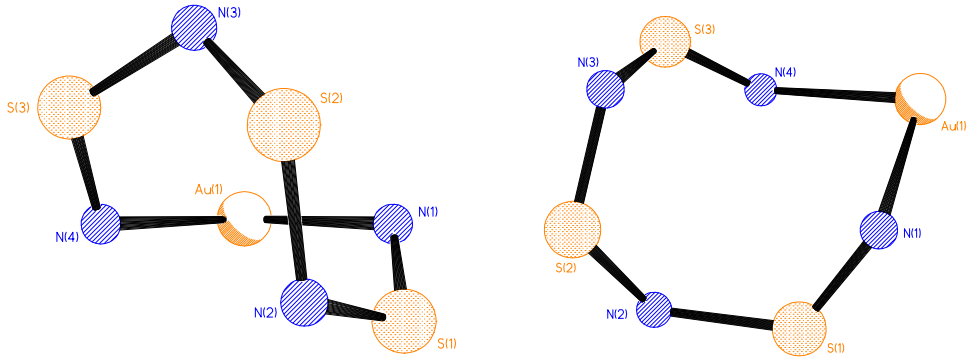

Figure 49: X-ray crystal structure of the backbone in **40** showing the twist-boat conformation

The ring within the structure of **39** adopts a less twisted version of the standard conformation (Figure 50). This can be attributed to the aryl overlap between one of the phenyl groups on S(3) and the bipyridyl group, which results in a reduced S(3)-N(4)-Pd angle compared to the other structures. **39** also exhibits a lower dihedral angle between the S(1)-N(1)-M and N(1)-M-N(4) planes than the other structures, such that S(1) is nearly in the same plane as the N(1)-Pd-N(4) angle.

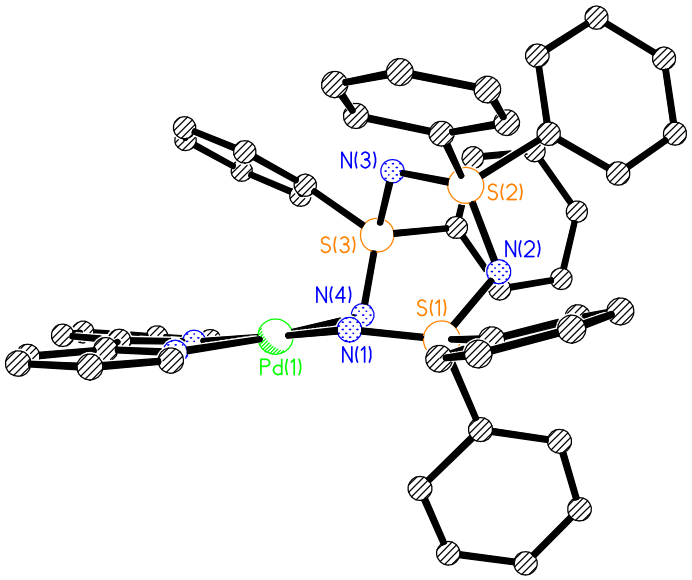

Figure 50: X-ray crystal structure of **39**

In the structure of **37** (Figure 51) the Pt-P bond lengths and P-Pt-P bond angle were comparable to those observed in **5** and **16**. In accordance with the assertions of Chapter 4, Pt-P(1), which corresponds to the phosphonate ligand and the lower $^{1}J_{Pt\text{-}P}$ value, is longer than Pt-P(2), which corresponds to the phosphite group and the higher $^{1}J_{Pt\text{-}P}$ value. The structure of **37** also exhibited disorder about one of the methoxy groups on the phosphite ligand.

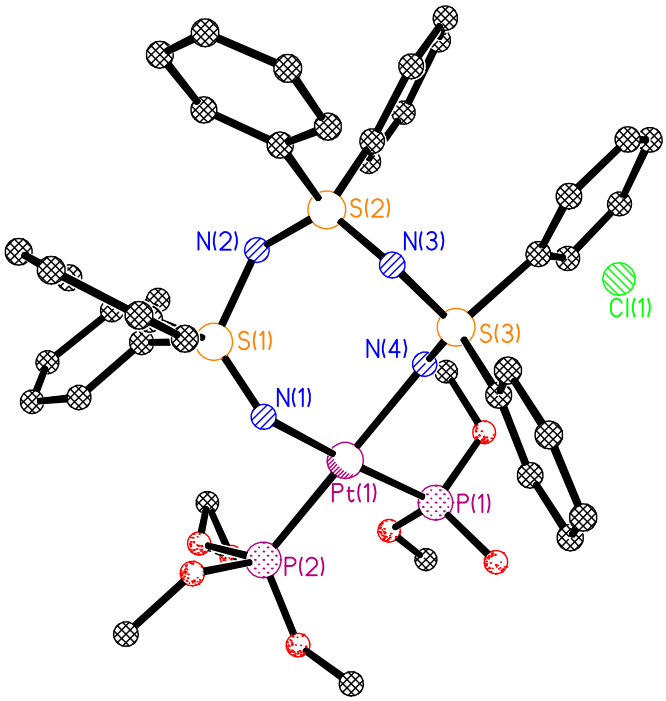

Figure 51: X-ray crystal structure of **37**

Table 25: Selected bond lengths (Å) for **36**-**40**

	36·CH_2Cl_2	**37**·$2H_2O$	**38**·$2CH_2Cl_2$	**39**·$2CH_2Cl_2$·$2H_2O$	**40**
M-N(1)	2.030(10)	2.130(13)	2.044(11)	1.992(10)	2.03(2)
N(1)-S(1)	1.465(9)	1.450(12)	1.499(11)	1.507(9)	1.47(2)
S(1)-N(2)	1.674(10)	1.672(14)	1.654(11)	1.666(9)	1.69(3)
N(2)-S(2)	1.544(11)	1.546(12)	1.575(10)	1.545(9)	1.55(2)
S(2)-N(3)	1.566(11)	1.532(13)	1.536(12)	1.569(10)	1.53(2)
N(3)-S(3)	1.665(10)	1.684(14)	1.661(11)	1.639(9)	1.67(2)
S(3)-N(4)	1.460(10)	1.481(12)	1.473(11)	1.457(9)	1.45(2)
N(4)-M	2.062(10)	2.087(11)	2.042(10)	2.049(8)	2.07(2)
M-P(1)		2.260(4)			
M-P(2)		2.211(4)			
M-N(5)				2.027(8)	
M-N(6)				2.023(9)	
M-Cl(1)					2.303(8)
M-Cl(2)					2.345(10)

Table 26: Selected bond angles (°) for **34**-**38**

	36·CH_2Cl_2	**37**·$2H_2O$	**38**·$2CH_2Cl_2$	**39**·$2CH_2Cl_2$·$2H_2O$	**40**
M-N(1)-S(1)	133.2(6)	123.6(8)	120.6(7)	125.6(5)	122.3(16)
N(1)-S(1)-N(2)	122.7(6)	122.3(7)	122.0(6)	122.4(5)	122.8(15)
S(1)-N(2)-S(2)	117.9(6)	121.0(8)	115.5(7)	117.2(5)	115.5(15)
N(2)-S(2)-N(3)	120.2(6)	121.3(6)	120.1(6)	119.9(5)	117.7(14)
S(2)-N(3)-S(3)	116.6(6)	119.3(8)	118.5(7)	117.0(5)	119.3(16)
N(3)-S(3)-N(4)	121.0(6)	120.7(6)	124.1(6)	121.2(5)	122.7(14)
S(3)-N(4)-M	126.0(6)	129.9(8)	125.1(6)	114.5(4)	122.0(14)
N(4)-M-N(1)	90.3(4)	89.6(4)	91.5(4)	92.9(3)	92.4(10)
P(1)-M-P(2)		92.36(18)			
N(5)-M-N(6)				80.5(4)	
Cl(1)-M-Cl(2)					92.9(3)

Chapter 6: Experimental

10. Experimental

10.1. General Experimental

The reagents, purchased from Sigma-Aldrich or Alfa Aesar were used without further purification. The ndsdsd ligand was prepared by the Fujii group at Nihon University, Japan. Unless otherwise stated, all reactions were carried out under an oxygen-free nitrogen atmosphere using pre-dried solvents and standard Schlenk techniques, subsequent chromatographic and work up procedures were performed in air. Solvents were dried and purified using a Braun Solvent Drying System. ^{31}P (109 MHz, H_3PO_4) and ^{1}H (270 MHz, $SiMe_4$) NMR spectra were recorded with C_6D_6 as an external lock at 25 ºC (unless stated otherwise) on a JEOL GSX 270. IR spectra were recorded as KBr discs in the range of 4000-200 cm^{-1} on a Perkin-Elmer 2000 FTIR/Raman spectrometer. Microanalysis was performed by the University of St Andrews microanalysis service.

Crystal structure data were collected for **1, 4-7, 21, 36** and **38** at 93 K on a Rigaku MM007 confocal optics/Saturn CCD diffractometer using Mo-K_α radiation (λ = 0.71073 Å) and for **2**, **8-9**, **16-20**, **23-24, 26-35, 37** and **39-40** at 125 K using a Rigaku SCX-Mini. All data was corrected for absorption. The structure were solved

by direct methods and refined by full-matrix least-squares methods on F^2 values of all data. Refinements were performed using SHELXL.

10.2. Preparation of Starting Materials and Reagents

10.2.1. Preparation of $[S_4N_3]Cl$[2]

Ammonium chloride (300 g, 5.61 mol) and sulfur flowers (60 g, 0.230 mol) was placed in a wide-necked flask to which sulfur monochloride (S_2Cl_2) (300 mL, 3.75 mol) was added. After being mixed together using a glass rod the flask was fitted with an air condenser with a calcium chloride drying tube and gently refluxed at 150 °C for 20 h. The orange brown crystals of $[S_3N_2Cl]Cl$ were removed from the inside of the air condenser and dried *in vacuo*. $[S_3N_2Cl]Cl$ (14 g, 72 mmol) was then added to a solution of S_2Cl_2 (50 mL, 0.63 mol) in dry carbon tetrachloride (CCl_4) (50 mL) at -20 °C. The solution was then refluxed for 5 h at 95 °C before being filtered yielding the bright yellow product which was washed with CCl_4 (50 mL) and dried *in vacuo*.
Yield: 7.0 g (34 mmol), 71 %.

10.2.2. Preparation of S_7NH[173]

Hexamethylphosphoramide (HMPA) (500 mL) was dried with calcium hydride (10 g) and enough potassium metal to turn the solution blue. The solvent was then distilled under vacuum between 70 and 90 °C with the first 30 mL and the last 70 mL being discarded. The remaining solvent was then degassed with nitrogen flow and stirring. Sodium azide (23.75 g, 0.365 mol) and sulfur flowers (25 g, 0.097 mol) were

added to the HMPA which turned inky blue within 20 mins. The solution was stirred for 3 days before being poured into 10 % hydrochloric acid (500 mL) of at 0 °C producing a pale yellow precipitate which was allowed to settle for 3 h before being filtered off, washed with water (250 mL) and dried *in vacuo*. The residue was then extracted with diethyl ether (8 × 50 mL) in a mortar and pestle. The extracts were combined and the solvent allowed to evaporate giving yellow crystals. The product was then recrystallised from methanol. Yield (from sulfur): 1.690 g (7.07 mmol), 7 %. Elemental Analysis (%, calculated in brackets): H, 0.24 (0.42); N, 5.33 (5.85).

10.2.3. Preparation of $PtCl_2(COD)$[148]

Potassium tetrachloroplatinate (5 g, 12 mmol) was dissolved in water (50 mL) and filtered into a 250 mL round bottom flask. A further 20 mL of water was then used to wash the filtered solid. Glacial acetic acid (100 mL) was added after which 1,5-cyclooctadiene (5 mL, 12 mmol) was added to the solution. The reaction mixture was then stirred at 90 °C for 30 mins. The mixture was allowed to cool to room temperature and was placed in a fridge overnight. The white crystalline material formed was filtered and then washed with water, ethanol and diethyl ether. Yield: 4.10 g (11 mmol), 91 %.

10.2.4. Preparation of $PtCl_2(PhCN)_2$[174]

A suspension of platinum(II) chloride (1 g, 3.76 mmol) in benzonitrile (25 mL) of was heated to 110 °C until the solid dissolved. The solution was then filtered hot

and cooled in an ice bath. The yellow, crystalline product was then filtered and washed with 30 mL of hexane. Yield: 1.29 g (2.73 mmol), 73 %

10.2.5. Preparation of $PtCl_2(bipy)$[175]

Potassium tetrachloroplatinate (0.5 g, 1.2 mmol) was dissolved in water (150 mL) to which 2M hydrochloric acid (8 mL) was added. To this 2,2′-bipyridine (0.19 g, 1.2 mmol) of was added and the solution heated under reflux for 2 h. The resulting yellow precipitate was filtered, washed with water (50 mL) and dried in an oven at 100 °C. Yield: 0.295 g (0.7 mmol), 58 %.

10.2.6. Preparation of *trans*-$PtBr_2(PhCN)_2$[70]

Potassium tetrachloroplatinate (3.6 g, 8.7 mmol) and potassium bromide (6 g, 50.8 mmol) were dissolved in water (120 mL). To this, benzonitrile (12 mL) was added and the solution was stirred at 70 °C for 5 h. The resulting dark yellow precipitate was filtered and washed with water (50 mL), ethanol (50 mL) and diethyl ether (50 mL). Yield: 3.620 g (6.5 mmol), 74 %.

10.2.7. Preparation of *trans*-$PtI_2(PhCN)_2$[70]

Potassium tetrachloroplatinate (3.6 g, 8.7 mmol) and potassium iodide (6 g, 36.1 mmol) were dissolved in water (120 mL). To this, benzonitrile (12 mL) was added and the solution was stirred at 70 °C for 5 h. The resulting brown precipitate was filtered and washed with water (50 mL), ethanol (50 mL) and diethyl ether (50 mL). Yield: 4.452 g (8.0 mmol), 92 %.

10.2.8. Preparation of $Pd(COD)Cl_2$

Bis(benzonitrile)palladium(II) dichloride (1 g, 2.6 mmol) of was dissolved in dichloromethane (30 mL) to which 1,5-cyclooctadiene (0.32 mL, 2.6 mmol) was added. After stirring for 1 h the volume of the solution was reduced to *ca.* 5 mL and the product was precipitated *via* addition of hexane (20 mL). Yield: 0.308 g (1.1 mmol), 42 %.

10.2.9. Preparation of $PdCl_2(bipy)$[176]

Palladium(II) chloride (2.67 g, 15 mmol) was dissolved in water (300 mL) to which 2M hydrochloric acid (15 mL) was added. The solution was then heated at 75 °C for 30 mins. After filtering of the solution and adjusting the pH to 2-3 by addition of aqueous NaOH the solution was cooled to room temperature. A solution of 2,2′-bipyridine (2.34 g, 15 mmol) in water (30 mL) was then added and the solution stirred for 3 h. The resulting yellow precipitate was filtered, washed with water (50 mL), ethanol (50 mL) and diethyl ether (50 mL). Yield: 4.464 g (13.4 mmol), 89 %.

10.3. Preparation of $MX_2(PR_3)_2$ Complexes

10.3.1. Preparation of *cis*-$PtCl_2(PMe_2Ph)_2$[69]

(1,5-cyclooctadiene)platinum(II) dichloride (1 g, 2.7 mmol) was dissolved in the minimum volume of dichloromethane (30 mL) under an inert atmosphere. To this dimethyl phenylphosphine (0.76 mL, 5.3 mmol) was added. The mixture was stirred

at room temperature for 30 mins before being filtered and precipitated *via* slow addition of diethyl ether to give a white powder. Yield: 0.335 g (0.6 mmol), 22 %.

$^{31}P\{^{1}H\}$ NMR (C_6D_6, 298 K): δ = -14.4 ($^{1}J_{P\text{-}Pt}$= 3549 Hz).

10.3.2. Preparation of *cis*-$PtCl_2(P(OPh)_3)_2$

(1,5-cyclooctadiene)platinum(II) dichloride (1 g, 2.7 mmol) was dissolved in the minimum volume of dichloromethane (30 mL) under an inert atmosphere. To this triphenylphosphite (1.39 mL, 5.3 mmol) was added. The solution was stirred at room temperature for 30 mins before being filtered and precipitated *via* slow addition of hexane to give a white powder. Yield: 1.982 g (2.4 mmol), 90 %.

$^{31}P\{^{1}H\}$ NMR (C_6D_6, 297 K): δ = 59.7 ($^{1}J_{P\text{-}Pt}$= 5793 Hz).

10.3.3. Preparation of *cis*-$PtCl_2(P(O^{n}Bu)_3)_2$

(1,5-cyclooctadiene)platinum(II) dichloride (1 g, 2.7 mmol) was dissolved in the minimum volume of dichloromethane (30 mL) under an inert atmosphere. To this tributylphosphite (1.46 mL, 5.3 mmol) was added. The solution was stirred at room temperature for 30 mins before being filtered. The product could not be precipitated *via* the addition of hexane yet NMR of the solution with its volume reduced to 5 mL confirmed the presence of the desired product.

$^{31}P\{^{1}H\}$ NMR (C_6D_6, 297 K): δ = 71.3 ($^{1}J_{P\text{-}Pt}$= 5634 Hz).

10.3.4. Preparation of *cis*-$PtCl_2(P(O^{i}Pr)_3)_2$ (20)

(1,5-cyclooctadiene)platinum(II) dichloride (0.5 g, 1.5 mmol) was dissolved in the minimum volume of dichloromethane (15 mL) under an inert atmosphere. To this

triisopropylphosphite (0.520 mL, 2.6 mmol) was added. The solution was stirred at room temperature for 30 mins before being filtered and precipitated *via* slow addition of hexane to give a colourless, crystalline powder. Yield: 0.833 g (1.2 mmol), 94 %. $^{31}P\{^{1}H\}$ NMR (C_6D_6, 297 K): $\delta = 61.7$ ($^{1}J_{P\text{-}Pt} = 5812$ Hz).

10.3.5. Preparation of *cis*-$PtCl_2(P(OEt)_3)_2$ (21)

(1,5-cyclooctadiene)platinum(II) dichloride (1 g, 2.7 mmol) was dissolved in the minimum volume of dichloromethane (30 mL) under an inert atmosphere. To this triethylphosphite (0.91 mL, 5.3 mmol) was added. The solution was stirred at room temperature for 30 mins before being filtered and precipitated *via* slow addition of hexane to give a white crystalline solid. Yield: 0.925 g (1.5 mmol), 57 %. $^{31}P\{^{1}H\}$ NMR (C_6D_6, 297 K): $\delta = 68.1$ ($^{1}J_{P\text{-}Pt} = 5697$ Hz).

10.3.6. Preparation of *cis*-$PtCl_2(P(OMe)_3)_2$ (22)

(1,5-cyclooctadiene)platinum(II) dichloride (1 g, 2.7 mmol) was dissolved in the minimum volume of dichloromethane (30 mL) under an inert atmosphere. To this trimethylphosphite (0.625 mL, 5.3 mmol) was added. The solution was stirred at room temperature for 30 mins before being filtered and precipitated *via* slow addition of hexane to give a colourless, crystalline powder. Yield: 1.011 g (1.8 mmol), 75 %. $^{31}P\{^{1}H\}$ NMR (C_6D_6, 297 K): $\delta = 73.7$ ($^{1}J_{P\text{-}Pt} = 5707$ Hz).

10.3.7. Preparation of *cis*-$PtCl_2(P(OMe)_2Ph)_2$ (23)

(1,5-cyclooctadiene)platinum(II) dichloride (1 g, 2.7 mmol) of was dissolved in the minimum volume of dichloromethane (30 mL) under an inert atmosphere. To this

dimethyl phenylphosphonite (0.84 mL, 5.3 mmol) was added. The solution was stirred at room temperature for 30 mins before being filtered and then precipitated by slow addition of hexane to give a white crystalline solid. Crystals were grown for X-ray crystallography *via* slow diffusion of hexane into a solution of the product in dichloromethane. Yield: 0.607 g (1.0 mmol), 37 %.

$^{31}P\{^{1}H\}$ NMR (C_6D_6, 297 K): $\delta = 97.2$ ($^{1}J_{P\text{-}Pt} = 4819$ Hz).

10.3.8. Preparation of *cis*-$PtCl_2(P(OMe)Ph_2)_2$ (24)

(1,5-cyclooctadiene)platinum(II) dichloride (0.8 g, 2.1 mmol) was dissolved in the minimum volume of dichloromethane (30 mL) under an inert atmosphere. To this methyl diphenylphosphinite (0.92 mL, 4.6 mmol) was added. The solution was stirred at room temperature for 30 mins before being filtered and then precipitated by slow addition of hexane to give a white crystalline solid. Crystals were grown for X-ray crystallography *via* slow diffusion of hexane into a solution of the product in dichloromethane. Yield: 1.347 g (1.9 mmol), 90 %.

$^{31}P\{^{1}H\}$ NMR (C_6D_6, 296 K): $\delta = 85.2$ ($^{1}J_{P\text{-}Pt} = 4183$ Hz).

10.3.9. Preparation of *cis*-$PtCl_2(PPh_3)_2$ [71] (25)

A solution of potassium tetrachloroplatinate (1.8 g, 4.3 mmol) in water (30 mL) was added slowly to a solution of triphenylphosphine (2.55 g, 9.7 mmol) in ethanol (30 mL) under an inert atmosphere. The solution was refluxed until a white precipitate formed. The mixture was allowed to cool before being filtered and washed with ethanol. Yield: 2.941 g (3.7 mmol), 86 %.

$^{31}P\{^{1}H\}$ NMR (C_6D_6, 297 K): $\delta = 14.5$ ($^{1}J_{P\text{-}Pt} = 3679$ Hz).

10.3.10. Preparation of *cis*-$PtBr_2(P(OMe)_3)_2$[70] (26)

trans-bis(benzonitrile)platinum(II) dibromide (1 g, 1.8 mmol) was vigorously stirred in acetone (40 mL), to which trimethylphosphite (0.424 mL, 3.6 mmol) was added affording a clear solution. The volume of acetone was reduced to *ca.* 10 mL. The product was precipitated upon addition of diethyl ether (50 mL). The solid was filtered and washed with diethyl ether to give a colourless, crystalline solid. Crystals were grown for X-ray crystallography *via* slow diffusion of hexane into a solution of the product in dichloromethane. Yield: 0.375 g (0.6 mmol), 35 %.

$^{31}P\{^1H\}$ NMR (C_6D_6, 297 K): $\delta = 75.2$ ($^1J_{P\text{-}Pt} = 5662$ Hz).

10.3.11. Preparation of *cis*-$PtBr_2(P(OMe)_2Ph)_2$[93] (27)

trans-bis(benzonitrile)platinum(II) dibromide (1 g, 1.8 mmol) was vigorously stirred in acetone (40 mL), to which dimethyl phenylphosphonite (0.571 mL, 3.6 mmol) was added affording a clear solution. The volume of acetone was reduced to *ca.* 10 mL with a colourless precipitate forming. The remaining product was precipitated upon addition of diethyl ether (50 mL). The solid was filtered and washed with diethyl ether to give a colourless, crystalline solid. Crystals were grown for X-ray crystallography *via* slow diffusion of hexane into a solution of the product in dichloromethane. Yield: 0.812 g (1.2 mmol), 65 %.

$^{31}P\{^1H\}$ NMR (C_6D_6, 297 K): $\delta = 97.0$ ($^1J_{P\text{-}Pt} = 4777$ Hz).

10.3.12. Preparation of *cis*-$PtBr_2(P(OMe)Ph_2)_2$[93] (28)

trans-bis(benzonitrile)platinum(II) dibromide (1 g, 1.8 mmol) was vigorously stirred in acetone (40 mL), to which methyl diphenylphosphinite (0.726 mL, 3.6

mmol) was added affording a clear solution. The volume of acetone was reduced to *ca.* 10 mL with a colourless precipitate forming. The solid was filtered and washed with diethyl ether to give a colourless powder. Crystals were grown for X-ray crystallography *via* slow diffusion of hexane into a solution of the product in dichloromethane. Yield: 1.129 g (1.43 mmol), 79 %.

$^{31}P\{^{1}H\}$ NMR (C_6D_6, 297 K): $\delta = 84.9$ ($^{1}J_{P\text{-}Pt} = 4141$ Hz).

10.3.13. Preparation of $PtBr_2(PPh_3)_2$[74] (29)

trans-bis(benzonitrile)platinum(II) dibromide (0.5 g, 0.9 mmol) was vigorously stirred in acetone (20 mL), to which triphenylphosphine (0.472 g, 1.8 mmol) dissolved in of acetone (20 mL) was added affording a yellow precipitate. The solid was then filtered and washed with diethyl ether to give a colourless, crystalline solid. Crystals were grown for X-ray crystallography *via* slow diffusion of hexane into a solution of the product in chloroform. Yield: 0.726 g (0.8 mmol), 92 %.

$^{31}P\{^{1}H\}$ NMR (C_6D_6, 297 K): $\delta = 14.0$ ($^{1}J_{P\text{-}Pt} = 3627$ Hz).

10.3.14. Preparation of *cis*-$PtI_2(P(OMe)_3)_2$[70] (30)

trans-bis(benzonitrile)platinum(II) diiodide (1 g, 1.53 mmol) of was vigorously stirred in acetone (40 mL), to which trimethylphosphite (0.360 mL, 3.05 mmol) was added affording a clear yellow solution. The volume of acetone was reduced to *ca.* 10 mL. The product was precipitated upon addition of diethyl ether (50 mL). The solid was filtered and washed with diethyl ether to give a yellow, crystalline solid. Crystals were grown for X-ray crystallography *via* slow diffusion of hexane into a solution of the product in dichloromethane. Yield: 0.313 g (0.45 mmol), 29 %.

$^{31}P\{^{1}H\}$ NMR (C_6D_6, 297 K): δ = 77.6 ($^{1}J_{P\text{-}Pt}$ = 5477 Hz).

10.3.15. Preparation of *cis*-$PtI_2(P(OMe)_2Ph)_2$ (31)

trans-bis(benzonitrile)platinum(II) diiodide (1 g, 1.53 mmol) was vigorously stirred in acetone (40 mL), to which dimethyl phenylphosphonite (0.48 mL, 3.05 mmol) was added affording a clear yellow solution. The volume of acetone was reduced to *ca.* 10 mL, with a yellow precipitate forming. The remaining product was precipitated upon addition of diethyl ether (50 mL). The solid was filtered and washed with diethyl ether to give a crystalline, yellow solid, mp 172-174 °C. Crystals were grown for X-ray crystallography *via* slow diffusion of hexane into a solution of the product in dichloromethane. Yield: 0.632 g (0.8 mmol), 52 %.

Elemental Analysis (%, calculated in brackets): C, 24.65 (24.33); H, 2.51 (2.79).

^{1}H NMR ($CDCl_3$, 291 K): δ = 3.66 (d, 12H, methyl, $^{3}J_{PH}$ = 12.9 Hz), 7.41-7.77 (m, 10H, phenyl).

$^{31}P\{^{1}H\}$ NMR (C_6D_6, 295 K): δ = 96.4 ($^{1}J_{P\text{-}Pt}$ = 4618 Hz).

Infra Red: 2938w, 2831w, 1480w, 1434m, 1308w, 1175m, 1118m, 1045m, 1018m, 820m, 807m, 776m, 749m, 711m, 693m, 579m, 555m, 486m, 317w, 202m, 188s, 163s, 150m cm^{-1}.

10.3.16. Preparation of *cis*-$PtI_2(P(OMe)Ph_2)_2$ (32)

trans-bis(benzonitrile)platinum(II) diiodide (1 g, 1.53 mmol) was vigorously stirred in acetone (40 mL), to which methyl diphenylphosphinite (0.61 mL, 3.05 mmol) was added affording a clear yellow solution. The volume of acetone was reduced to *ca.* 10 mL, with a yellow precipitate forming. The solid was filtered and

washed with diethyl ether to give a yellow powder, mp 182-186 °C. Crystals were grown for X-ray crystallography *via* slow diffusion of hexane into a solution of the product in dichloromethane. Yield: 1.255 g (1.43 mmol), 93 %.

Elemental Analysis (%, calculated in brackets): C, 35.52 (35.41); H, 2.66 (2.95).

^{1}H NMR ($CDCl_3$, 291 K): δ = 3.31 (d, 6H, methyl, $^{3}J_{PH}$ = 12.4 Hz), 7.36-7.79 (m, 20H, phenyl).

$^{31}P\{^{1}H\}$ NMR (C_6D_6, 295 K): δ = 83.5 ($^{1}J_{P\text{-}Pt}$ = 3995 Hz).

Infra Red: 2937w, 1586w, 1573w, 1480m, 1436m, 1312m, 1280w, 1182m, 1105m, 1032m, 743m, 693m, 568m, 548w, 526m, 502w, 482w, 218w, 206m, 175s, 167s, 151s cm^{-1}.

10.3.17. Preparation of *cis*-$PtI_2(PPh_3)_2$[74] (33)

cis-bis(triphenylphosphine)platinum(II) dichloride (1 g, 1.3 mmol) and sodium iodide (7.6 g, 50.7 mmol) was refluxed in 10 mL each of acetone, chloroform, ethanol and water for 1 h. The resulting yellow precipitate was filtered and washed with diethyl ether to give a yellow solid. Crystals were grown for X-ray crystallography *via* slow diffusion of hexane into a solution of the product in chloroform. Yield: 1.023 g (1.05 mmol), 81 %.

$^{31}P\{^{1}H\}$ NMR (C_6D_6, 297 K): δ = 11.6 ($^{1}J_{P\text{-}Pt}$ = 3472 Hz).

10.3.18. Preparation of *trans*-$PtI_2(PPh_3)_2$ (33a)

trans-bis(benzonitrile)platinum(II) diiodide (0.5 g, 0.77 mmol) was vigorously stirred in acetone (20 mL) to which triphenylphosphine (0.404 g, 1.53 mmol) dissolved in acetone (20 mL) was added affording a yellow precipitate. The solid was

then filtered and washed with diethyl ether to give a yellow powder. Crystals were grown for X-ray crystallography *via* slow diffusion of hexane into a solution of the product in dichloromethane. Yield: 0.515 g (0.53 mmol), 69 %.

$^{31}P\{^{1}H\}$ NMR (C_6D_6, 297 K): $\delta = 12.6$ ($^{1}J_{P\text{-}Pt} = 2491$ Hz).

10.3.19. Preparation of *cis*-$PdCl_2(P(OMe)_3)_2$ (34)

(1,5-cyclooctadiene)palladium(II) dichloride (0.5 g, 1.75 mmol) was dissolved in the minimum volume of dichloromethane (10 mL) under an inert atmosphere. To this, trimethylphosphite (0.414 mL, 3.5 mmol) was added. The solution was stirred at room temperature for 30 mins before being filtered and precipitated by slow addition of hexane to give a pale yellow powder. Crystals were grown for X-ray crystallography *via* slow diffusion of hexane into a solution of the product in dichloromethane. Yield: 0.578 g (1.4 mmol), 78 %.

$^{31}P\{^{1}H\}$ NMR (C_6D_6, 297 K): $\delta = 97.9$.

10.3.20. Preparation of *cis*-$PdCl_2(P(OMe)_2Ph)_2$[177] (35)

Potassium tetrachloropalladate (0.3 g, 0.93 mmol) was dissolved in ethanol (10 mL), to which dimethyl phenylphosphonite (0.147 mL, 1.86 mmol) was added. The solution was stirred at room temperature for 30 mins before being filtered and then precipitated by slow addition of hexane to give a white crystalline solid. Crystals were grown for X-ray crystallography *via* slow diffusion of hexane into a solution of the product in dichloromethane. Yield: 0.204 g (0.40 mmol), 68 %.

$^{31}P\{^{1}H\}$ NMR (C_6D_6, 297 K): $\delta = 125.8$.

10.3.21. Preparation of *cis*-$Pd_2Cl_4(P(OMe)_2Ph)_2$[178]

bis(benzonitrile)palladium(II) dichloride (1 g, 2.6 mmol) was dissolved in dichloromethane (25 mL) to which dimethyl phenylphosphonite (0.84 mL, 5.3 mmol) was added. The solution was stirred at room temperature for 30 mins before being filtered and then precipitated by slow addition of hexane to give a pale yellow solid. Crystals were grown for X-ray crystallography *via* slow diffusion of hexane into a solution of the product in dichloromethane. Yield: 0.321 g (0.46 mmol), 19 %.

10.4. Preparation of Disulfur-Dinitrido Complexes

10.4.1. Preparation of $Sb(S_2N_2)Ph_3$[179]

Liquid ammonia (30 mL) was condensed under nitrogen using an ammonia condenser filled with dry ice and acetone into a dry Schlenk tube in a dry ice/acetone bath. To this, $[S_4N_3]Cl$ (0.102 g, 0.5 mmol) was added. After stirring for 30 mins, triphenylstibene dichloride (0.212 g, 0.5 mmol) was added rapidly. The solution was then allowed to warm to room temperature and the ammonia gas blown off under a stream of nitrogen. The residue was placed under vacuum to remove any excess ammonia, before being dissolved in dichloromethane and filtered through celite. The product was precipitated by slow addition of hexane to give a yellow powder. Crystals were grown *via* slow diffusion of hexane into a solution of the product in dichloromethane. These crystals were of a good enough quality for X-ray crystallography.

Elemental Analysis (%, calculated in brackets): C, 45.28 (48.65); H, 3.41 (3.41); N, 4.61 (6.31).

10.4.2. Preparation of $Pt(S_2N_2)(PMe_2Ph)_2$[28] (1)

Liquid ammonia (30 mL) was condensed under nitrogen using an ammonia condenser filled with dry ice and acetone into a dry Schlenk tube in a dry ice/acetone bath. To this, $[S_4N_3]Cl$ (0.102 g, 0.5 mmol) was added. After stirring for 30 mins, *cis*-$PtCl_2(PMe_2Ph)_2$ (0.271 g, 0.5 mmol) was added rapidly. The solution was then allowed to warm to room temperature and the ammonia gas blown off under a stream of nitrogen. The residue was placed under vacuum to remove any excess ammonia before being dissolved in dichloromethane, filtered through celite and precipitated by slow addition of hexane to give a tan-brown powder. Crystals were grown *via* the slow diffusion of hexane into a solution of the product in dichloromethane. Yield: 0.142 g (2.5 mmol), 50 %.

$^{31}P\{^1H\}$ NMR ($CDCl_3$, 297 K): δ_A = -24.0 ($^1J_{P\text{-}Pt}$= 2812 Hz), δ_X = -7.4 ($^1J_{P\text{-}Pt}$= 2737 Hz), $^2J_{P\text{-}P}$= 25.8.

10.4.3. Preparation of $Pt(S_2N_2)(P(OPh)_3)_2$ (2)

Liquid ammonia (30 mL) was condensed under nitrogen using an ammonia condenser filled with dry ice and acetone into a dry Schlenk tube in a dry ice/acetone bath. To this, $[S_4N_3]Cl$ (0.102 g, 0.5 mmol) was added. After stirring for 30 mins, *cis*-$PtCl_2(P(OPh)_3)_2$ (0.443 g, 0.5 mmol) was added rapidly. The solution was allowed to warm to room temperature and the ammonia gas blown off under a stream of nitrogen.

The residue was placed under vacuum to remove any excess ammonia before being dissolved in dichloromethane and filtered through celite and precipitated by slow addition of hexane to give a dark brown powder. Crystals were grown *via* the slow diffusion of hexane into a solution of the product in dichloromethane. Yield: 0.145 g (0.15 mmol), 32 %.

Elemental Analysis for $Pt(S_2N_2)(P(OPh)_3)_2 \cdot 0.5CH_2Cl_2$ (%, calculated in brackets): C, 45.90 (46.13); H, 3.12(3.28); N, 3.27 (2.95).

$^{31}P\{^1H\}$ NMR (C_6D_6, 296 K): $\delta_A = 89.6$ ($^1J_{P\text{-}Pt} = 4634$ Hz), $\delta_X = 96.7$ ($^1J_{P\text{-}Pt} = 4503$ Hz), $^2J_{P\text{-}P} = 54$.

Infra Red: 3423w, 3062w, 2962w, 1945w, 1590s, 1488s, 1455m, 1261m, 1186s, 1161s, 1103w, 1072m, 1052m, 1025m, 1007m, 928s, 805w, 759s, 687s, 618m, 596m, 564w, 491s, 380w, 357w cm^{-1}.

10.4.4. Preparation of $Pt(S_2N_2)(P(O^nBu)_3)_2$ (3)

Liquid ammonia (30 mL) was condensed under nitrogen using an ammonia condenser filled with dry ice and acetone into a dry Schlenk tube in a dry ice/acetone bath. To this, $[S_4N_3]Cl$ (0.102 g, 0.5 mmol) was added. After stirring for 30 mins, the solution obtained in the preparation of *cis*-$PtCl_2(P(O$*n*-$Bu)_3)_2$ was added rapidly. The solution was allowed to warm to room temperature and the ammonia gas blown off under a stream of nitrogen. Dichloromethane was added to the remaining solution which was then filtered through celite. Precipitation of the product as a solid *via* slow addition of hexane was not achieved, however the ^{31}P NMR spectrum displayed an AX splitting characteristic of an $[S_2N_2]^{2-}$ complex.

$^{31}P\{^1H\}$ NMR (C_6D_6, 297 K): $\delta_A = 102.8$ ($^1J_{P\text{-}Pt} = 4470$ Hz), $\delta_X = 109.0$ ($^1J_{P\text{-}Pt} = 4334$ Hz), $^2J_{P\text{-}P} = 49$.

10.4.5. Preparation of $Pt(S_2N_2)(P(OEt)_3)_2$ (4)

Liquid ammonia gas (30 mL) was condensed under nitrogen using an ammonia condenser filled with dry ice and acetone into a dry Schlenk tube in a dry ice/acetone bath. To this, $[S_4N_3]Cl$ (0.102 g, 0.5 mmol) was added. After stirring for 30 mins, *cis*-$PtCl_2(P(OEt)_3)_2$ (0.299 g, 0.5 mmol) was added rapidly. The solution was allowed to warm to room temperature and the ammonia gas blown off under a stream of nitrogen. The residue was placed under vacuum to remove any excess ammonia before being dissolved in dichloromethane, filtered through celite and precipitated by slow addition of hexane to give tan-brown, plate-like crystals. These crystals were of a good enough quality for X-ray crystallography. Yield: 0.146 g (0.24 mmol), 47 %).

Elemental Analysis (%, calculated in brackets): C, 23.25 (23.26); H, 4.78 (4.88); N, 3.73 (4.52).

$^{31}P\{^1H\}$ NMR (C_6D_6, 298 K): $\delta_A = 98.5$ ($^1J_{P\text{-}Pt} = 4498$ Hz), $\delta_X = 105.5$ ($^1J_{P\text{-}Pt} = 4415$ Hz), $^2J_{P\text{-}P} = 49$.

Infra Red: 3424w, 3225w, 2982s, 2938m, 2900s, 1945w, 1836w, 1739w, 1474m, 1444m, 1390s, 1156m, 1103s, 1020s, 961s, 802s, 766m, 748m, 686s, 618m, 576s, 554s, 469m, 434w, 370m, 355m, 330m cm^{-1}.

10.4.6. Preparation of $Pt(S_2N_2)(P(OMe)_3)_2$ (5)

Liquid ammonia (30 mL) was condensed under nitrogen using an ammonia condenser filled with dry ice and acetone into a dry Schlenk tube in a dry ice/acetone bath. To this, $[S_4N_3]Cl$ (0.102 g, 0.5 mmol) was added. After stirring for 30 mins, *cis*-$PtCl_2(P(OMe)_3)_2$ (0.206 g, 0.5 mmol) was added rapidly. The solution was allowed to warm to room temperature and the ammonia gas blown off under a stream of nitrogen.

The residue was dried under vacuum to remove any excess ammonia before being dissolved in dichloromethane, filtered through celite and precipitated via slow addition of hexane to give tan-brown needle-like crystals. These crystals were of a good enough quality for X-ray crystallography. Yield: 0.123 g (0.23 mmol), 58 %. Elemental Analysis (%, calculated in brackets): C, 14.23 (13.46); H, 3.08 (3.39); N, 4.68 (5.23).

$^{31}P\{^{1}H\}$ NMR ($CDCl_3$, 300 K): $\delta_A = 105.3$ ($^{1}J_{P\text{-}Pt} = 4502$ Hz), $\delta_X = 110.9$ ($^{1}J_{P\text{-}Pt} = 4395$ Hz), $^{2}J_{P\text{-}P} = 51$.

Infra Red: 3421w, 2999w, 2949s, 2844m, 1839w, 1559w, 1442s, 1179s, 1019s, 818s, 780m, 756s, 682s, 615m, 537s, 467m, 398m, 372m, 354w, 319w cm^{-1}.

10.4.7. Preparation of $Pt(S_2N_2)(P(OMe)_2Ph)_2$ (6)

Liquid ammonia (30 mL) was condensed under nitrogen using an ammonia condenser filled with dry ice and acetone into a dry Schlenk tube in a dry ice/acetone bath. To this, $[S_4N_3]Cl$ (0.102 g, 0.5 mmol) was added. After stirring for 30 mins, *cis*-$PtCl_2(P(OMe)_2Ph)_2$ (0.303 g, 0.5 mmol) was added rapidly. The solution was allowed to warm to room temperature and the ammonia gas blown off under a stream of nitrogen. The residue was placed under vacuum to remove any excess ammonia before being dissolved in dichloromethane, filtered through celite and precipitated via slow addition of hexane to give a tan-brown, granular solid. Crystals for X-ray crystallography were grown *via* slow diffusion of hexane into a solution of the product in dichloromethane. Yield: 0.194 g (0.31 mmol), 62 %).

Elemental Analysis for $Pt(S_2N_2)(P(OMe)_2Ph)_2 \cdot 0.5CH_2Cl_2$ (%, calculated in brackets): C, 29.74 (29.58); H, 3.38 (3.46); N, 4.72 (4.18).

$^{31}P\{^{1}H\}$ NMR (C_6D_6, 296 K): δ_A = 120.4 ($^{1}J_{P\text{-}Pt}$= 3864 Hz), δ_X = 126.2 ($^{1}J_{P\text{-}Pt}$= 3761 Hz), $^{2}J_{P\text{-}P}$= 38.

Infra Red: 3425w, 3054w, 2987w, 2940m, 2835w, 1972w, 1832w, 1776w, 1588w, 1573w, 1480w, 1437s, 1309w, 1179m, 1118s, 1047s, 1024s, 803s, 749m, 710s, 694m, 684m, 614w, 579s, 556s, 491m, 467m, 371m, 355m, 320m cm^{-1}.

10.4.8. Preparation of $Pt(S_2N_2)(P(OMe)Ph_2)_2$ (7)

Liquid ammonia (30 mL) was condensed under nitrogen using an ammonia condenser filled with dry ice and acetone into a dry Schlenk tube in a dry ice/acetone bath. To this, $[S_4N_3]Cl$ (0.102 g, 0.5 mmol) was added. After stirring for 30 mins, *cis*-$PtCl_2(P(OMe)_2Ph)_2$ (0.365 g, 0.5 mmol) was added rapidly. The solution was allowed to warm to room temperature and the ammonia gas blown off under a stream of nitrogen. The residue was placed under vacuum to remove any excess ammonia before being dissolved in dichloromethane, filtered through celite and precipitated via slow addition of hexane to give a red-brown, granular solid. Crystals for X-ray crystallography were grown *via* slow diffusion of hexane into a solution of the product in dichloromethane. Yield: 0.215 g (0.30 mmol), 60 %).

Elemental Analysis (%, calculated in brackets): C, 43.22 (43.39); H, 3.79 (3.64); N, 4.23 (3.89).

$^{31}P\{^{1}H\}$ NMR (C_6D_6, 296 K): δ_A = 91.8 ($^{1}J_{P\text{-}Pt}$= 3287 Hz), δ_X = 104.1 ($^{1}J_{P\text{-}Pt}$= 3249 Hz), $^{2}J_{P\text{-}P}$= 28.

Infra Red: 3425w, 3214w, 3050w, 2940w, 1968w, 1896w, 1817w 1571w, 1480m, 1435s, 1310m 1260w, 1177m, 1158w, 1105s, 1062m, 1042s, 925w, 853w, 800w, 773m, 758m, 696s, 680m, 615w, 566m, 548s, 503m, 476m, 462m, 445m, 360w, 349w cm^{-1}.

10.4.9. Preparation of [Pd(S_2N_2H)(bipy)][$^nBu_2SnCl_3$] (8)

$PdCl_2$(bipy) (0.2 g, 0.6 mmol) was suspended in of dry dichloromethane (20 mL) with rapid stirring. [$^nBu_2Sn(S_2N_2)]_2$ (0.16 g, 0.3 mmol) was then added to the suspension which was stirred for a further 30 mins during which time the suspension turned dark red in colour. The solution was then filtered through celite and the volume reduced to *ca.* 5 mL. Purification of the product was achieved *via* column chromatography (bio-beads) and crystals were successfully grown for X-ray crystallography. Yield: 96 mg (0.14 mmol), 23 %.
Elemental Analysis (%, calculated in brackets): C, 33.56 (31.10); H, 3.67 (3.92); N, 7.41 (8.06).

10.4.10. Preparation of [Pd(S_2N_2H)(bipy)][Cl] (9)

$PdCl_2$(bipy) (0.2 g, 0.6 mmol) was suspended in a solution of $NaPF_6$ (0.1 g, 0.6 mmol) in dry dichloromethane (20 mL) with rapid stirring. [$^nBu_2Sn(S_2N_2)]_2$ (0.16 g, 0.3 mmol) was then added to the suspension which was stirred for a further 30 mins during which time the suspension turned dark red in colour. The solution was then filtered through celite and evaporated to dryness. The red-brown residue was then extracted with methanol (*ca.* 30 mL) producing a golden-yellow solution which was filtered through celite once more. The volume of the solution was then reduced to *ca.* 5 mL and the orange product was precipitated upon layering with diethyl ether (20 mL). The solid was then filtered and dried *in vacuo*. Crystals for X-ray crystallography were grown *via* slow diffusion of diethyl ether into a solution of the product in methanol. Yield: 0.103 g (0.25 mmol), 41 %.

Elemental Analysis for $[Pd(S_2N_2H)(bipy)][Cl]\cdot MeOH\cdot 0.5H_2O$ (%, calculated in brackets): C, 31.05 (30.56); H, 2.93 (3.26); N, 12.51 (12.96).

^{1}H NMR (CD_2Cl_2, 293 K, Figure 31): δ = 7.39-7.44 (dd, 1H, H^7), 7.65-7.69 (dd, 1H, H^4), 7.98-8.10 (m, 4H, H^3, H^5, H^6, H^8), 8.45-8.47 (d, 1H, H^9, $^3J_{H\text{-}H}$ = 5.5 Hz), 9.51-9.53 (d, 1H, H^2, $^3J_{H\text{-}H}$ = 5.2 Hz), 11.4-12.0 (s, 1H, H^1).

10.4.11. Preparation of $Pd(S_2N_2)(bipy)$ (10)

$PdCl_2(bipy)$ (0.2 g, 0.6 mmol) was suspended in dry dichloromethane (20 mL) with rapid stirring. $[^nBu_2Sn(S_2N_2)]_2$ (0.16 g, 0.3 mmol) was then added to the suspension, which was stirred for a further 30 mins, during which time the suspension turned dark red in colour. The solution was then filtered through celite and evaporated to dryness. The red-brown residue was then extracted with methanol (*ca.* 30 mL) producing a golden-yellow solution which was filtered through celite once more. The volume of the solution was then reduced to *ca.* 5 mL and 3 drops of DBU were added producing a dark red colour. The solution was evaporated to dryness once more and the residue washed with ether. Crystals for X-ray crystallography were grown *via* slow diffusion of hexane into a solution of the product in dichloromethane. Yield: 72 mg (0.2 mmol), 34 %.

Elemental Analysis for $Pd(S_2N_2)(bipy)\cdot 0.5CH_2Cl_2$ (%, calculated in brackets): C, 32.60 (31.75); H, 2.58 (2.28); N, 14.09 (14.10).

10.4.12. Preparation of $Pt(S_2N_2)(bipy)$ (11)

$PtCl_2(bipy)$ (0.14 g, 0.36 mmol) was suspended in dichloromethane (120 mL) in a 250 mL round-bottomed flask wrapped in aluminium foil so as to prevent light

coming into contact with the reaction. [^{n}Bu$_2$Sn(S$_2$N$_2$)]$_2$ (0.12 g, 0.18 mmol) was added to the suspension, which was stirred for a further 30 mins, during which time the suspension turned dark purple in colour. The solution was then filtered through celite and evaporated to dryness. The dark red-brown residue was then extracted with methanol (*ca.* 30 mL) producing a red solution which was filtered through celite once more. The volume of the solution was then reduced to *ca.* 5 mL and 3 drops of DBU were added. The solution was evaporated to dryness once more and the residue washed with diethyl ether. Crystals for X-ray crystallography were grown in darkness *via* slow diffusion of hexane into a solution of the product in dichloromethane. Yield: 38 mg (0.09 mmol), 25 %.

Elemental Analysis (%, calculated in brackets): C, 30.32 (27.09); H, 2.35 (1.82); N, 11.50 (12.64).

10.4.13. Preparation of [Pt(S$_2$N$_2$H)(bipy)][BF$_4$] (12)

PtCl$_2$(bipy) (0.14 g, 0.36 mmol) was suspended in dichloromethane(120 mL) in a 250 mL round-bottomed flask wrapped in aluminium foil so as to prevent light coming into contact with the reaction. [^{n}Bu$_2$Sn(S$_2$N$_2$)]$_2$ (0.12 g, 0.18 mmol) was added to the suspension, which was stirred for a further 30 mins, during which time the suspension turned dark purple in colour. The solution was then filtered through celite and 3 drops of HBF$_4$ (50-54% w/v in diethyl ether) were added producing a brown precipitate. Attempts to grow crystals for X-ray crystallography were unsuccessful. Yield: 0.026 g (0.05 mmol), 14 %.

Elemental Analysis (%, calculated in brackets): C, 24.10 (22.61); H, 1.43 (1.71); N, 10.06 (10.54).

10.4.14. Attempted preparation of $Pt(S_2N_2)(PPh_3)_2$

Liquid ammonia (30 mL) was condensed under nitrogen using an ammonia condenser filled with dry ice and acetone into a dry Schlenk tube in a dry ice/acetone bath. To this, $[S_4N_3]Cl$ (0.102 g, 0.5 mmol) was added. After stirring for 30 mins, *cis*-$PtCl_2(PPh_3)_2$ (0.395 g , 0.5 mmol) was added rapidly. The solution was allowed to warm to room temperature and the ammonia gas blown off under a stream of nitrogen. The residue was placed under vacuum to remove any excess ammonia before being dissolved in dichloromethane and filtered through celite. Precipitation of the product could not be achieved through addition of hexane, however crystals were grown *via* the slow diffusion of hexane into a solution of the crude product in dichloromethane. X-ray crystallography revealed the pink crystals formed to be the *trans*-isomer of the starting material.

10.5. Preparation of Trisulfur-Mononitrido Complexes

10.5.1. Preparation of $[Pt(S_3N)(P(OMe)_3)_2][BF_4]$ (13)

$Hg(OC_2H_5)_2$ (133 mg, 0.45 mmol) and $[S_7N]H$ (216 mg, 0.9 mmol) were stirred together in methanol (40 mL) for 30 mins at -35 °C. The resulting pale yellow precipitate ($Hg(S_7N)_2$) was filtered off. $Hg(S_7N)_2$ (0.21 g, 0.31 mmol), $PtCl_2(P(OMe)_3)_2$ (0.16 g, 0.31 mmol) and $AgBF_4$ (0.064 g, 0.31 mmol) were dissolved in dichloromethane (10 mL) and stirred for 1 h. The resulting yellow solution was filtered through celite. Attempts to isolate the product or grow crystals

suitable for crystallography were unsuccessful, however the ^{31}P NMR spectrum displayed an AX splitting characteristic of an $[S_3N]^-$ complex.

$^{31}P\{^1H\}$ NMR (C_6D_6, 296 K): $\delta_A = 80.8$ ($^1J_{P\text{-}Pt} = 4953$ Hz), $\delta_X = 92.2$ ($^1J_{P\text{-}Pt} = 4176$ Hz), $^2J_{P\text{-}P} = 38$.

10.5.2. Preparation of $[Pt(S_3N)(P(OMe)_2Ph)_2][BF_4]$ (14)

$Hg(OC_2H_5)_2$ (133 mg, 0.45 mmol) and $[S_7N]H$ (216 mg, 0.9 mmol) were stirred together in methanol (40 mL) for 30 mins at -35 °C. The resulting pale yellow precipitate ($Hg(S_7N)_2$) was filtered off. $Hg(S_7N)_2$ (0.21 g, 0.31 mmol), $PtCl_2(P(OMe)_2Ph)_2$ (0.19 g, 0.31 mmol) and $AgBF_4$ (0.064 g, 0.31 mmol) were dissolved in dichloromethane (10 mL) and stirred for 1 h. The resulting yellow solution was filtered through celite. Attempts to isolate the product or grow crystals suitable for crystallography were unsuccessful, however the ^{31}P NMR spectrum displayed an AX splitting characteristic of an $[S_3N]^-$ complex.

$^{31}P\{^1H\}$ NMR (C_6D_6, 297 K): $\delta_A = 104.4$ ($^1J_{P\text{-}Pt} = 4073$ Hz), $\delta_X = 114.4$ ($^1J_{P\text{-}Pt} = 3446$ Hz), $^2J_{P\text{-}P} = 31$.

10.5.3. Preparation of $[Pt(S_3N)(P(OMe)Ph_2)_2][BF_4]$ (15)

$Hg(OC_2H_5)_2$ (133 mg, 0.45 mmol) and $[S_7N]H$ (216 mg, 0.9 mmol) were stirred together in methanol (40 mL) for 30 mins at -35 °C. The resulting pale yellow precipitate ($Hg(S_7N)_2$) was filtered off. $Hg(S_7N)_2$ (0.3 g, 0.44 mmol), $PtCl_2(P(OMe)_2Ph)_2$ (0.31 g, 0.44 mmol) and $AgBF_4$ (0.085 g, 0.44 mmol) were dissolved in dichloromethane (10 mL) and stirred for 1 h. The resulting yellow solution was filtered through celite. Attempts to isolate the product or grow crystals

suitable for crystallography were unsuccessful, however the ^{31}P NMR spectrum displayed an AX splitting characteristic of an $[S_3N]^-$ complex.

$^{31}P\{^1H\}$ NMR (C_6D_6, 294 K): $\delta_A = 89.7$ ($^1J_{P\text{-}Pt}$= 3578 Hz), $\delta_X = 93.7$ ($^1J_{P\text{-}Pt}$= 3045 Hz), $^2J_{P\text{-}P}$= 24.

10.6. Preparation of Monoselenium-Monosulfur-Dinitrido Complexes

10.6.1. Preparation of $Pt(SeSN_2)(P(OMe)_3)_2$ (16)

Liquid ammonia (30 mL) was condensed under nitrogen using an ammonia condenser filled with dry ice and acetone into a dry Schlenk tube in a dry ice/acetone bath. To this, $[S_4N_3]Cl$ (0.16 g, 0.78 mmol) and $SeCl_4$ (0.858 g, 3.9 mmol) was added. After stirring for 30 mins, *cis*-$PtCl_2(P(OMe)_3)_2$ (0.206 g, 0.5 mmol) was added rapidly. The solution was allowed to warm to room temperature and the ammonia gas blown off under a stream of nitrogen. The residue was dried under vacuum to remove any excess ammonia, before being dissolved in dichloromethane and filtered through celite. The product was obtained by column chromatography using a silica column and 90 % CH_2Cl_2-10 % MeOH as the eluent and then precipitating *via* slow addition of hexane to the fraction to give yellow-brown crystals. Crystals for X-ray crystallography were grown *via* slow diffusion of hexane into a solution of the product in dichloromethane. Yield: 0.222 g (0.38 mmol), 76 %.

Elemental Analysis (%, calculated in brackets): C, 12.76 (12.37); H, 2.70 (3.12); N, 4.94 (4.81).

$^{31}P\{^{1}H\}$ NMR (C_6D_6, 297 K): δ_A = 106.0 ($^{1}J_{P\text{-}Pt}$= 4530 Hz), δ_X = 108.1 ($^{1}J_{P\text{-}Pt}$= 4571 Hz), $^{2}J_{P\text{-}P}$= 49, $^{2}J_{P\text{-}Se(trans)}$= 94.

Infra Red: 3426m, 3020w, 2949m, 2840m, 1834w, 1560w, 1439s, 1179s, 1068s, 1023s, 923m, 815s, 760s, 705s, 633m, 541s, 492s, 401m, 357m, 315w cm^{-1}

10.6.2. Preparation of $Pt(SeSN_2)(P(OMe)_2Ph)_2$ (17)

Liquid ammonia (30 mL) was condensed under nitrogen using an ammonia condenser filled with dry ice and acetone into a dry Schlenk tube in a dry ice/acetone bath. To this, $[S_4N_3]Cl$ (0.16 g, 0.78 mmol) and $SeCl_4$ (0.858 g, 3.9 mmol) was added. After stirring for 30 mins, *cis*-$PtCl_2(P(OMe)_2Ph)_2$ (0.303 g, 0.5 mmol) was added rapidly. The solution was allowed to warm to room temperature and the ammonia gas blown off under a stream of nitrogen. The residue was placed under vacuum to remove any excess ammonia, before being dissolved in dichloromethane and filtered through celite. The product was obtained by column chromatography using a silica column and 90 % CH_2Cl_2-10 % MeOH as the eluent and then precipitating *via* slow addition of hexane to the fraction to give a tan-brown solid. Crystals for X-ray crystallography were grown *via* slow diffusion of hexane into a solution of the product in dichloromethane. Yield: 0.172 g (0.26 mmol), 51 %).

Elemental Analysis for $Pt(SeSN_2)(P(OMe)_2Ph)_2 \cdot 0.5CH_2Cl_2$ (%, calculated in brackets): C, 27.38 (27.64); H, 2.82 (3.23); N, 4.71 (3.91).

$^{31}P\{^{1}H\}$ NMR (C_6D_6, 297 K): δ_A = 122.9 ($^{1}J_{P\text{-}Pt}$= 3868 Hz), δ_X = 124.8 ($^{1}J_{P\text{-}Pt}$= 3900 Hz), $^{2}J_{P\text{-}P}$= 33, $^{2}J_{P\text{-}Se(trans)}$= 75.

Infra Red: 3208m, 3052w, 2989w, 2939s, 2836m, 2705m, 1983w, 1831m, 1777m, 1619w, 1589w, 1572w, 1482m, 1437s, 1336w, 1307w, 1255m, 1179s, 1118s, 1071s,

1021s, 925m, 814s, 756s, 710s, 634m, 617m, 578s, 556s, 490s, 402w, 357m, 318w, 298w cm^{-1}.

10.6.3. Preparation of $Pt(SeSN_2)(P(OMe)Ph_2)_2$ (18)

Liquid ammonia (30 mL) was condensed under nitrogen using an ammonia condenser filled with dry ice and acetone into a dry Schlenk tube in a dry ice/acetone bath. To this, $[S_4N_3]Cl$ (0.16 g, 0.78 mmol) and $SeCl_4$ (0.858 g, 3.9 mmol) was added. After stirring for 30 mins, *cis*-$PtCl_2(P(OMe)_2Ph)_2$ (0.365 g, 0.5 mmol) was added rapidly. The solution was allowed to warm to room temperature and the ammonia gas blown off under a stream of nitrogen. The residue was placed under vacuum to remove any excess ammonia, before being dissolved in dichloromethane and filtered through celite. The product was obtained by column chromatography using a silica column and 90 % CH_2Cl_2-10 % MeOH as the eluent and then precipitating *via* slow addition of hexane to the fraction to give a dark grey-brown solid. Crystals for X-ray crystallography were grown *via* slow diffusion of hexane into a solution of the product in dichloromethane. Yield: 0.242 g (0.32 mmol), 63 %).

Elemental Analysis for $Pt(SeSN_2)(P(OMe)Ph_2)_2 \cdot 0.5CH_2Cl_2$ (%, calculated in brackets): C, 39.42 (39.34); H, 2.96 (3.36); N, 4.14 (3.46).

$^{31}P\{^1H\}$ NMR (C_6D_6, 297 K): $\delta_A = 89.3$ ($^1J_{P\text{-}Pt} = 3309$ Hz), $\delta_X = 103.1$ ($^1J_{P\text{-}Pt} = 3391$ Hz), $^2J_{P\text{-}P} = 26$, $^2J_{P\text{-}Se(trans)} = 66$.

Infra Red: 3430m, 3052w, 2941m, 2839w, 1970w, 1819w, 1628m, 1588w, 1572w, 1481m, 1435s, 1310w, 1178m, 1159m, 1106s, 1059s, 1040s, 999m, 922w, 853w, 774m, 746s, 697s, 634m, 617w, 567m, 542s, 504m, 476m, 446w, 402w, 355w cm^{-1}.

10.6.4. Preparation of $Pt(SeSN_2)(PPh_3)_2$[43] (19)

Liquid ammonia (30 mL) was condensed under nitrogen using an ammonia condenser filled with dry ice and acetone into a dry Schlenk tube in a dry ice/acetone bath. To this, $[S_4N_3]Cl$ (0.16 g, 0.78 mmol) and $SeCl_4$ (0.858 g, 3.9 mmol) was added. After stirring for 30 mins, *cis*-$PtCl_2(PPh_3)_2$ (0.395 g, 0.5 mmol) was added rapidly. The solution was allowed to warm to room temperature and the ammonia gas blown off under a stream of nitrogen. The residue was placed under vacuum to remove any excess ammonia, before being dissolved in dichloromethane and filtered through celite. The product was obtained by column chromatography using a silica column and 90 % CH_2Cl_2-10 % MeOH as the eluent. Crystals were grown *via* the slow diffusion of hexane into a solution of the crude product in dichloromethane. $^{31}P\{^1H\}$ NMR (C_6D_6, 294 K): $\delta_A = 7.2$ ($^1J_{P\text{-}Pt} = 2956$ Hz), $\delta_X = 22.6$ ($^1J_{P\text{-}Pt} = 2995$ Hz), $^2J_{P\text{-}P} = 21$, $^2J_{P\text{-}Se(trans)} = 54$.

10.7. Preparation of ndsdsd-containing Complexes

10.7.1. Preparation of [Pt(ndsdsd)(COD)][2Cl] (36)

ndsdsd (80 mg, 0.13 mmol) and $PtCl_2(COD)$ (48 mg, 0.13 mmol) were dissolved in dichloromethane (15 mL) and stirred for 12 h. The solution was then filtered through celite and reduced in volume to *ca.* 5 mL. The product was then precipitated upon addition of hexane to give an off-white solid. Crystals suitable for X-ray crystallography were grown *via* slow diffusion of hexane into a solution of the product in dichloromethane. Yield: 105 mg (0.098 mmol), 75 %.

Elemental Analysis for [Pt(ndsdsd)(COD)][2Cl]·CH_2Cl_2 (%, calculated in brackets): C, 49.98 (50.33); H, 4.49 (4.13); N, 5.29 (5.21).

10.7.2. Preparation of [Pt(ndsdsd)(P(OMe)$_3$)(P(O)(OMe)$_2$)][Cl] (37)

$PtCl_2(P(OMe)_3)_2$ (150 mg, 0.3 mmol) and ndsdsd (180 mg, 0.3 mmol) was dissolved in wet dichloromethane (20 mL) and stirred for 1 h. The solution was then filtered through celite and the volume reduced to *ca.* 5 mL. The product was then precipitated upon addition of hexane to give an off-white solid. Crystals suitable for X-ray crystallography were grown *via* slow diffusion of hexane into a solution of the product in dichloromethane. Yield: 258 mg (0.23 mmol), 77 %.

Elemental Analysis for [Pt(ndsdsd)(P(OMe)$_3$)(P(O)(OMe)$_2$)][Cl]·CH_2Cl_2 (%, calculated in brackets): C, 43.25 (43.36); H, 3.79 (4.07); N, 4.69 (4.82).

$^{31}P\{^1H\}$ NMR (C_6D_6, 297 K): δ_A = 31.4 ($^1J_{P\text{-}Pt}$= 6207 Hz), δ_X = 84.2 ($^1J_{P\text{-}Pt}$= 4812 Hz), $^2J_{P\text{-}P}$= 40.

Infra Red (KBr): 3407s, 1639m, 1472m, 1446s, 1306w, 1261s, 1139s, 1074s, 1026s, 982s cm^{-1}.

10.7.3. Preparation of [Pd(ndsdsd)$_2$][Pd$_2$Cl$_6$] (38)

$PtCl_2(PhCN)_2$ (38 mg, 0.08 mmol) and ndsdsd (50 mg, 0.08 mmol) were dissolved in dichloromethane (60 mL) and stirred for 24 h. The solution was then filtered through celite and the volume reduced to *ca.* 5 mL. Yellow, aserose crystals of the product were grown *via* slow diffusion of hexane into this solution. Yield: 65 mg (0.035 mmol), 44 %.

Elemental Analysis for $[Pd(ndsdsd)_2][Pd_2Cl_6]\cdot 0.5CH_2Cl_2$ (%, calculated in brackets): C, 48.48 (48.27); H, 3.39 (3.41); N, 6.15 (6.21).

Infra Red (KBr): 3450s, 1630w, 1472m, 1445s, 1307w, 1261m, 1207s, 1075s, 1030s, 982s cm^{-1}.

10.7.4. Preparation of [Pd(ndsdsd)(bipy)][2Cl] (39)

$PdCl_2$(bipy) (0.1 g, 0.3 mmol) was suspended in dichloromethane (60 mL) *via* rapid stirring. To this, ndsdsd (0.184 g, 0.3 mmol) was added upon which the solution turned a clear yellow colour. The solution was then filtered through celite and the volume reduced to *ca.* 5 mL. The product was precipitated upon addition of hexane to give a bright yellow, crystalline solid. Crystals suitable for X-ray crystallography were grown *via* slow diffusion of hexane into a solution of the product in dichloromethane. Yield: 0.264 g (0.25 mmol), 82 %.

Elemental Analysis for $[Pd(ndsdsd)(bipy)][2Cl]\cdot CH_2Cl_2\cdot 2H_2O$ (%, calculated in brackets): C, 52.94 (52.79); H, 3.72 (4.15); N, 8.01 (7.86).

Infra Red (KBr): 3374s, 1643m, 1604s, 1471s, 1446s, 1309w, 1262m, 1071s, 1011s, 979s cm^{-1}.

10.7.5. Preparation of $[AuCl_2(ndsdsd)][AuCl_4]$ (40)

$AuCl_3$ (49 mg, 0.163 mmol) and ndsdsd (100 mg, 0.163 mmol) were dissolved in dichloromethane (10 mL) and stirred for 1 h after which time the product had precipitated as a yellow powder. Crystals suitable for X-ray crystallography were grown *via* slow diffusion of diethyl ether into a solution of the product in methanol. Yield: 123 mg (0.10 mmol), 62 %.

Elemental Analysis (%, calculated in brackets): C, 37.01 (35.40); H, 1.85 (2.48); N, 4.63 (4.59).

Infra Red (KBr): 3449m, 1473m, 1447s, 1310w, 1260m, 1145s, 1065s, 1013m, 982s cm^{-1}.

10.7.6. Preparation of $[AuCl_2(ndsdsd)][PF_6]$ (41)

$AuCl_3$ (49 mg, 0.163 mmol) and LiCl (1 mg, 0.025 mmol) were dissolved in dichloromethane (3 mL) to which 1 drop of methanol had been added. To this, a solution of ndsdsd (100 mg, 0.163 mmol) in dichloromethane (3 mL) was added. $NaPF_6$ (27 mg, 0.163 mmol) was then added and the solution was then stirred under reflux for 1 h after which time the product had precipitated as a yellow powder. Attempts to grow crystals were unsuccessful. Yield: 150 mg (0.15 mmol), 90 %.

Elemental Analysis (%, calculated in brackets): C, 41.59 (42.07); H, 2.32 (2.94); N, 5.45 (4.96).

^1H NMR (CD_2Cl_2, 292 K): δ = 7.44-7.55 (m, 12H), 7.60-7.64 (m, 6H), 7.79-7.82 (m, 4H), 7.94-7.97 (m, 8H).

$^{31}P\{^1H\}$ NMR (C_6D_6, 297 K): δ = -143.8 (sep, 1P, $^1J_{P\text{-}F}$ = 711 Hz).

Infra Red (KBr): 3449m, 1472m, 1447s, 1310w, 1262m, 1206w, 1145s, 1070s, 1013s, 982s cm^{-1}.

Further Work

In the area of metal-centred, 5-membered $[E_2N_2]^{2-}$ and $[E_2N_2H]^-$ complexes a great deal of work can still be done. $Pt(E_2N_2)(P(OR')_nR_{3-n})_2$ and $[Pt(E_2N_2H)(P(OR')_nR_{3-n})_2][X]$ complexes for the known ligands $[S_2N_2H]^-$, $[SeSN_2H]^-$, $[Se_2N_2]^{2-}$, $[Se_2N_2H]^-$, $[TeSN_2]^{2-}$ and $[TeSN_2H]^-$ have yet to be synthesised. The study of these complexes would give a fuller picture of the *trans*-influence of the chalcogen-nitrogen fragments and the effect of the different electrical properties of $P(OR')_nR_{3-n}$ ligands on the bond order within the rings. Synthesis of the as yet unreported ligands $[Te_2N_2]^{2-}$, $[Te_2N_2H]^-$, $[TeSeN_2]^{2-}$ and $[TeSeN_2H]^-$ may also be possible, though new synthetic strategies will need to be devised for these as proposed in section 1.3. Developing selenium, tellurium and mixed-chalcogen analogues of the metathetical reagent $[R_2Sn(S_2N_2)]_2$ would also be a useful strategy to this end.

In addition to the $P(OR')_nR_{3-n}$-containing complexes, metal-chalcogen-nitrogen compounds containing ligands without phosphorus could also be possible, though most would be more difficult to assess by NMR. Moving down group 15, arsine and stibine dichloride compounds with platinum centres are known.[180] These compounds should behave in a similar fashion to phosphines. Other potential ligands which could also be investigated include SR_2, SOR_2, SeR_2 and TeR_2 for all of which the relevant platinum dichlorides are known.[181]

Work into attaching disulfur dinitrido ligands to new central atoms and planar backbones can be attempted. Theoretically, complexes where the central atom is boron, aluminium, carbon and silicon are possible and some work could be attempted

to this end.[182] One seemingly plausible strategy for a boron centred complex would be the reaction of the compound $PtCl(PR_3)_2BCl_2$[183] with $[S_4N_3]Cl$ in liquid ammonia.

Working towards a more accurate indicator of Pt-P bond length using the $^1J_{Pt\text{-}P}$ value, a more extensive literature survey will be required. Further studies in the *trans*-$PtX_2(P(OR')_nR_{3-n})_2$ complexes could also prove interesting as few examples of *trans*-phosphite, phosphonite or phosphinite complexes are known. $PtX_2(P(OR')_nR_{3-n})_2$ complexes could be further studied using solid-state NMR; as many of the complexes exhibit two distinct bond lengths in their X-ray crystal structures, yet only one ^{31}P NMR signal in solution, couplings specific to individual bond lengths could be measured in solid-state.

Further work involving the ndsdsd ligand should revolve around growing better quality crystals of the complexes reported in Chapter 5. This could potentially be achieved using counter-ions other than Cl^- such as ClO_4^- and PF_6. Further attempts to synthesise a $P(OR')_nR_{3-n}$ series for this ligand would also be very useful in probing its *trans*-influence and donor properties.

References

[1] P. F. Kelly, J. D. Woollins, *Transition Met. Chem.* **1988**, *13*, 77.
[2] W. L. Jolly, M. Becke-Goering, *Inorg. Chem.* **1962**, *1*, 76.
[3] D. Clarke, *J. Chem. Soc.* **1952**, 1615.
[4] J. M. Jolliffe, P. F. Kelly, J. D. Woollins, *J. Chem. Soc., Dalton Trans.* **1989**, 2179.
[5] C. W. Allen, P. F. Kelly, J. D. Woollins, *J. Chem. Soc., Dalton Trans.* **1991**, 1343.
[6] P. F. Kelly, A. M. Z. Slawin, D. J. Williams, J. D. Woollins, *Polyhedron* **1991**, *10*, 2337.
[7] R. L. Patton, K. N. Raymond, *Inorg. Chem.* **1969**, *8*, 2426.
[8] U. Thewalt, B. Müller, *Z. Anorg. Allg. Chem.* **1980**, *462*, 214.
[9] U. Thewalt, *Z. Anorg. Allg. Chem.* **1982**, *37B*, 276.
[10] V. C. Ginn, P. F. Kelly, A. M. Z. Slawin, D. J. Williams, J. D. Woollins, *J. Chem. Soc., Dalton Trans.* **1992**, 963
[11] M. B. Hursthouse, M. Motevalli, P. F. Kelly, J. D. Woollins, *Polyhedron* **1989**, *8*, 997.
[12] P. F. Kelly, J. D. Woollins, *Polyhedron* **1989**, *8*, 2907.
[13] P. F. Kelly, R. N. Sheppard, J. D. Woollins, *Polyhedron* **1992**, *11*, 2605.
[14] B. J. McCormick, B. M. Anderson, *J. Inorg. Nucl. Chem.* **1970**, *32*, 3414.
[15] A. A. Bhattacharyya, J. A. McLean, A. G. Turner, *Inorg. Chim. Acta.* **1979**, *34*, L199.
[16] F. Edelmann, *J. Organomet. Chem.* **1982**, *228*, C47.
[17] R. Jones, P. F. Kelly, D. J. Williams, J. D. Woollins, *Polyhedron* **1985**, *4*, 1947.
[18] J. Bojes, T. Chivers, I. Drummond, G. MacLean, *Inorg. Chem.* **1978**, *17*, 3668.
[19] P. A. Bates, M. B. Hursthouse, P. F. Kelly, J. D. Woollins, *J. Chem. Soc., Dalton Trans.* **1986**, 2367
[20] R. Jones, P. F. Kelly, C. P. Warrens, D. J. Williams, J. D. Woollins, *J. Chem. Soc., Chem. Commun.* **1986**, 711
[21] J. Weiss, *Fortsch. Chem. Forsch.* **1966**, *5*, 635.
[22] J. D. Woollins, R. Grinter, M. K. Johnson, A. J. Thomson, *J. Chem. Soc., Dalton Trans.* **1980**, 1910.
[23] P. F. Kelly, J. D. Woollins, *Polyhedron* **1986**, *5*, 607.
[24] R. Jones, P. F. Kelly, D. J. Williams, J. D. Woollins, *Polyhedron* **1987**, *6*, 1541.
[25] H. W. Roesky, H. Wiezer, *Angew. Chem.* **1975**, *87*, 254.
[26] R. Jones, C. P. Warrens, D. J. Williams, J. D. Woollins, *J. Chem. Soc., Dalton Trans.* **1987**, 907
[27] R. Jones, P. F. Kelly, D. J. Williams, J. D. Woollins, *J. Chem. Soc., Dalton Trans.* **1988**, 803
[28] P. F. Kelly, J. D. Woollins, *J. Chem. Soc., Dalton Trans.* **1988**, 1053.
[29] H. Prestel, U. Schindewolf, *Z. Anorg. Allg. Chem.* **1987**, *551*, 21.
[30] P. Dubois, J. P. Lelieur, G. Lepoutre, *Inorg. Chem.* **1988**, *27*, 73.

[31] P. S. Belton, I. P. Parkin, D. J. Williams, J. D. Woollins, *J. Chem. Soc., Chem. Commun.* **1988**, 1479.
[32] T. Chivers, K. J. Schmidt, *J. Chem. Soc., Chem. Commun.* **1990**, 1342.
[33] I. P. Parkin, J. D. Woollins, *J. Chem. Soc., Dalton Trans.* **1990**, 519.
[34] R. Short, M. B. Hursthouse, T. G. Purcell, J. D. Woollins, *J. Chem. Soc., Chem. Commun.* **1987**, 407.
[35] I. P. Parkin, A. M. Z. Slawin, D. J. Williams, J. D. Woollins, *Polyhedron* **1989**, *8*, 835.
[36] J. Weiss, *Z. Anorg. Allg. Chem.* **1985**, *521*, 44.
[37] J. Weiss, *Z. Anorg. Allg. Chem.* **1986**, *532*, 184.
[38] J. Weiss, *Z. Anorg. Allg. Chem.* **1986**, *542*, 137.
[39] K. Bergemann, M. Kustos, P. Krüger, R. Steudel, *Angew. Chem. Int. Ed.* **1995**, *34*, 1330.
[40] P. F. Kelly, A. M. Z. Slawin, *Angew. Chem. Int. Ed.* **1995**, *34*, 1758.
[41] P. F. Kelly, A. M. Z. Slawin, A. Soriano-Rama, *J. Chem. Soc., Dalton Trans.* **1997**, 559.
[42] C. A. O'Mahoney, I. P. Parkin, D. J. Williams, J. D. Woollins, *Polyhedron* **1989**, *8*, 2215.
[43] I. P. Parkin, J. D. Woollins, *J. Chem. Soc., Dalton Trans.* **1990**, 925
[44] J. Adel, C. Ergezinger, R. Figge, K. Dehnicke, *Z. Naturforsch., B: Chem. Sci.* **1988**, *43*, 639.
[45] P. F. Kelly, I. P. Parkin, A. M. Z. Slawin, D. J. Williams, J. D. Woollins, *Angew. Chem. Int. Ed.* **1989**, *28*, 1047.
[46] P. F. Kelly, A. M. Z. Slawin, D. J. Williams, J. D. Woollins, *Polyhedron* **1990**, *9*, 1567.
[47] P. F. Kelly, J. D. Woollins, *Polyhedron* **1993**, *12*, 1129.
[48] V. C. Ginn, P. F. Kelly, J. D. Woollins, *Polyhedron* **1994**, *13*, 1501.
[49] A. G. Awere, J. Passmore, P. S. White, T. Klapoetke, *J. Chem. Soc., Chem. Commun.* **1989**, 1415
[50] W. Massa, C. Lau, M. Möhlen, B. Neumüller, K. Dehnicke, *Angew. Chem. Int. Ed.* **1998**, *37*, 2840.
[51] A. Haas, J. Kasprowski, M. Pryka, *J. Chem. Soc., Chem. Commun.* **1992**, 1144.
[52] P. F. Kelly, A. M. Z. Slawin, D. J. Williams, J. D. Woollins, *Polyhedron* **1990**, *9*, 2659.
[53] A. V. Zibarev, G. G. Furin, G. G. Yakobson, *Izv. Akad. Nauk. SSSR* **1985**, 2774.
[54] M. Björgvinsson, H. W. Roesky, F. Pauer, D. Stalke, G. M. Sheldrick, *Inorg. Chem.* **1990**, *29*, 5140.
[55] O. Glemser, H. Schröder, *Z. Anorg. Allg. Chem.* **1956**, *284*, 97.
[56] O. Glemser, H. Richert, *Z. Anorg. Allg. Chem.* **1961**, *307*, 313.
[57] H. Richert, O. Glemser, *Z. Anorg. Allg. Chem.* **1961**, *307*, 328.
[58] A. F. Clifford, C. S. Kobayashi, *Inorg. Chem.* **1965**, *4*, 571.
[59] A. F. Clifford, J. S. Harman, *J. Chem. Soc., Dalton Trans.* **1974**, 571.
[60] A. F. Clifford, J. L. Howell, D. L. Wooton, *J. Fluorine Chem.* **1977**, *11*, 433.
[61] T. Yoshimura, K. Hamada, M. Imado, K. Hamata, K. Tomoda, T. Fujii, H. Morita, C. Shimasaki, S. Ono, E. Tsukurimichi, N. Furukawa, T. Kimura, *J. Org. Chem.* **1997**, *62*, 3802.
[62] T. Fujii, A. Itoh, K. Hamata, T. Yoshimura, *Tetrahedron Lett.* **2001**, *42*, 5041.
[63] T. Fujii, T. Kousaka, T. Yoshimura, *Tetrahedron Lett.* **2002**, *43*, 5841.

[64] T. Yoshimura, T. Fujii, S. Murotani, S. Miyoshi, T. Fujimori, M. Ohkubo, S. Ono, H. Morita, *J. Organomet. Chem.* **2000**, *611*, 272.
[65] T. Fujii, T. Fujimori, S. Miyoshi, S. Murotani, M. Ohkubo, T. Yoshimura, *Heteroat. Chem.* **2001**, *12*, 263.
[66] T. Fujii, M. Kanno, M. Hirata, T. Fujimori, T. Yoshimura, *Inorg. Chem.* **2005**, *44*, 8653.
[67] T. Yoshimura, T. Fujii, H. Dai, *Chem. Lett.* **2002**, 1000.
[68] T. Fujii, M. Kanno, M. Hirata, T. Nakahodo, T. Wakahara, T. Akasaka, *Inorg. Chim. Acta.* **2008**, *361*, 2540.
[69] J. Bailar, H. Itatani, *Inorg. Chem.* **1965**, *4*, 1618.
[70] M. J. Church, M. J. Mays, *J. Inorg. Nucl. Chem.* **1971**, *33*, 253.
[71] F. J. Ramos-Lima, A. G. Quiroga, J. M. Pérez, M. Font-Bardía, X. Solans, C. Navarro-Ranninger, *Eur. J. Inorg. Chem.* **2003**, *2003*, 1591.
[72] S. H. Mastin, P. Haake, *J. Chem. Soc. D* **1970**, 202.
[73] R. D. Gillard, M. F. Pilbrow, *J. Chem. Soc., Dalton Trans.* **1974**, 2320.
[74] S. H. Mastin, *Inorg. Chem.* **1974**, *13*, 1003.
[75] A. Yahav, I. Goldberg, A. Vigalok, *J. Am. Chem. Soc.* **2003**, *125*, 13634.
[76] T. G. Appleton, H. C. Clark, L. E. Manzer, *Coord. Chem. Rev.* **1973**, *10*, 335.
[77] L. J. Manojlovic-Muir, K. W. Muir, *Inorg. Chim. Acta.* **1974**, *10*, 47.
[78] D. S. Marynick, *J. Am. Chem. Soc.* **1984**, *106*, 4064.
[79] A. G. Orpen, N. G. Connelly, *J. Chem. Soc., Chem. Commun.* **1985**, 1310.
[80] W. Strohmeier, F.-J. Müller, *Chem. Ber.* **1967**, *100*, 2812.
[81] W. D. Horrocks Jr, R. C. Taylor, *Inorg. Chem.* **1963**, *2*, 723.
[82] F. H. Allen, A. Pidcock, C. R. Waterhouse, *J. Chem. Soc. A.* **1970**, 2087.
[83] Q.-B. Bao, S. J. Geib, A. L. Rheingold, T. B. Brill, *Inorg. Chem.* **1987**, *26*, 3453.
[84] T. Allman, *J. Magn. Res.* **1989**, *83*, 637.
[85] S. O. Grim, R. L. Keiter, W. McFarlane, *Inorg. Chem.* **1967**, *6*, 1133.
[86] R. Favez, R. Roulet, A. A. Pinkerton, D. Schwartzenbach, *Inorg. Chem.* **1980**, *19*, 1356.
[87] R. Mas-Ballesté, G. Aullón, P. A. Champkin, W. Clegg, C. Mégret, P. González-Duarte, A. Lledós, *Chem. Eur. J.* **2003**, *9*, 5023.
[88] J. A. Rahn, L. Baltusis, J. H. Nelson, *Inorganic Chemistry* **1990**, *29*, 750.
[89] L. Rigamonti, C. Manassero, M. Rusconi, M. Manassero, A. Pasini, *J. Chem. Soc., Dalton Trans.* **2009**, 1206.
[90] T. Cardolaccia, Y. Li, K. S. Schanze, *J. Am. Chem. Soc.* **2008**, *130*, 2535.
[91] V. P. Balema, J. W. Wiench, M. Pruski, V. K. Pecharsky, *Chem. Commun.* **2002**, 1606.
[92] N. Ahmad, E. W. Ainscough, T. A. James, S. D. Robinson, *J. Chem. Soc., Dalton Trans.* **1973**, 1148
[93] D. A. Couch, S. D. Robinson, J. N. Wingfield, *J. Chem. Soc., Dalton Trans.* **1974**, 1309.
[94] R. Favez, R. Roulet, *Inorg. Chem.* **1981**, *20*, 1598.
[95] S. J. Sabounchei, V. Jodaien, S. Samiee, *Phosphorus, Sulfur Silicon Relat. Elem.* **2004**, *179*, 473.
[96] S. O. Grim, R. L. Keiter, *Inorg. Chim. Acta.* **1970**, *4*, 56.
[97] S. J. Sabounchei, A. Naghipour, *Asian J. Chem.* **2001**, *13*, 1011.
[98] G. G. Messmer, E. L. Amma, *Inorg. Chem.* **2002**, *5*, 1775.
[99] H.-K. Fun, S. Chantrapromma, Y.-C. Liu, Z.-F. Chen, H. Liang, *Acta Crystallogr. Sect. E: Struct. Rep. Online* **2006**, *62*, m1252.

[100] A. Del Pra, G. Zanotti, *Cryst. Struct. Commun.* **1979**, *8*, 737.
[101] W. M. Attia, G. Balducci, M. Calligaris, *Acta Crystallogr., Sect. C: Cryst. Struct. Commun.* **1987**, *43*, 1053.
[102] K.-C. Ho, G. M. McLaughlin, M. McPartlin, G. B. Robertson, *Acta Crystallogr., Sect. B: Struct. Crystallogr. Cryst. Chem.* **1982**, *38*, 421.
[103] S. Otto, A. J. Muller, *Acta Crystallogr., Sect. C: Cryst. Struct. Commun.* **2001**, *57*, 1405.
[104] W. Domanska-Babul, J. Chojnacki, J. Pikies, *Acta Crystallogr. Sect. E: Struct. Rep. Online* **2007**, *63*, m1956.
[105] W. Domanska-Babul, J. Pikies, J. Chojnacki, *Acta Crystallogr. Sect. E: Struct. Rep. Online* **2007**, *63*, m2583.
[106] S. J. Sabounchei, A. Naghipour, *Molecules* **2001**, *6*, 777.
[107] P. B. Hitchcock, B. Jacobson, A. Pidcock, *J. Organomet. Chem.* **1977**, *133*, 273.
[108] N. P. Rath, V. S. S. Kumar, M. Janka, G. K. Anderson, *Inorg. Chim. Acta.* **2007**, *360*, 2997.
[109] G. B. Robertson, P. A. Tucker, W. A. Wickramasinghe, *Aust. J. Chem.* **1986**, *39*, 1495.
[110] M. H. Johansson, S. Otto, *Acta Crystallogr., Sect. C: Cryst. Struct. Commun.* **2000**, *56*, e12.
[111] N. M. Boag, K. Mohan Rao, N. J. Terrill, *Acta Crystallogr., Sect. C: Cryst. Struct. Commun.* **1991**, *47*, 1064.
[112] P. B. Hitchcock, B. Jacobson, A. Pidcock, *J. Chem. Soc., Dalton Trans.* **1977**, 2038
[113] R. A. Jacobson, L. L. Martin, *Inorg. Chem.* **1971**, *10*, 1795.
[114] W. L. Steffen, G. J. Palenik, *Inorg. Chem.* **1976**, *15*, 2432.
[115] G. Ferguson, R. McCrindle, A. J. McAlees, M. Parvez, *Acta Crystallogr., Sect. B: Struct. Sci.* **1982**, *B38*, 2679.
[116] N. W. Alcock, J. H. Nelson, *Acta Crystallogr., Sect. C: Cryst. Struct. Commun.* **1985**, *C41*, 1748.
[117] G. Schultz, N. Y. Subbotina, C. M. Jensen, J. A. Golen, I. Hargittai, *Inorg. Chim. Acta.* **1992**, *191*, 85.
[118] I. Y. Guzman-Jimenez, K. H. Whitmire, *Acta Crystallogr., Sect. C: Cryst. Struct. Commun.* **1999**, *C55*, IUC9900028.
[119] A. M. Trzeciak, H. Bartosz-Bechowski, Z. Ciunik, K. Niesyty, J. J. Ziolkowski, *Can. J. Chem.* **2001**, *79*, 752.
[120] D. R. Powell, R. A. Jacobson, *Cryst. Struct. Commun.* **1980**, *9*, 1023.
[121] S. J. Sabounchei, A. Naghipour, J. F. Bickley, *Acta Crystallogr., Sect. C: Cryst. Struct. Commun.* **2000**, *C56*, e280.
[122] C. M. Crawforth, S. Burling, I. J. S. Fairlamb, A. R. Kapdi, R. J. K. Taylor, A. C. Whitwood, *Tetrahedron* **2005**, *61*, 9736.
[123] T. Debaerdemaeker, A. Kutoglu, G. Schmid, L. Weber, *Acta Crystallogr., Sect. B: Struct. Sci.* **1973**, *29*, 1283.
[124] A. M. Magill, B. F. Yates, K. J. Cavell, B. W. Skelton, A. H. White, *J. Chem. Soc., Dalton Trans.* **2007**, 3398.
[125] G. G. Mather, A. Pidcock, G. J. N. Rapsey, *J. Chem. Soc., Dalton Trans.* **1973**, 2095.
[126] R. J. Blau, J. H. Espenson, *Inorg. Chem.* **1986**, *25*, 878.
[127] J. S. Miller, A. J. Epstein, *Prog. Inorg. Chem.* **1976**, *20*, 1.

[128] H. M. Nugent, M. Rosenblum, P. Klemarcyzk, *J. Am. Chem. Soc.* **1993**, *115*, 3848.
[129] L. B. Coleman, M. J. Cohen, D. J. Sandman, F. G. Yamagishi, A. F. Garito, A. J. Heeger, *Solid. State. Comm.* **1973**, *12*, 1125.
[130] T. J. Kistenmacher, *Ann. N. Y. Acad. Sci.* **1978**, *313*, 333.
[131] A. J. Schultz, G. D. Stucky, R. H. Blessing, P. Coppens, *J. Am. Chem. Soc.* **1976**, *98*, 3194.
[132] M. Fontana, H. Chanzy, W. R. Caseri, P. Smith, A. P. H. J. Schenning, E. W. Meijer, F. Grohn, *Chem. Mater.* **2002**, *14*, 1730.
[133] J. Bremi, M. Fontana, W. Caseri, P. Smith, *Macromol. Symp.* **2006**, *235*, 80.
[134] L. V. Interrante, R. P. Messmer, *Inorg. Chem.* **1971**, *10*, 1174.
[135] J. Bremi, D. Brovelli, W. Caseri, G. Hahner, P. Smith, T. Tervoort, *Chem. Mater.* **1999**, *11*, 977.
[136] K. Krogmann, *Angew. Chem. Int. Ed.* **1969**, *8*, 35.
[137] T. R. Koch, P. L. Johnson, J. M. Williams, *Inorg. Chem.* **1977**, *16*, 640.
[138] J. M. Williams, A. J. Schultz, K. B. Cornett, R. E. Besinger, *J. Am. Chem. Soc.* **1978**, *100*, 5572.
[139] E. P. Goodings, *Endeavour* **1975**, *34*, 123.
[140] A. J. Schultz, C. C. Coffey, G. C. Lee, J. M. Williams, *Inorg. Chem.* **1977**, *16*, 2129.
[141] C.-H. Hsu, M. M. Labes, *J. Chem. Phys.* **1974**, *61*, 4640.
[142] H. G. Heal, *Academic Press* **1980**.
[143] R. Jones, P. F. Kelly, D. J. Williams, J. D. Woollins, *J. Chem. Soc., Chem. Commun.* **1985**, 1325
[144] S. M. Aucott, P. Bhattacharyya, H. L. Milton, A. M. Z. Slawin, J. D. Woollins, *New J. Chem.* **2003**, *27*, 1466.
[145] T. Chivers, F. Edelmann, U. Behrens, R. Drews, *Inorg. Chim. Acta.* **1986**, *116*, 145.
[146] S. M. Aucott, A. M. Z. Slawin, J. D. Woollins, *Can. J. Chem.* **2002**, *80*, 1481.
[147] B. D. Read, A. M. Z. Slawin, J. D. Woollins, *Acta Crystallogr. Sect. E: Struct. Rep. Online* **2007**, *63*, m751.
[148] D. Drew, J. R. Doyle, *Inorg. Synth.* **1972**, *13*, 47.
[149] P. F. Kelly, A. M. Z. Slawin, D. J. Williams, J. D. Woollins, *Polyhedron* **1988**, *7*, 1925.
[150] M. Maekawa, M. Munakata, S. Kitagawa, M. Nakamura, *Anal. Sci.* **1991**, *7*, 521.
[151] R. Jones, T. G. Purcell, D. J. Williams, J. D. Woollins, *Polyhedron* **1987**, *6*, 2165.
[152] G. Wolmershauser, C. R. Brulet, G. B. Street, *Inorg. Chem.* **1978**, *17*, 3586.
[153] I. P. Parkin, J. D. Woollins, P. S. Belton, *J. Chem. Soc., Dalton Trans.* **1990**, 511.
[154] M. Herberhold, W. Ehrenreich, *Angew. Chem.* **1982**, *94*, 637.
[155] P. F. Kelly, I. P. Parkin, R. N. Sheppard, J. D. Woollins, *Heteroat. Chem.* **1991**, *2*, 301.
[156] B. Rosenberg, L. Van Camp, T. Krigas, *Nature* **1965**, *205*, 698.
[157] A. Pidcock, *Adv. Chem. Ser.* **1982**, *196*, 1.
[158] A. Pidcock, R. E. Richards, L. M. Venanzi, *J. Chem. Soc., A* **1966**, 1707.
[159] K. S. Knirik, A. D. Troitskaya, R. R. Shagidullin, *Tr. Kazan. Khim.-Tekhnol. Inst.* **1967**, *No. 36*, 116.
[160] J. M. Jenkins, J. G. Verkade, *Inorg. Chem.* **1967**, *6*, 2250.

[161] A. M. Z. Slawin, P. G. Waddell, J. D. Woollins, *Acta Crystallogr., Sect. E: Struct. Rep. Online* **2009**, *E65*, m1392.
[162] A. M. Z. Slawin, P. G. Waddell, J. D. Woollins, *Acta Crystallogr. Sect. E: Struct. Rep. Online* **2007**, *63*, m2017.
[163] A. M. Z. Slawin, P. G. Waddell, J. D. Woollins, *Acta Crystallogr. Sect. E: Struct. Rep. Online* **2007**, *63*, m2018.
[164] P. Sharma, A. Cabrera, C. Alvarez, N. Rosas, E. Gomez, A. Toscano, *Anal. Sci.* **2003**, *19*, 1341.
[165] A. M. Z. Slawin, P. G. Waddell, J. D. Woollins, *Acta Crystallogr., Sect. E: Struct. Rep. Online* **2009**, *E65*, m1391.
[166] A. M. Z. Slawin, P. G. Waddell, J. D. Woollins, *Acta Crystallogr. Sect. E: Struct. Rep. Online* **2010**, *66*, m321.
[167] L. Rigamonti, A. Forni, M. Manassero, C. Manassero, A. Pasini, *Inorg. Chem. (Washington, DC, U. S.)* **2010**, *49*, 123.
[168] I. M. Al-Najjar, *Inorg. Chim. Acta.* **1987**, *128*, 93.
[169] G. J. Grant, D. F. Galas, D. G. VanDerveer, *Polyhedron* **2002**, *21*, 879.
[170] S. A. Aucott, A. M. Z. Slawin, J. D. Woollins, *Polyhedron* **2000**, *19*, 499.
[171] A. L. Fuller, F. R. Knight, A. M. Z. Slawin, J. D. Woollins, *in press*.
[172] Q.-B. Bao, T. B. Brill, *Inorg. Chem.* **1987**, *26*, 3447.
[173] J. Bojes, T. Chivers, I. Drummond, *Inorg. Synth.* **1978**, *18*, 203.
[174] P. Braunstein, R. Bender, J. Jud, *Inorg. Synth.* **1989**, *26*.
[175] G. T. Morgan, F. H. Burstall, *J. Chem. Soc.* **1934**, 965.
[176] M. R. Shehata, *Transition Met. Chem.* **2001**, *26*, 198.
[177] J. M. Jenkins, B. L. Shaw, *J. Chem. Soc. A.* **1966**, 770.
[178] A. M. Z. Slawin, P. G. Waddell, J. D. Woollins, *Acta Crystallogr. Sect. E: Struct. Rep. Online* **2010**, *E66*, m499.
[179] A. M. Z. Slawin, P. G. Waddell, J. D. Woollins, *Acta Crystallogr. Sect. E: Struct. Rep. Online* **2010**, *66*, m418.
[180] R. J. Goodfellow, J. G. Evans, P. L. Goggin, D. A. Duddell, *J. Chem. Soc. A.* **1968**, 1604.
[181] P. L. Goggin, R. J. Goodfellow, S. R. Haddock, B. F. Taylor, I. R. H. Marshall, *J. Chem. Soc., Dalton Trans.* **1976**, 459
[182] J. Van Droogenbroeck, C. Van Alsenoy, F. Blockhuys, *J. Phys. Chem. A.* **2005**, *109*, 4847.
[183] J. P. H. Charmant, C. Fan, N. C. Norman, P. G. Pringle, *J. Chem. Soc., Dalton Trans.* **2007**, 114.

Appendices

A: Crystallographic Data

Table A. 1: Crystal data and structure refinement for **1**

Identification code	pwas9
Empirical formula	C16 H22 N2 P2 Pt S2
Formula weight	563.51
Temperature	93(2) K
Wavelength	0.71073 Å
Crystal System	Monoclinic
Space group	C2/c
Unit cell dimensions	a = 16.936(4) Å α= 90°
	b = 13.475(3) Å β= 109.913(9)°
	c = 17.633(4) Å γ = 90°
Volume	3783.5(13) $Å^3$
Z	8
Density (calc.)	1.979 Mg/m^3
Absorption coefficient	7.807 mm^{-1}
F(000)	2176
Crystal size	0.100 x 0.080 x 0.020 mm^3
Theta range for data collection	2.46 to 25.35°
Index ranges	-20<=h<=13, -15<=k<=15, -15<=l<=20
Reflection collected	10569
Independent reflections (R_{int})	3239 [R(int) = 0.0410]
Completeness to theta = 25.00°	95.5 %
Absorption correction	multiscan
Max and min. transmission	1.0000 and 0.6497
Refinement method	Full-matrix least-squares on F^2
Data / restraints / parameters	3239 / 0 / 213
Goodness of fit on F^2	1.084
Final R indices [I>2sigma(I)]	R1 = 0.0294, wR2 = 0.0585
R indices (all data)	R1 = 0.0427, wR2 = 0.0644
Largest diff. peak and hole	1.051 and -0.916 e.$Å^{-3}$

Table A. 2: Crystal data and structure refinement for **2**

Identification code	pwas14
Empirical formula	C36 H30 N2 O6 P2 Pt S2
Formula weight	907.77
Temperature	125(2) K
Wavelength	0.71073 Å
Crystal System	Triclinic
Space group	P-1
Unit cell dimensions	a = 10.8476(13) Å α= 78.290(3)°
	b = 13.2659(15) Å β= 78.106(3)°
	c = 13.4783(16) Å γ = 67.963(3)°
Volume	1742.3(4) $Å^3$
Z	2
Density (calc.)	1.730 Mg/m^3
Absorption coefficient	4.288 mm^{-1}
F(000)	896
Crystal size	0.15 x 0.15 x 0.08 mm^3
Theta range for data collection	3.06 to 25.35°
Index ranges	-13<=h<=13, -15<=k<=15, -16<=l<=16
Reflection collected	15146
Independent reflections (R_{int})	6341 [R(int) = 0.1000]
Completeness to theta = 25.00°	99.5 %
Absorption correction	multiscan
Max and min. transmission	1.0000 and 0.4139
Refinement method	Full-matrix least-squares on F^2
Data / restraints / parameters	6341 / 0 / 443
Goodness of fit on F^2	1.094
Final R indices [I>2sigma(I)]	R1 = 0.0783, wR2 = 0.1599
R indices (all data)	R1 = 0.1084, wR2 = 0.1748
Largest diff. peak and hole	3.091 and -2.635 $e.Å^{-3}$

Table A. 3: Crystal data and structure refinement for **4**

Identification code	pwas18
Empirical formula	C12 H30 N2 O6 P2 Pt S2
Formula weight	619.53
Temperature	93(2) K
Wavelength	0.71073 Å
Crystal System	Monoclinic
Space group	$P2_1/c$
Unit cell dimensions	a = 8.900(7) Å α= 90°
	b = 13.719(10) Å β= 101.345(11)°
	c = 18.519(13) Å γ = 90°
Volume	2217(3) $Å^3$
Z	4
Density (calc.)	1.856 Mg/m^3
Absorption coefficient	6.689 mm^{-1}
F(000)	1216
Crystal size	0.0600 x 0.0600 x 0.01 mm^3
Theta range for data collection	2.69 to 25.31°
Index ranges	-10<=h<=10, -16<=k<=16, -22<=l<=22
Reflection collected	21249
Independent reflections (R_{int})	4006 [R(int) = 0.1219]
Completeness to theta = 25.00°	99.3 %
Absorption correction	multiscan
Max and min. transmission	1.0000 and 0.7920
Refinement method	Full-matrix least-squares on F^2
Data / restraints / parameters	4006 / 40 / 257
Goodness of fit on F^2	1.134
Final R indices [I>2sigma(I)]	R1 = 0.0449, wR2 = 0.0972
R indices (all data)	R1 = 0.0565, wR2 = 0.1024
Largest diff. peak and hole	2.591 and -1.418 $e.Å^{-3}$

Table A. 4: Crystal data and structure refinement for **5**

Identification code	pwas11
Empirical formula	C6 H18 N2 O6 P2 Pt S2
Formula weight	535.37
Temperature	93(2) K
Wavelength	0.71073 Å
Crystal System	Monoclinic
Space group	$P2_1$
Unit cell dimensions	a = 8.299(4) Å α= 90°
	b = 6.783(3) Å β= 101.864(6)°
	c = 14.587(6) Å γ = 90°
Volume	803.7(6) $Å^3$
Z	2
Density (calc.)	2.212 Mg/m^3
Absorption coefficient	9.207 mm^{-1}
F(000)	512
Crystal size	0.2000 x 0.0100 x 0.0100 mm^3
Theta range for data collection	2.51 to 25.33°
Index ranges	-9<=h<=9, -8<=k<=7, -17<=l<=17
Reflection collected	7958
Independent reflections (R_{int})	2882 [R(int) = 0.0490]
Completeness to theta = 25.00°	99.9 %
Absorption correction	Multiscan
Max and min. transmission	1.0000 and 0.7396
Refinement method	Full-matrix least-squares on F^2
Data / restraints / parameters	2882 / 1 / 179
Goodness of fit on F^2	0.988
Final R indices [I>2sigma(I)]	R1 = 0.0418, wR2 = 0.0963
R indices (all data)	R1 = 0.0455, wR2 = 0.0997
Largest diff. peak and hole	2.049 and -1.099 $e.Å^{-3}$

Table A. 5: Crystal data and structure refinement for **6**

Identification code	pwas15
Empirical formula	C16 H22 N2 O4 P2 Pt S2
Formula weight	627.51
Temperature	93(2) K
Wavelength	0.71073 Å
Crystal System	Monoclinic
Space group	$P2_1/c$
Unit cell dimensions	a = 19.622(2) Å α= 90°
	b = 13.4726(11) Å β= 117.33(3)°
	c = 18.8268(18) Å γ = 90°
Volume	4421.6(7) $Å^3$
Z	8
Density (calc.)	1.885 Mg/m^3
Absorption coefficient	6.704 mm^{-1}
F(000)	2432
Crystal size	0.2000 x 0.2000 x 0.2000 mm^3
Theta range for data collection	1.91 to 25.36°
Index ranges	-23<=h<=23, -9<=k<=16, -22<=l<=18
Reflection collected	28208
Independent reflections (R_{int})	8052 [R(int) = 0.0455]
Completeness to theta = 25.00°	99.7 %
Absorption correction	Multiscan
Max and min. transmission	1.0000 and 0.6958
Refinement method	Full-matrix least-squares on F^2
Data / restraints / parameters	8052 / 0 / 496
Goodness of fit on F^2	1.063
Final R indices [I>2sigma(I)]	R1 = 0.0353, wR2 = 0.0795
R indices (all data)	R1 = 0.0438, wR2 = 0.0842
Largest diff. peak and hole	3.854 and -1.439 $e.Å^{-3}$

Table A. 6: Crystal data and structure refinement for **7**

Identification code	pwas17
Empirical formula	C26 H26 N2 O2 P2 Pt S2
Formula weight	719.64
Temperature	93(2) K
Wavelength	0.71073 Å
Crystal System	Orthorhombic
Space group	$P2_12_12_1$
Unit cell dimensions	a = 10.2231(11) Å α= 90°
	b = 14.6259(16) Å β= 90°
	c = 17.7113(19) Å γ = 90°
Volume	2648.2(5) $Å^3$
Z	4
Density (calc.)	1.805 Mg/m^3
Absorption coefficient	5.604 mm^{-1}
F(000)	1408
Crystal size	0.050 x 0.050 x 0.050 mm^3
Theta range for data collection	2.69 to 25.35°
Index ranges	-12<=h<=8, -17<=k<=17, -21<=l<=16
Reflection collected	15867
Independent reflections (R_{int})	4803 [R(int) = 0.1261]
Completeness to theta = 25.00°	99.5 %
Absorption correction	Multiscan
Max and min. transmission	1.0000 and 0.9710
Refinement method	Full-matrix least-squares on F^2
Data / restraints / parameters	4803 / 6 / 319
Goodness of fit on F^2	1.060
Final R indices [I>2sigma(I)]	R1 = 0.0442, wR2 = 0.1092
R indices (all data)	R1 = 0.0457, wR2 = 0.1105
Largest diff. peak and hole	1.394 and -1.725 $e.Å^{-3}$

Table A. 7: Crystal data and structure refinement for **8**

Identification code	paul28
Empirical formula	C18 H26 Cl3 N4 Pd S2 Sn
Formula weight	693.99
Temperature	125(2) K
Wavelength	0.71073 Å
Crystal System	Triclinic
Space group	P-1
Unit cell dimensions	a = 7.3169(9) Å α= 61.097(11)°
	b = 19.976(3) Å β= 86.927(12)°
	c = 20.014(3) Å γ = 86.875(13)°
Volume	2556.0(6) $Å^3$
Z	4
Density (calc.)	1.803 Mg/m^3
Absorption coefficient	2.171 mm^{-1}
F(000)	1364
Crystal size	0.24 x 0.07 x 0.06 mm^3
Theta range for data collection	2.96 to 25.35°
Index ranges	-8<=h<=8, -24<=k<=24, -24<=l<=24
Reflection collected	21243
Independent reflections (R_{int})	9276 [R(int) = 0.2721]
Completeness to theta = 25.00°	99.3 %
Absorption correction	Multiscan
Max and min. transmission	1.0000 and 0.6239
Refinement method	Full-matrix least-squares on F^2
Data / restraints / parameters	9276 / 13 / 328
Goodness of fit on F^2	0.933
Final R indices [I>2sigma(I)]	R1 = 0.1161, wR2 = 0.1925
R indices (all data)	R1 = 0.3321, wR2 = 0.2642
Largest diff. peak and hole	1.238 and -1.022 $e.Å^{-3}$

Table A. 8: Crystal data and structure refinement for **9**

Identification code	Paul34
Empirical formula	C17 H22 Cl2 N8 O2 Pd2 S4
Formula weight	782.37
Temperature	125(2) K
Wavelength	0.71070 Å
Crystal System	Triclinic
Space group	P-1
Unit cell dimensions	a = 7.347(15) Å α= 94.76(4)°
	b = 9.97(2) Å β= 99.03(4)°
	c = 20.08(4) Å γ = 92.450(17)°
Volume	1445(5) $Å^3$
Z	2
Density (calc.)	1.798 Mg/m^3
Absorption coefficient	1.748 mm^{-1}
F(000)	772
Crystal size	0.20 x 0.20 x 0.20 mm^3
Theta range for data collection	2.05 to 25.00°
Index ranges	-8<=h<=8, -11<=k<=11, -23<=l<=23
Reflection collected	11978
Independent reflections (R_{int})	5069 [R(int) = 0.1552]
Completeness to theta = 25.00°	99.6 %
Absorption correction	multiscan
Max and min. transmission	0.7212 and 0.7212
Refinement method	Full-matrix least-squares on F^2
Data / restraints / parameters	5069 / 0 / 354
Goodness of fit on F^2	1.000
Final R indices [I>2sigma(I)]	R1 = 0.0955, wR2 = 0.1982
R indices (all data)	R1 = 0.1869, wR2 = 0.2565
Largest diff. peak and hole	1.548 and -1.338 e.$Å^{-3}$

Table A. 9: Crystal data and structure refinement for **16**

Identification code	Paul37
Empirical formula	C6 H18 N2 O6 P2 Pt S Se
Formula weight	582.27
Temperature	125(2) K
Wavelength	0.71075 Å
Crystal System	Monoclinic
Space group	$P2_1/c$
Unit cell dimensions	a = 15.1888(8) Å α= 90°
	b = 6.8320(4) Å β= 109.6820(10)°
	c = 16.4967(9) Å γ = 90°
Volume	1611.85(15) $Å^3$
Z	4
Density (calc.)	2.399 Mg/m^3
Absorption coefficient	11.310 mm^{-1}
F(000)	1096
Crystal size	0.40 x 0.27 x 0.18 mm^3
Theta range for data collection	3.16 to 24.99°
Index ranges	-18<=h<=18, -8<=k<=8, -19<=l<=19
Reflection collected	13159
Independent reflections (R_{int})	2834 [R(int) = 0.1017]
Completeness to theta = 24.99°	99.9 %
Absorption correction	multiscan
Max and min. transmission	0.2353 and 0.0930
Refinement method	Full-matrix least-squares on F^2
Data / restraints / parameters	2834 / 0 / 179
Goodness of fit on F^2	1.077
Final R indices [I>2sigma(I)]	R1 = 0.0416, wR2 = 0.1029
R indices (all data)	R1 = 0.0487, wR2 = 0.1062
Largest diff. peak and hole	3.318 and -2.188 $e.Å^{-3}$

Table A. 10: Crystal data and structure refinement for **17**

Identification code	paul35
Empirical formula	C16 H22 N2 O4 P2 Pt S Se
Formula weight	674.41
Temperature	125(2) K
Wavelength	0.71075 Å
Crystal System	Monoclinic
Space group	$P2_1/n$
Unit cell dimensions	a = 9.0315(3) Å α= 90°
	b = 17.8064(5) Å β= 102.6460(10)°
	c = 13.5320(4) Å γ = 90°
Volume	2123.40(11) $Å^3$
Z	4
Density (calc.)	2.110 Mg/m^3
Absorption coefficient	8.595 mm^{-1}
F(000)	1288
Crystal size	0.29 x 0.15 x 0.12 mm^3
Theta range for data collection	3.05 to 27.48°
Index ranges	-11<=h<=11, -23<=k<=23, -17<=l<=17
Reflection collected	22112
Independent reflections (R_{int})	4854 [R(int) = 0.0625]
Completeness to theta = 25.00°	99.8 %
Absorption correction	multiscan
Max and min. transmission	0.4253 and 0.1895
Refinement method	Full-matrix least-squares on F^2
Data / restraints / parameters	4854 / 0 / 249
Goodness of fit on F^2	1.085
Final R indices [I>2sigma(I)]	R1 = 0.0326, wR2 = 0.0588
R indices (all data)	R1 = 0.0420, wR2 = 0.0619
Largest diff. peak and hole	1.513 and -1.238 $e.Å^{-3}$

Table A. 11: Crystal data and structure refinement for **18**

Identification code	paul38
Empirical formula	C26 H26 N2 O2 P2 Pt S Se
Formula weight	766.54
Temperature	125(2) K
Wavelength	0.71075 Å
Crystal System	Orthorhombic
Space group	$P2_12_12_1$
Unit cell dimensions	a = 10.1701(4) Å α= 90°
	b = 14.7525(5) Å β= 90°
	c = 18.0251(6) Å γ = 90°
Volume	2704.39(17) $Å^3$
Z	4
Density (calc.)	1.883 Mg/m^3
Absorption coefficient	6.757 mm^{-1}
F(000)	1480
Crystal size	0.42 x 0.23 x 0.20 mm^3
Theta range for data collection	3.02 to 25.00°
Index ranges	-12<=h<=12, -17<=k<=17, -21<=l<=21
Reflection collected	23268
Independent reflections (R_{int})	4744 [R(int) = 0.0638]
Completeness to theta = 25.00°	99.7 %
Absorption correction	multiscan
Max and min. transmission	0.3451 and 0.1636
Refinement method	Full-matrix least-squares on F^2
Data / restraints / parameters	4744 / 6 / 319
Goodness of fit on F^2	1.083
Final R indices [I>2sigma(I)]	R1 = 0.0311, wR2 = 0.0642
R indices (all data)	R1 = 0.0332, wR2 = 0.0648
Largest diff. peak and hole	1.502 and -0.744 $e.Å^{-3}$

Table A. 12: Crystal data and structure refinement for **19**

Identification code	paul40
Empirical formula	C36 H34 N2 O2 P2 Pt S Se
Formula weight	894.70
Temperature	125(2) K
Wavelength	0.71075 Å
Crystal System	Triclinic
Space group	P-1
Unit cell dimensions	a = 11.3630(4) Å α= 93.4760(10)°
	b = 12.1702(5) Å β= 108.3000(10)°
	c = 16.5588(7) Å γ = 113.4650(10)°
Volume	1948.47(13) $Å^3$
Z	2
Density (calc.)	1.525 Mg/m^3
Absorption coefficient	4.701 mm^{-1}
F(000)	876
Crystal size	0.49 x 0.24 x 0.23 mm^3
Theta range for data collection	3.08 to 25.00°
Index ranges	-13<=h<=13, -14<=k<=14, -19<=l<=19
Reflection collected	16900
Independent reflections (R_{int})	6859 [R(int) = 0.0426]
Completeness to theta = 25.00°	99.8 %
Absorption correction	multiscan
Max and min. transmission	0.4111 and 0.2066
Refinement method	Full-matrix least-squares on F^2
Data / restraints / parameters	6859 / 24 / 425
Goodness of fit on F^2	1.084
Final R indices [I>2sigma(I)]	R1 = 0.0502, wR2 = 0.1501
R indices (all data)	R1 = 0.0569, wR2 = 0.1545
Largest diff. peak and hole	2.761 and -1.269 $e.Å^{-3}$

Table A. 13: Crystal data and structure refinement for **20**

Identification code	paul20
Empirical formula	C18 H42 Cl2 O6 P2 Pt
Formula weight	682.45
Temperature	125(2) K
Wavelength	0.71075 Å
Crystal System	Monoclinic
Space group	$P2_1/c$
Unit cell dimensions	a = 10.8962(4) Å α= 90°
	b = 18.9114(8) Å β= 104.7460(10)°
	c = 14.2754(6) Å γ = 90°
Volume	2844.7(2) $Å^3$
Z	4
Density (calc.)	1.593 Mg/m^3
Absorption coefficient	5.259 mm^{-1}
F(000)	1360
Crystal size	0.26 x 0.22 x 0.13 mm^3
Theta range for data collection	3.02 to 25.00°
Index ranges	-12<=h<=12, -22<=k<=22, -16<=l<=16
Reflection collected	24157
Independent reflections (R_{int})	4995 [R(int) = 0.0396]
Completeness to theta = 25.00°	99.8 %
Absorption correction	multiscan
Max and min. transmission	0.5480 and 0.3417
Refinement method	Full-matrix least-squares on F^2
Data / restraints / parameters	4995 / 0 / 275
Goodness of fit on F^2	1.107
Final R indices [I>2sigma(I)]	R1 = 0.0239, wR2 = 0.0372
R indices (all data)	R1 = 0.0308, wR2 = 0.0383
Largest diff. peak and hole	0.569 and -0.491 $e.Å^{-3}$

Table A. 14: Crystal data and structure refinement for **21**

Identification code	pwas12
Empirical formula	C12 H30 Cl2 O6 P2 Pt
Formula weight	598.29
Temperature	93(2) K
Wavelength	0.71073 Å
Crystal System	Triclinic
Space group	P-1
Unit cell dimensions	a = 9.952(6) Å α= 88.92(3)°
	b = 14.063(9) Å β= 85.04(3)°
	c = 15.851(8) Å γ = 89.90(4)°
Volume	2210(2) $Å^3$
Z	4
Density (calc.)	1.798 Mg/m^3
Absorption coefficient	6.757 mm^{-1}
F(000)	1168
Crystal size	0.1000 x 0.1000 x 0.1000 mm^3
Theta range for data collection	1.45 to 25.37°
Index ranges	-11<=h<=11, -14<=k<=16, -19<=l<=18
Reflection collected	11501
Independent reflections (R_{int})	6698 [R(int) = 0.0453]
Completeness to theta = 25.00°	83.6 %
Absorption correction	multiscan
Max and min. transmission	1.0000 and 0.5058
Refinement method	Full-matrix least-squares on F^2
Data / restraints / parameters	6698 / 102 / 417
Goodness of fit on F^2	1.114
Final R indices [I>2sigma(I)]	R1 = 0.1485, wR2 = 0.3616
R indices (all data)	R1 = 0.1593, wR2 = 0.3681
Largest diff. peak and hole	6.066 and -7.245 $e.Å^{-3}$

Table A. 15: Crystal data and structure refinement for **23**

Identification code	pwas16
Empirical formula	C16 H22 Cl2 O4 P2 Pt
Formula weight	606.27
Temperature	125(2) K
Wavelength	0.71073 Å
Crystal System	Monoclinic
Space group	C2/c
Unit cell dimensions	a = 10.9734(7) Å α= 90°
	b = 9.2290(6) Å β= 102.398(2)°
	c = 20.7002(14) Å γ = 90°
Volume	2047.5(2) $Å^3$
Z	4
Density (calc.)	1.967 Mg/m^3
Absorption coefficient	7.288 mm^{-1}
F(000)	1168
Crystal size	0.29 x 0.16 x 0.07 mm^3
Theta range for data collection	3.21 to 25.34°
Index ranges	-13<=h<=13, -11<=k<=10, -24<=l<=24
Reflection collected	5869
Independent reflections (R_{int})	1869 [R(int) = 0.0354]
Completeness to theta = 25.00°	99.4 %
Absorption correction	Multiscan
Max and min. transmission	0.6295 and 0.2264
Refinement method	Full-matrix least-squares on F^2
Data / restraints / parameters	1869 / 0 / 117
Goodness of fit on F^2	1.065
Final R indices [I>2sigma(I)]	R1 = 0.0214, wR2 = 0.0418
R indices (all data)	R1 = 0.0246, wR2 = 0.0425
Largest diff. peak and hole	0.621 and -0.692 e.$Å^{-3}$

Table A. 16: Crystal data and structure refinement for **24**

Identification code	paul1
Empirical formula	Pt C26 H26 O2 Cl2 P2
Formula weight	698.43
Temperature	125(1) K
Wavelength	0.71075 Å
Crystal System	Monoclinic
Space group	$P2_1/n$
Unit cell dimensions	a = 12.4262(6) Å α= 90°
	b = 13.6280(7) Å β = 93.5316(11)°
	c = 15.0494(8) Å γ = 90°
Volume	2543.7(2) $Å^3$
Z	4
Density (calc.)	1.824 Mg/m^{-3}
Absorption coefficient	58.520 cm^{-1}
F(000)	1360
Crystal size	0.25 x 0.15 x 0.12 mm^3
Theta range for data collection	3.21 to 25.34°
Index ranges	-13<=h<=13, -11<=k<=10, -24<=l<=24
Reflection collected	26133
Independent reflections (R_{int})	5827 [R(int) = 0.057]
Completeness to theta = 25.00°	99.4 %
Absorption correction	multiscan
Max and min. transmission	0.377 and 0.495
Refinement method	Full-matrix least-squares on F^2
Data / restraints / parameters	5827 / 0 / 299
Goodness of fit on F^2	1.133
Final R indices [I>2sigma(I)]	R1 = 0.0405, wR2 = 0.0621
R indices (all data)	R1 = 0.0562, wR2 = 0.0621
Largest diff. peak and hole	0.99 and -1.02 $e.Å^{-3}$

Table A. 17: Crystal data and structure refinement for **26**

Identification code	paul64
Empirical formula	C6 H18 Br2 O6 P2 Pt
Formula weight	603.05
Temperature	125(2) K
Wavelength	0.71075 Å
Crystal System	Orthorhombic
Space group	$Pna2_1$
Unit cell dimensions	a = 12.6116(9) Å α= 90°
	b = 7.6773(6) Å β= 90°
	c = 16.0931(12) Å γ = 90°
Volume	1558.2(2) $Å^3$
Z	4
Density (calc.)	2.571 Mg/m^3
Absorption coefficient	14.349 mm^{-1}
F(000)	1120
Crystal size	0.14 x 0.11 x 0.07 mm^3
Theta range for data collection	3.11 to 24.98°
Index ranges	-14<=h<=14, -9<=k<=9, -19<=l<=19
Reflection collected	12415
Independent reflections (R_{int})	2730 [R(int) = 0.0848]
Completeness to theta = 25.00°	99.8 %
Absorption correction	multiscan
Max and min. transmission	0.4333 and 0.2386
Refinement method	Full-matrix least-squares on F^2
Data / restraints / parameters	2730 / 1 / 161
Goodness of fit on F^2	1.054
Final R indices [I>2sigma(I)]	R1 = 0.0335, wR2 = 0.0653
R indices (all data)	R1 = 0.0368, wR2 = 0.0664
Largest diff. peak and hole	1.362 and -0.918 $e.Å^{-3}$

Table A. 18: Crystal data and structure refinement for **27**

Identification code	paul63
Empirical formula	C16 H22 Br2 O4 P2 Pt
Formula weight	695.19
Temperature	125(2) K
Wavelength	0.71075 Å
Crystal System	Triclinic
Space group	P-1
Unit cell dimensions	a = 9.1545(7) Å α= 110.452(8)°
	b = 9.9510(8) Å β= 94.763(7)°
	c = 13.1489(10) Å γ = 108.745(8)°
Volume	1036.71(14) $Å^3$
Z	2
Density (calc.)	2.227 Mg/m^3
Absorption coefficient	10.793 mm^{-1}
F(000)	656
Crystal size	0.23 x 0.13 x 0.12 mm^3
Theta range for data collection	3.24 to 25.00°.
Index ranges	0<=h<=10, -11<=k<=11, -15<=l<=15
Reflection collected	3629
Independent reflections (R_{int})	3629 [R(int) = 0.0000]
Completeness to theta = 25.00°	99.4 %
Absorption correction	multiscan
Max and min. transmission	0.3575 and 0.1904
Refinement method	Full-matrix least-squares on F^2
Data / restraints / parameters	3629 / 0 / 231
Goodness of fit on F^2	1.144
Final R indices [I>2sigma(I)]	R1 = 0.0199, wR2 = 0.0429
R indices (all data)	R1 = 0.0211, wR2 = 0.0434
Largest diff. peak and hole	0.500 and -0.675 $e.Å^{-3}$

Table A. 19: Crystal data and structure refinement for **28**

Identification code	paul61
Empirical formula	C26 H26 Br2 O2 P2 Pt
Formula weight	787.32
Temperature	125(2) K
Wavelength	0.71070 Å
Crystal System	Monoclinic
Space group	$P2_1/n$
Unit cell dimensions	a = 12.675(3) Å α= 90°
	b = 13.753(5) Å β= 93.283(9)°
	c = 14.938(10) Å γ = 90°
Volume	2600(2) $Å^3$
Z	4
Density (calc.)	2.012 Mg/m^3
Absorption coefficient	8.617 mm^{-1}
F(000)	1504
Crystal size	0.20 x 0.20 x 0.20 mm^3
Theta range for data collection	2.01 to 25.00°
Index ranges	-15<=h<=15, -16<=k<=16, -17<=l<=17
Reflection collected	22176
Independent reflections (R_{int})	4568 [R(int) = 0.0497]
Completeness to theta = 25.00°	99.9 %
Absorption correction	multiscan
Max and min. transmission	0.2776 and 0.2776
Refinement method	Full-matrix least-squares on F^2
Data / restraints / parameters	4568 / 0 / 301
Goodness of fit on F^2	1.078
Final R indices [I>2sigma(I)]	R1 = 0.0265, wR2 = 0.0600
R indices (all data)	R1 = 0.0317, wR2 = 0.0624
Largest diff. peak and hole	1.155 and -0.995 $e.Å^{-3}$

Table A. 20: Crystal data and structure refinement for **29**

Identification code	paul60
Empirical formula	C37 H31 Br2 Cl3 P2 Pt
Formula weight	998.82
Temperature	125(2) K
Wavelength	0.71075 Å
Crystal System	Triclinic
Space group	P-1
Unit cell dimensions	a = 11.1265(7) Å α= 90.826(6)°
	b = 11.7130(7) Å β= 98.341(7)°
	c = 14.2633(10) Å γ = 106.986(7)°
Volume	1755.8(2) $Å^3$
Z	2
Density (calc.)	1.889 Mg/m^3
Absorption coefficient	6.618 mm^{-1}
F(000)	964
Crystal size	0.28 x 0.12 x 0.11 mm^3
Theta range for data collection	3.03 to 25.00°
Index ranges	-13<=h<=13, -13<=k<=13, -16<=l<=16
Reflection collected	15229
Independent reflections (R_{int})	6155 [R(int) = 0.0362]
Completeness to theta = 25.00°	99.8 %
Absorption correction	multiscan
Max and min. transmission	0.5297 and 0.2587
Refinement method	Full-matrix least-squares on F^2
Data / restraints / parameters	6155 / 0 / 407
Goodness of fit on F^2	1.097
Final R indices [I>2sigma(I)]	R1 = 0.0285, wR2 = 0.0581
R indices (all data)	R1 = 0.0330, wR2 = 0.0595
Largest diff. peak and hole	1.001 and -0.881 $e.Å^{-3}$

Table A. 21: Crystal data and structure refinement for **29a**

Identification code	paul59
Empirical formula	C37 H33 Br2 Cl P2 Pt
Formula weight	929.93
Temperature	125(2) K
Wavelength	0.71075 Å
Crystal System	Monoclinic
Space group	C2/c
Unit cell dimensions	a = 12.2581(11) Å α= 90°
	b = 14.5375(13) Å β= 92.402(6)°
	c = 20.1433(18) Å γ = 90°
Volume	3586.4(5) $Å^3$
Z	4
Density (calc.)	1.722 Mg/m^3
Absorption coefficient	6.329 mm^{-1}
F(000)	1800
Crystal size	0.20 x 0.12 x 0.09 mm^3
Theta range for data collection	3.02 to 25.00°
Index ranges	-14<=h<=14, -17<=k<=17, -23<=l<=23
Reflection collected	14789
Independent reflections (R_{int})	3161 [R(int) = 0.0431]
Completeness to theta = 25.00°	99.8 %
Absorption correction	multiscan
Max and min. transmission	0.5997 and 0.3642
Refinement method	Full-matrix least-squares on F^2
Data / restraints / parameters	3161 / 0 / 214
Goodness of fit on F^2	1.095
Final R indices [I>2sigma(I)]	R1 = 0.0278, wR2 = 0.0444
R indices (all data)	R1 = 0.0420, wR2 = 0.0475
Largest diff. peak and hole	0.583 and -0.714 $e.Å^{-3}$

Table A. 22: Crystal data and structure refinement for **30**

Identification code	paul69
Empirical formula	C6 H18 I2 O6 P2 Pt
Formula weight	697.03
Temperature	125(2) K
Wavelength	0.71075 Å
Crystal System	Monoclinic
Space group	$P2_1/n$
Unit cell dimensions	a = 9.0554(4) Å α= 90°
	b = 14.7571(7) Å β= 98.251(7)°
	c = 12.8733(9) Å γ = 90°
Volume	1702.46(16) $Å^3$
Z	4
Density (calc.)	2.719 Mg/m^3
Absorption coefficient	12.066 mm^{-1}
F(000)	1264
Crystal size	0.18 x 0.10 x 0.05 mm^3
Theta range for data collection	3.19 to 25.00°
Index ranges	-10<=h<=10, -17<=k<=17, -15<=l<=15
Reflection collected	14469
Independent reflections (R_{int})	2993 [R(int) = 0.0508]
Completeness to theta = 25.00°	99.8 %
Absorption correction	multiscan
Max and min. transmission	0.5837 and 0.2200
Refinement method	Full-matrix least-squares on F^2
Data / restraints / parameters	2993 / 0 / 161
Goodness of fit on F^2	1.155
Final R indices [I>2sigma(I)]	R1 = 0.0276, wR2 = 0.0460
R indices (all data)	R1 = 0.0329, wR2 = 0.0472
Largest diff. peak and hole	0.761 and -0.932 $e.Å^{-3}$

Table A. 23: Crystal data and structure refinement for **31**

Identification code	paul68
Empirical formula	C16 H22 I2 O4 P2 Pt
Formula weight	789.17
Temperature	125(2) K
Wavelength	0.71070 Å
Crystal System	Triclinic
Space group	P-1
Unit cell dimensions	a = 9.496(3) Å α= 66.910(15)°
	b = 10.044(3) Å β= 71.546(18)°
	c = 13.743(4) Å γ = 71.621(15)°
Volume	1116.0(6) $Å^3$
Z	2
Density (calc.)	2.349 Mg/m^3
Absorption coefficient	9.213 mm^{-1}
F(000)	728
Crystal size	0.20 x 0.20 x 0.20 mm^3
Theta range for data collection	1.65 to 24.99°
Index ranges	-11<=h<=11, -11<=k<=11, -16<=l<=16
Reflection collected	9745
Independent reflections (R_{int})	3922 [R(int) = 0.0350]
Completeness to theta = 24.99°	99.9 %
Absorption correction	multiscan
Max and min. transmission	0.2602 and 0.2602
Refinement method	Full-matrix least-squares on F^2
Data / restraints / parameters	3922 / 0 / 231
Goodness of fit on F^2	1.091
Final R indices [I>2sigma(I)]	R1 = 0.0287, wR2 = 0.0592
R indices (all data)	R1 = 0.0348, wR2 = 0.0625
Largest diff. peak and hole	1.251 and -1.658 $e.Å^{-3}$

Table A. 24: Crystal data and structure refinement for **32**

Identification code	paul66
Empirical formula	C26 H26 I2 O2 P2 Pt
Formula weight	881.30
Temperature	125(2) K
Wavelength	0.71070 Å
Crystal System	Monoclinic
Space group	Cc
Unit cell dimensions	a = 10.456(4) Å α= 90°
	b = 17.143(7) Å β= 104.500(3)°
	c = 15.597(6) Å γ = 90°
Volume	2706.7(19) $Å^3$
Z	4
Density (calc.)	2.163 Mg/m^3
Absorption coefficient	7.605 mm^{-1}
F(000)	1648
Crystal size	0.14 x 0.11 x 0.05 mm^3
Theta range for data collection	2.34 to 25.00°
Index ranges	-12<=h<=12, -20<=k<=20, -18<=l<=18
Reflection collected	11522
Independent reflections (R_{int})	4748 [R(int) = 0.0352]
Completeness to theta = 25.00°	100.0 %
Absorption correction	multiscan
Max and min. transmission	0.7023 and 0.4157
Refinement method	Full-matrix least-squares on F^2
Data / restraints / parameters	4748 / 2 / 301
Goodness of fit on F^2	0.807
Final R indices [I>2sigma(I)]	R1 = 0.0267, wR2 = 0.0452
R indices (all data)	R1 = 0.0294, wR2 = 0.0467
Largest diff. peak and hole	0.945 and -0.997 $e.Å^{-3}$

Table A. 25: Crystal data and structure refinement for **33**

Identification code	paul73
Empirical formula	C36 H32 I2 O P2 Pt
Formula weight	991.45
Temperature	125(2) K
Wavelength	0.71075 Å
Crystal System	Triclinic
Space group	P-1
Unit cell dimensions	a = 9.8227(5) Å α= 86.757(6)°
	b = 10.4993(6) Å β= 77.704(5)°
	c = 17.7426(13) Å γ = 70.376(5)°
Volume	1683.79(17) $Å^3$
Z	2
Density (calc.)	1.956 Mg/m^3
Absorption coefficient	6.123 mm^{-1}
F(000)	940
Crystal size	0.16 x 0.09 x 0.09 mm^3
Theta range for data collection	3.10 to 25.00°
Index ranges	-11<=h<=11, -12<=k<=12, -21<=l<=21
Reflection collected	14529
Independent reflections (R_{int})	5893 [R(int) = 0.0457]
Completeness to theta = 25.00°	99.5 %
Absorption correction	multiscan
Max and min. transmission	0.6088 and 0.4408
Refinement method	Full-matrix least-squares on F^2
Data / restraints / parameters	5893 / 0 / 389
Goodness of fit on F^2	1.076
Final R indices [I>2sigma(I)]	R1 = 0.0403, wR2 = 0.0879
R indices (all data)	R1 = 0.0535, wR2 = 0.0922
Largest diff. peak and hole	2.016 and -1.152 $e.Å^{-3}$

Table A. 26: Crystal data and structure refinement for **33a**

Identification code	paul65
Empirical formula	C38 H32 Cl2 I2 P2 Pt
Formula weight	1070.37
Temperature	125(2) K
Wavelength	0.71070 Å
Crystal System	Monoclinic
Space group	$P2_1/a$
Unit cell dimensions	a = 8.215(3) Å α= 90°
	b = 20.314(7) Å β= 94.925(3)°
	c = 11.771(4) Å γ = 90°
Volume	1956.9(12) $Å^3$
Z	2
Density (calc.)	1.817 Mg/m^3
Absorption coefficient	5.406 mm^{-1}
F(000)	1016
Crystal size	0.20 x 0.20 x 0.20 mm^3
Theta range for data collection	1.74 to 25.00°
Index ranges	-9<=h<=9, -24<=k<=24, -13<=l<=13
Reflection collected	16334
Independent reflections (R_{int})	3410 [R(int) = 0.0894]
Completeness to theta = 25.00°	99.3 %
Absorption correction	multiscan
Max and min. transmission	0.4111 and 0.4111
Refinement method	Full-matrix least-squares on F^2
Data / restraints / parameters	3410 / 24 / 215
Goodness of fit on F^2	1.083
Final R indices [I>2sigma(I)]	R1 = 0.1106, wR2 = 0.3031
R indices (all data)	R1 = 0.1200, wR2 = 0.3088
Largest diff. peak and hole	13.517 and -2.528 $e.Å^{-3}$

Table A. 27: Crystal data and structure refinement for **34**

Identification code	paul10
Empirical formula	C6 H18 Cl2 O6 P2 Pd
Formula weight	425.44
Temperature	125(2) K
Wavelength	0.71075 Å
Crystal System	Monoclinic
Space group	Cc
Unit cell dimensions	a = 6.8059(19) Å α= 90°
	b = 16.897(5) Å β= 100.086(7)°
	c = 13.374(4) Å γ = 90°
Volume	1514.2(7) $Å^3$
Z	4
Density (calc.)	1.866 Mg/m^3
Absorption coefficient	1.799 mm^{-1}
F(000)	848
Crystal size	0.24 x 0.16 x 0.13 mm^3
Theta range for data collection	3.09 to 24.99°
Index ranges	-8<=h<=8, -20<=k<=20, -15<=l<=15
Reflection collected	6323
Independent reflections (R_{int})	2639 [R(int) = 0.0715]
Completeness to theta = 24.99°	99.9 %
Absorption correction	multiscan
Max and min. transmission	0.7998 and 0.6720
Refinement method	Full-matrix least-squares on F^2
Data / restraints / parameters	2639 / 2 / 161
Goodness of fit on F^2	1.074
Final R indices [I>2sigma(I)]	R1 = 0.0540, wR2 = 0.0875
R indices (all data)	R1 = 0.0655, wR2 = 0.0903
Largest diff. peak and hole	1.264 and -0.712 $e.Å^{-3}$

Table A. 28: Crystal data and structure refinement for **35**

Identification code	paul74
Empirical formula	C16 H22 Cl2 O4 P2 Pd
Formula weight	517.58
Temperature	125(2) K
Wavelength	0.71075 Å
Crystal System	Monoclinic
Space group	C2/c
Unit cell dimensions	a = 10.876(7) Å α= 90°
	b = 9.174(5) Å β= 102.196(7)°
	c = 20.722(13) Å γ = 90°
Volume	2021(2) $Å^3$
Z	4
Density (calc.)	1.701 Mg/m^3
Absorption coefficient	1.359 mm^{-1}
F(000)	1040
Crystal size	0.16 x 0.15 x 0.09 mm^3
Theta range for data collection	2.93 to 24.99°
Index ranges	-12<=h<=12, -10<=k<=10, -24<=l<=24
Reflection collected	8406
Independent reflections (R_{int})	1775 [R(int) = 0.0320]
Completeness to theta = 24.99°	99.6 %
Absorption correction	multiscan
Max and min. transmission	0.8875 and 0.8119
Refinement method	Full-matrix least-squares on F^2
Data / restraints / parameters	1775 / 0 / 117
Goodness of fit on F^2	1.091
Final R indices [I>2sigma(I)]	R1 = 0.0230, wR2 = 0.0485
R indices (all data)	R1 = 0.0260, wR2 = 0.0500
Largest diff. peak and hole	1.146 and -0.314 $e.Å^{-3}$

Table A. 29: Crystal data and structure refinement for **36**

Identification code	pwas22
Empirical formula	C45 H44 Cl4 N4 Pt S3
Formula weight	1073.91
Temperature	93(2) K
Wavelength	0.71073 Å
Crystal System	Monoclinic
Space group	$P2_1/c$
Unit cell dimensions	a = 17.610(3) Å α= 90°
	b = 14.268(2) Å β= 102.063(3)°
	c = 18.364(3) Å γ = 90°
Volume	4512.4(12) $Å^3$
Z	4
Density (calc.)	1.581 Mg/m^3
Absorption coefficient	3.522 mm^{-1}
F(000)	2144
Crystal size	0.0500 x 0.0500 x 0.0500 mm^3
Theta range for data collection	1.82 to 25.34°
Index ranges	-21<=h<=17, -11<=k<=17, -20<=l<=22
Reflection collected	29181
Independent reflections (R_{int})	8234 [R(int) = 0.1044]
Completeness to theta = 25.00°	99.9 %
Absorption correction	Multiscan
Max and min. transmission	1.0000 and 0.8626
Refinement method	Full-matrix least-squares on F^2
Data / restraints / parameters	8234 / 0 / 533
Goodness of fit on F^2	1.079
Final R indices [I>2sigma(I)]	R1 = 0.0857, wR2 = 0.2141
R indices (all data)	R1 = 0.1261, wR2 = 0.2489
Largest diff. peak and hole	4.236 and -1.899 $e.Å^{-3}$

Table A. 30: Crystal data and structure refinement for **37**

Identification code	paul46
Empirical formula	C41 H49 Cl N4 O8 P2 Pt S3
Formula weight	1114.50
Temperature	125(2) K
Wavelength	0.71075 Å
Crystal System	Triclinic
Space group	P-1
Unit cell dimensions	a = 10.8195(18) Å α= 80.088(4)°
	b = 11.0779(19) Å β= 86.071(4)°
	c = 19.618(3) Å γ = 80.417(4)°
Volume	2282.1(7) $Å^3$
Z	2
Density (calc.)	1.622 Mg/m^3
Absorption coefficient	3.395 mm^{-1}
F(000)	1120
Crystal size	0.29 x 0.15 x 0.09 mm^3
Theta range for data collection	2.98 to 25.00°
Index ranges	-12<=h<=12, -13<=k<=13, -23<=l<=23
Reflection collected	18353
Independent reflections (R_{int})	7925 [R(int) = 0.1967]
Completeness to theta = 25.00°	98.7 %
Absorption correction	multiscan
Max and min. transmission	0.7498 and 0.4393
Refinement method	Full-matrix least-squares on F^2
Data / restraints / parameters	7925 / 6 / 555
Goodness of fit on F^2	1.052
Final R indices [I>2sigma(I)]	R1 = 0.1105, wR2 = 0.2218
R indices (all data)	R1 = 0.1856, wR2 = 0.2630
Largest diff. peak and hole	2.272 and -1.152 $e.Å^{-3}$

Table A. 31: Crystal data and structure refinement for **38**

Identification code	pwas24
Empirical formula	C74 H64 Cl10 N8 Pd3 S6
Formula weight	1931.39
Temperature	93(2) K
Wavelength	0.71073 Å
Crystal System	Monoclinic
Space group	$P2_1/n$
Unit cell dimensions	a = 15.720(3) Å α= 90°
	b = 15.247(3) Å β= 97.504(5)°
	c = 19.495(4) Å γ = 90°
Volume	4632.5(15) $Å^3$
Z	2
Density (calc.)	1.385 Mg/m^3
Absorption coefficient	1.040 mm^{-1}
F(000)	1936
Crystal size	0.2000 x 0.0500 x 0.0500 mm^3
Theta range for data collection	1.87 to 25.34°
Index ranges	-18<=h<=14, -18<=k<=15, -21<=l<=23
Reflection collected	28936
Independent reflections (R_{int})	8360 [R(int) = 0.0718]
Completeness to theta =	98.8 %
Absorption correction	Multiscan
Max and min. transmission	1.0000 and 0.8465
Refinement method	Full-matrix least-squares on F^2
Data / restraints / parameters	8360 / 0 / 458
Goodness of fit on F^2	1.622
Final R indices [I>2sigma(I)]	R1 = 0.1456, wR2 = 0.4145
R indices (all data)	R1 = 0.1744, wR2 = 0.4370
Largest diff. peak and hole	7.108 and -0.983 $e.Å^{-3}$

Table A. 32: Crystal data and structure refinement for **39**

Identification code	paul25
Empirical formula	C48 H46 Cl6 N6 O2 Pd S3
Formula weight	1154.19
Temperature	125(2) K
Wavelength	0.71075 Å
Crystal System	Triclinic
Space group	P-1
Unit cell dimensions	a = 11.5037(12) Å α= 81.851(3)°
	b = 11.6636(12) Å β= 84.774(3)°
	c = 19.177(2) Å γ = 83.702(3)°
Volume	2524.2(5) $Å^3$
Z	2
Density (calc.)	1.519 Mg/m^3
Absorption coefficient	0.855 mm^{-1}
F(000)	1176
Crystal size	0.20 x 0.17 x 0.11 mm^3
Theta range for data collection	3.23 to 25.00°
Index ranges	-13<=h<=13, -13<=k<=13, -22<=l<=22
Reflection collected	20742
Independent reflections (R_{int})	8823 [R(int) = 0.1840]
Completeness to theta = 25.00°	99.1 %
Absorption correction	multiscan
Max and min. transmission	0.9118 and 0.8476
Refinement method	Full-matrix least-squares on F^2
Data / restraints / parameters	8823 / 6 / 605
Goodness of fit on F^2	1.082
Final R indices [I>2sigma(I)]	R1 = 0.1176, wR2 = 0.2077
R indices (all data)	R1 = 0.2196, wR2 = 0.2514
Largest diff. peak and hole	0.935 and -0.974 $e.Å^{-3}$

Table A. 33: Crystal data and structure refinement for **40**

Identification code	paul33
Empirical formula	C36 H30 Au2 Cl6 N4 S3
Formula weight	1221.45
Temperature	125(2) K
Wavelength	0.71075 Å
Crystal System	Triclinic
Space group	P-1
Unit cell dimensions	a = 9.3202(14) Å α= 82.526(4)°
	b = 10.5215(15) Å β= 86.303(4)°
	c = 20.848(3) Å γ = 78.067(4)°
Volume	1981.7(5) $Å^3$
Z	2
Density (calc.)	2.047 Mg/m^3
Absorption coefficient	7.991 mm^{-1}
F(000)	1164
Crystal size	0.17 x 0.12 x 0.09 mm^3
Theta range for data collection	2.97 to 25.00°
Index ranges	-11<=h<=11, -12<=k<=12, -24<=l<=24
Reflection collected	16287
Independent reflections (R_{int})	6933 [R(int) = 0.1716]
Completeness to theta = 25.00°	99.5 %
Absorption correction	multiscan
Max and min. transmission	0.5333 and 0.3436
Refinement method	Full-matrix least-squares on F^2
Data / restraints / parameters	6933 / 102 / 461
Goodness of fit on F^2	1.175
Final R indices [I>2sigma(I)]	R1 = 0.1447, wR2 = 0.3170
R indices (all data)	R1 = 0.2026, wR2 = 0.3422
Largest diff. peak and hole	5.711 and -2.791 $e.Å^{-3}$

B: Publications

[1] '*cis*-Dichloridobis(dimethoxyphenylphosphino)platinum(II).'
A. M. Z. Slawin, P. G. Waddell, J. D. Woollins, *Acta Crystallogr. Sect. E: Struct. Rep. Online* **2007**, *63*, m2017.

[2] '*cis*-Dichloridobis(methoxydiphenylphosphino)platinum(II).'
A. M. Z. Slawin, P. G. Waddell, J. D. Woollins, *Acta Crystallogr. Sect. E: Struct. Rep. Online* **2007**, *63*, m2018.

[3] 'The preparation and X-ray structure of heptasulfurimidostearate.'
C. J. Bromley, A. M. Z. Slawin, P. G. Waddell, J. D. Woollins, *Inorg. Chem. Commun.* **2009**, *12*, 804.

[4] '*cis*-Dichloridobis(trimethoxyphosphine)palladium(II) at 125 K.'
A. M. Z. Slawin, P. G. Waddell, J. D. Woollins, *Acta Crystallogr., Sect. E: Struct. Rep. Online* **2009**, *E65*, m1391.

[5] '*cis*-Dichloridobis(triisopropoxyphosphine)platinum(II).'
A. M. Z. Slawin, P. G. Waddell, J. D. Woollins, *Acta Crystallogr., Sect. E: Struct. Rep. Online* **2009**, *E65*, m1392.

[6] '*cis*-Dichloridobis(dimethoxyphenylphosphino)palladium(II).'
A. M. Z. Slawin, P. G. Waddell, J. D. Woollins, *Acta Crystallogr. Sect. E: Struct. Rep. Online* **2010**, *E66*, m321.

[7] '(Disulfur dinitrido)triphenylantimony(V).'
A. M. Z. Slawin, P. G. Waddell, J. D. Woollins, *Acta Crystallogr. Sect. E: Struct. Rep. Online* **2010**, *E66*, m418.

[8] 'Di-μ-chlorido-bis[chlorido(dimethoxyphenylphosphine)palladium(II)].'
A. M. Z. Slawin, P. G. Waddell, J. D. Woollins, *Acta Crystallogr. Sect. E: Struct. Rep. Online* **2010**, *E66*, m499.

[9] 'The Preparation and Structure of $Pt(S_2N_2)\{P(OR)_nR'_{3-n}\}_2$ and $Pt(SeSN_2)\{P(OMe)_nPh_{3-n}\}_2$ (n = 0-3).'
P. G. Waddell, A. M. Z. Slawin, J. D. Woollins, *Eur. J. Inorg. Chem.*, submitted for publication.

[10] 'Correlating Pt-P Bond lengths and Pt-P Coupling Constants.'
P. G. Waddell, A. M. Z. Slawin, J. D. Woollins, *J. Chem. Soc., Dalton Trans.*, submitted for publication.